# A NOVEL, MATRIX-SPECIFIC GEF/GAP INTERACTION REGULATES RHO GTPASE CROSSTALK CRITICAL FOR 3D COLLAGEN MIGRATION

Matthew L. Kutys

A dissertation submitted to the faculty at the University of North Carolina at Chapel Hill in partial fulfillment of requirements for the degree of Doctor of Philosophy in the Department of Cell Biology and Physiology in the School of Medicine.

Chapel Hill
2014

Approved by:

Keith Burridge

Ken Jacobson

Stephanie Gupton

Steve Rodgers

Ken Yamada

© 2014
Matthew L. Kutys
ALL RIGHTS RESERVED

## ABSTRACT

Matthew L. Kutys: A novel, matrix-specific GEF/GAP interaction regulates Rho GTPase crosstalk critical for 3D collagen migration
(Under the direction of Kenneth M. Yamada)

Differential activation of the Rho family GTPases, Cdc42, Rac1, and RhoA, helps to govern the distinct morphological and migratory phenotypes downstream of adhesion to different extracellular matrix (ECM) proteins. However, it is not known how specific GTPase-dependent signaling pathways are activated in response to different ECM ligands. We hypothesized that adhesion to different ECM molecules, such as collagen and fibronectin, will trigger selective regulation of guanine nucleotide exchange factors (GEFs) to regulate the appropriate matrix-specific cell migratory response. We utilized an affinity precipitation-based mass spectrometry screen to isolate active GEFs from primary human fibroblasts migrating in collagen, fibronectin, or ECM-free environments. Among the GEFs identified, we found that βPix, a Rac1/Cdc42 GEF, was robustly activated only during migration in collagen matrices. Knockdown of βPix led to a collagen-specific migration defect characterized by rapid, spatially-deregulated protrusions, rounded morphology, the absence of stable leading and trailing edges, and robust contraction of the adjacent collagen matrix. In contrast to fibroblasts migrating on fibronectin, βPix in cells migrating in collagen did not localize to focal adhesions, but instead transiently accumulated on the membrane adjacent to areas of cellular protrusion as determined by live cell imaging, immunofluorescence staining, and biochemical

fractionation. Mechanistically, we found that βPix is critical for efficient migration in fibrillar collagen environments by restraining RhoA signaling. Live FRET imaging and RNAi knockdown established this suppression occurs through a mechanism of Rho GTPase crosstalk between Cdc42 and RhoA that is regulated by a collagen-specific functional interaction between βPix and the GTPase activating protein (GAP) srGAP1. Additionally, we identified that binding of $\alpha_2\beta_1$ integrin to fibrillar collagen leads, through PP2A, to loss of phosphorylation at T526 on βPix and promotes association with srGAP1. We conclude that ECM-dependent regulation of a specific GEF is a fundamental mechanism of migration in different microenvironments. Our results reveal a conserved, matrix-specific pathway controlling migration involving a GEF/GAP interaction of βPix with srGAP1 that is critical for maintaining suppressive crosstalk between Cdc42 and RhoA during 3D collagen migration.

## ACKNOWLEDGEMENTS

To my advisor Ken, thank you for providing the ideal environment and mentoring style to foster and develop my ability to conduct independent research. I will look to your example as a guide for not only exceptional research vision, but as a benchmark for integrity and managerial excellence throughout the course of my scientific career.

To my PhD advisory committee, Drs. Keith Burridge, Ken Jacobson, Stephanie Gupton, and Steve Rogers, thank you for providing advice, criticism, and direction throughout the course of my PhD. Your input was critical to surpassing many of the hurdles encountered in this project. I would also like to thank Dr. Rafael Garcia-Mata for previously serving on this committee and remaining a source of counsel thereafter.

Thank you to the members of the Yamada lab, particularly Andrew Doyle, Kaz Matsumoto, Jill Harunaga, Emily Joo, Ryan Petrie, and Will Daley, who were always willing to lend a critical eye, provide technical advice, or listen to vented frustrations. You made the lab an easy place to spend each day.

To my parents, Larry and Susan, words cannot express all that you have done for me, but they can convey my gratitude. Thank you to my mom, to whose memory this dissertation is dedicated, for teaching me to never be satisfied with achieving anything less than my best. Thank you to my dad, I would have undoubtedly never reached this point without your support. Thank you for being the first person to teach me how to

analytically approach a problem, to value both working with my hands and my mind, and for being a model of perseverance in the face of adversity. To the rest of my family, Anna, Greg, and Ginny, thank you for your unwavering support and for being an outlet for my sanity.

## TABLE OF CONTENTS

## LIST OF TABLES

## LIST OF FIGURES

## LIST OF ABREVIATIONS

| | |
|---|---|
| 3D | Three dimensional |
| BME | Basement membrane extract |
| CDM | Cell-derived matrix |
| COL | Collagen |
| ECM | Extracellular matrix |
| FN | Fibronectin |
| GAG | Glycosaminogylcan |
| GAP | GTPase-activating protein |
| GEF | Guanine nucleotide exchange factor |
| GDP | Guanosine diphosphate |
| GTP | Guanosine triphosphate |
| HFF | Human foreskin fibroblast |
| OKA | Okadaic acid |
| NS | Non-specific |
| p-Thr | Phosphothreonine |
| PBD | p21 binding domain of Pak1 |
| PG | Proteoglycan |
| PKA | Protein kinase A |
| PP2A | Protein phosphatase 2A |
| PPP2R1A | Protein phosphatase 2, regulatory subunit A, alpha isoform |
| RBD | Rho binding domain of Rhotekin |
| TIRF | Total internal reflection fluorescence |

# INTRODUCTION

## EXTRACELLULAR MATRIX AND THE CELL: A SYMBIOTIC RELATIONSHIP

The extracellular matrix (ECM) is the ubiquitous, non-cellular component found in all tissues and organs. Once merely considered a passive scaffold providing support for cells and tissues, we now appreciate that the ECM defines the chemical and physical interactions of the cell, directly influencing cellular physiology and behavior. Core ECM proteins such as collagens and laminins are highly conserved in metazoans, serving as adhesive substrates necessary for proper tissue development, differentiation, survival, and structural homeostasis (Engler et al., 2006; Frantz et al., 2010; Hynes, 2012). However, the distinct chemical composition and physical arrangement of the ECM are the dynamic product of cellular synthesis and remodeling, which are often unique to specific tissues. Thus a synergy exists between ECM matrix assembly/remodeling by the cell and the influence of the ECM on cellular and tissue function. This synergy plays a key role in determining how cells interact and respond to their environment, imbalance of which is the direct cause of many pathological conditions (Byron et al., 2013). To begin to elucidate the diverse cellular functions of the multitude of distinct ECM molecules found in vivo, this dissertation focuses on understanding how specific fibrous ECM proteins signal to stimulate distinct cellular migratory pathways.

**Composition and organization of the extracellular matrix**

The ECM is composed of several distinct families of complex, multifunctional molecules. While conserved proteins domains do exist across these families, arising over the course metazoan evolution through exon shuffling, ECM molecules are generally disparate in both origin and function (Hynes, 2009; Rozario and DeSimone, 2010). Over one hundred ECM proteins have been identified, with ~10-30% of that total being tissue-specific (Naba et al., 2012). This introduction will give a general overview of ECM composition and structure, and will focus on those ECM proteins relevant to this dissertation.

ECM proteins can be broadly grouped into two classes of macromolecules: proteoglycans (PGs) and fibrous proteins. PGs are ubiquitous molecules classified by their diverse protein cores and linked glycosaminoglycan (GAG) polysaccharide chains. PGs are secreted by the cell and either functionally integrate with other ECM constituents (perlecan and decorin) or exist on the cell surface/span the plasma membrane (syndecans and glypicans). PGs have a wide variety of functions, including contributing to tissue mechanical resistance, proliferation, hydration, and solute buffering (Aszodi et al., 2006; Friedl, 2010). In addition, through binding interactions, PGs can modulate the activity of secreted growth factors and cell-surface receptors to stimulate cell migration. In particular, the syndecan family of transmembrane PGs has recently been discovered to have significant influence on cell migration in response to ECM adhesion. Syndecan-4 regulates the directionality of cell migration in concert with fibronectin by modulating Rac1 activity through integrin recycling (Bass et al., 2007; Morgan et al., 2013), while

syndecan-1 controls cell migration by triggering focal adhesion turnover in response to type I collagen (Altemeier et al., 2012).

The second class of ECM macromolecules is fibrous matrix proteins, consisting mainly of laminins, fibronectins, collagens, and elastins. Collagens are composed of a triple helical organization of α chain subunits, where the differential combination of α chains defines the collagen type. While there are 28 known collagens, type I collagen is the most abundant protein in the human body and found in generally all interstitial ECMs, where the bulk of collagen is synthesized, secreted, and organized by fibroblasts, osteoblasts, and macrophages. In the case of type I collagen, two pro-α(1) chains combine with a pro-α(2) chain to form a triple-stranded procollagen precursor molecule. These collagen precursor molecules are secreted and cleaved in the extracellular environment by peptidases, which results in a collagen molecule capable of forming and crosslinking with collagen fibrils (Shoulders and Raines, 2009). The role of collagen was originally thought to be entirely structural, providing tensile strength and maintaining tissue integrity through crosslinking, fibril bundling, and cooperative interaction with the ECM protein elastin (Frantz et al., 2010; Wise and Weiss, 2009). However, collagens also regulate cell adhesion, haptotaxis and migration, cell polarity, and tissue development (Rozario and DeSimone, 2010). Mice deficient for the α(1) chain of type I collagen, *COL1A1*, are embryonic lethal due to impaired tissue development, morphogenesis, and severe integrity defects (Liu et al., 1995).

Fibronectin is another fibrous matrix protein that exists as a dimer of two polypeptide chains composed of a series of repeating modules (type I, II, III repeats), each with distinct functions and ability to bind other ECM components such as tenascins

and collagens (Singh et al., 2010). Fibroblasts secrete soluble fibronectin dimers into the surrounding microenvironment, which through concerted remodeling and deposition by additional cells form larger, insoluble fibronectin fibers (Wierzbicka-Patynowski and Schwarzbauer, 2003). Fibronectin is essential for cell migration during development; deletion of the fibronectin gene *FN1* results in embryonic lethality due to a multitude of morphogenic, developmental, and migratory defects in the mesoderm, neural tube, and vasculature (Rozario and DeSimone, 2010; Tsang et al., 2010). An important property of fibronectin required for both fiber assembly and signaling is that cellular traction on fibronectin fibrils causes it to stretch several times over its resting length, exposing cryptic binding sites. These sites promote self-association between fibronectin fibers, and cell adhesion to these cryptic sites has drastic effects on cellular behavior, implicating fibronectin as an extracellular mechanosensor (Klotzsch et al., 2009).

On a macroscale, the ECM is arranged primarily into basement membranes and interstitial matrix structures. Basement membranes surround epithelial and endothelial tissues, where cell adhesion to the basement membrane defines epithelial apical-basal polarity, and are essential for proper development and tissue homeostasis. The basement membrane confines the epithelium and separates it from the surrounding tissue stroma. All basement membranes are composed of a common set of interacting ECM proteins (type IV collagen, laminin, nidogen, and perlecan) (Daley and Yamada, 2013; Yurchenco, 2011). Surrounding the basement membrane layer, fibroblasts in the stroma assemble the interstitial matrix, consisting primarily of type I and III collagen, elastin, fibronectin, and a multitude of different PGs. The interstitial matrix maintains the structural integrity of the tissue and participates in dynamic regulatory crosstalk with the

epithelium that is necessary for the chemical and mechanical homeostatic maintenance of the entire tissue (Frantz et al., 2010).

**Cell migration and the extracellular matrix in homeostasis and disease**

The aim of this dissertation is to understand how cellular interaction with fibrous ECM proteins such as collagen and fibronectin stimulates cell migration. Physiologically this is most relevant to the interstitial matrix or stroma, an ECM structure that is essential for tissue homeostasis and often deregulated during disease. The distinct groups of ECM molecules previously discussed provide the capacity for a high degree of functional complexity and tissue-specific ECM composition. When assembled under normal conditions, these components are able to generate an interstitial matrix exhibiting diverse biochemical and biophysical properties that are necessary for regulation of cell behavior (Lu et al., 2012).

The compliance, or elasticity, of the stroma is attributed to a relaxed network of type I and III collagen, elastin, and fibronectin, which are surrounded by a hydrogel of GAG-containing PGs. This ECM network imparts resistance to the entire tissue against tensile and compressive stresses (Scott, 2003) and defines the physical properties of the interstitial matrix, which include its porosity, rigidity, elastic behavior, and topography. In addition to maintaining tissue integrity, these physical properties provide major environmental cues that determine cellular behaviors that include differentiation and gene expression, morphology, and migration (Engler et al., 2006; Petrie et al., 2012; Wolf et al., 2013). In regard to cell migration, differential matrix rigidity stimulates directed cell migration toward a substrate of greater stiffness in a process known as durotaxis (Lo et al., 2000), and ECM porosity can inhibit or direct the mode by which a cell migrates

(Wolf and Friedl, 2011). From a cellular perspective, physical ECM homeostasis is mediated by the coordinated deposition and arrangement of ECM molecules, secretion of ECM-degrading metalloproteinases (MMPs) and their agonist tissue inhibitors of metalloproteinases (TIMPs), controlled activity of ECM crosslinking enzymes such as lysyl oxidase and transglutaminase, and regulating the transmission of actomyosin-generated cellular forces to the ECM (Lucero and Kagan, 2006; Mott and Werb, 2004; Provenzano et al., 2008b).

The highly dynamic molecular composition of the stroma also imparts direct and indirect biochemical signals that influence cellular behavior. Charged polysaccharide GAG chains, such as heparan sulfate, bind a host of growth factors including BMPs, FGFs, and WNTs. Through this process, the interstitial matrix is able to limit the accessibility of growth factors to their receptors, establish gradients for chemotactic signaling, and create reservoirs of enzymatically accessible growth factors (Hynes, 2009). Additionally, fibrous proteins in the ECM can also initiate signaling by directly engaging cell-surface receptors. Fibroblast adhesion to fibronectin triggers migratory haptotaxis (Hynes and Yamada, 1982), and fibronectin deposition is essential for driving epithelial morphogenesis and cleft formation in the developing salivary gland (Sakai et al., 2003). Adhesion to type I collagen is also sufficient to stimulate migration and morphogenetic changes in human fibroblasts (da Rocha-Azevedo and Grinnell, 2013), and increased type I collagen deposition is a common marker of tissues undergoing epithelial-to-mesenchymal transitions (Kalluri and Weinberg, 2009).

The significance of maintaining the proper chemical and physical characteristics of the ECM for tissue and cell homeostasis is evident by the dysregulation of the ECM in

multiple diseases. Tissue fibrosis is the result of an abnormal collective wound healing response, characterized by hyperproliferation of fibroblasts, their differentiation into myofibroblasts, and excessive ECM synthesis, deposition, and remodeling (Cox and Erler, 2011). This excessive ECM deposition of collagen type I and III, fibronectin, and hyaluronic acid leads to elevated mechanical stress, which disrupts normal tissue function. During pulmonary fibrosis, increases in collagen concentration and crosslinking lead to drastic changes in tissue elastic properties and result in severe respiratory deficiencies (Suki and Bates, 2008). The increased deposition and remodeling of the ECM also promotes the directional migration of cells within the tissue toward the wound site. Fibronectin directs the migration of activated macrophages, which secrete and release growth factors and cytokines to promote angiogenesis, differentiation, and epithelial-to-mesenchymal transition (Schultz and Wysocki, 2009). Continual injury or failure to suppress the normal wound healing response compounds upon existing ECM changes, leading to further ECM synthesis, remodeling, and enhanced crosslinking, which results in chronic fibrosis.

Tumor progression involves the loss of tissue organization through aberrant behavior of transformed cellular components. Similar to fibrosis, the tumor microenvironment is comparable to wounds that have failed to heal, such that tumor cells and cancer-associated fibroblasts manipulate the surrounding microenvironment to enhance their survival. Tumors are characteristically more rigid than normal tissue with stiffening induced by ECM deposition, remodeling, and crosslinking by activated fibroblasts and the subsequent increased contractility of the transformed epithelium (Levental et al., 2009). Type I collagen and fibronectin are the most common and

abundant ECM components deposited during tumor progression, resulting in a dense fibrous tissue that typically surrounds the tumor (Provenzano et al., 2008a). In particular, the remodeling of fibrillar type I collagen surrounding the tumor is associated with metastatic progression. Linearization and perpendicular reorganization of collagen fibers to the tumor front is a classic marker of malignant transformation and metastatic potential (Levental et al., 2009; Provenzano et al., 2006). These changes in composition of the local ECM microenvironment are significant, as malignant breast cancer cells will not invade in a ECM consisting of basement membrane extract (primarily laminin), but do invade when the local ECM is changed to fibrillar type I collagen (Nguyen-Ngoc et al., 2012). Consequently, intravital imaging has revealed that tumor cells travel along aligned collagen fibers to facilitate invasion (Condeelis and Pollard, 2006), highlighting the importance of understanding the migratory signaling pathways downstream of adhesion to ECM fibers as potential targets of therapeutic intervention.

**Dimensionality, migration, and in vitro extracellular matrix models**

Characterization of cell migration signaling pathways in tissue culture in response to ECM proteins like fibronectin and collagen have helped establish the identity of the receptors and core cytoskeletal machinery involved in the migratory response. While these observations have guided our current understanding, recent investigations into cell migration in three-dimensional (3D) ECM models have revealed substantial differences between 2D and 3D migration (Baker and Chen, 2012; Doyle et al., 2013). However, as evident in Figure 1, these fundamental differences in cell migration are not simply a product of a change in “dimensionality,” but the many chemical and physical features that are inherent to each specific 3D ECM environment. Therefore, rather than simply

concluding that dimensionality directly affects cell migration, it is necessary to identify and understand the cell-regulatory features of each 3D ECM and to elucidate exactly what 3D migratory stimuli dominate that differ from more traditional 2D settings.

Cells migrating on 2D demonstrate a biphasic velocity dependence on ECM ligand concentration. In contrast, cells migrating on a 1D fibrillar ECM (which mimics migration along a 3D fiber) display increasing migration rates with increased ECM concentrations until reaching a plateau, with no inhibition of migration at high ligand concentration (Doyle et al., 2009). This conundrum is compounded further when extended to 3D systems, as changing the ECM protein concentration also alters stiffness, matrix pore size, degree of crosslinking, and topography. Recent investigations into ECM-dependent regulators of 3D migration concluded that deformation of the nucleus through the 3D porous matrix structure is generally the rate limiting factor during migration (Wolf et al., 2013). Inhibition of cell-generated actomyosin contractility decreases migration rates in 1D and 3D environments, but increases rates on 2D ECM (Doyle et al., 2012). Additionally, fibroblasts can respond to the elastic behavior of the ECM and switch their mode of migration from lobopodia-driven in linearly elastic environments (3D CDM) to lamellipodia-driven in nonlinear elastic environments (3D collagen or fibrin) (Petrie et al., 2012). However in addition to these physical parameters, it is clear that the chemical composition of 3D ECM significantly affects both the morphology and migratory behavior of cells. Direct comparisons of fibroblast morphology, migration rates, and focal adhesion structure across four different 3D ECM models revealed quantitative differences that were dependent on the specific ECM chemical composition (Hakkinen et al., 2011). Therefore, it is necessary to carefully

dissect both the physical and chemical cell-ECM interactions that stimulate migration, which is achieved through the combined analysis of 3D in vivo and 3D in vitro reductionist models.

Undoubtedly, the optimal way to study cell-ECM interactions is in vivo. Mouse models provide accurate, physiologically representative insight into cellular interactions with complex ECM microenvironments. However, mouse models often focus on manipulation of cellular aspects rather than directly on the ECM, have limited ability directly to induce chemical and mechanical changes in the local ECM environment, require sensitive and sophisticated imaging/quantification techniques, and are both time- and cost-intensive (Cox and Erler, 2011; Yamada and Cukierman, 2007). In vitro 3D ECM models, while sacrificing the physiological accuracy of mouse models, provide environments to precisely manipulate and quantify chemical and physical changes in the ECM and their effect on cell migration in a controlled setting.

In vitro models for 3D ECM study fall into two categories: synthetic, functionalized hydrogels and hydrogels based on natural ECM proteins. Polyethylene glycol (PEG) hydrogels have been developed with tunable mechanics and incorporated functionalities (such as tethered ECM adhesive domains, growth factors, and cleavable sites) mimicking natural ECM properties (Hern and Hubbell, 1998). Other common synthetic substrates are based on sugars (hyaluronan and dextran), which due to the abundance of functional sites along the polymer backbone, offer more flexibility than PEG in terms of chemical modifications (Trappmann and Chen, 2013). Recently, “designer ECMs” have combined the complex physical features of natural matrices with the versatility of synthetic matrices. For example, a recent PEG hydrogel system

incorporated a collagen peptide mimetic that allowed for in vivo-like triple helical assembly, allowing cells to naturally crosslink the synthetic matrix (Stahl et al., 2010; Trappmann and Chen, 2013). While synthetic matrices allow for heightened manipulation of precise physical/structural parameters, they lack the many physiological subtleties found in natural protein gels.

Natural ECM protein gels such as type I collagen, fibrin, and basement membrane extract are composed of proteins that self-assemble in vitro under proper experimental conditions into 3D fibrous networks mimicking in vivo environments. While these ECMs provide a clear physiological advantage in replicating in vivo chemical interactions between the cell and fibrous ECMs, it is difficult in these systems to isolate and manipulate individual properties, both physical and chemical, without inducing additional changes to the matrix. Figure 2a illustrates the methodology behind the preparation of cell-derived matrix (which is a product of cellular synthesis and discussed below), fibrin, basement membrane extract, and collagen gels. In cell migration studies using 3D collagen gels, globular, acid-solubilized rat tail type I collagen is equilibrated with fibroblasts at proper pH and ionic concentration and polymerized into a hydrated collagen lattice when incubated at the proper temperature (Grinnell and Petroll, 2010). 3D collagen gels generally consist of a dense network of collagen fibrils that lack any specific orientation and can range to depths of 100 - 200 microns. It is important to note that collagen gel polymerization can vary greatly between research groups and even individual experiments if there are differences in the preparation conditions. For example, polymerizing collagen at lower temperature ($4^{o}$C) yields a matrix with thick collagen bundles and large pore sizes, while polymerization at higher temperature ($37^{o}$C) yields a

reticular network of short fibers and smaller pore size (Raub et al., 2007), both of which will significantly affect cell migratory behavior.

Fibroblast-generated cell-derived matrix (CDM) is a heterogeneous fibrous matrix consisting primarily of a meshwork of linear fibronectin fibrils, the predominant adhesive ligand, which can be oriented in parallel or more random in organization (Figure 2a). Additional matrix proteins such as collagen I and IV, perlecan, tenascin-C, hyaluronic acid, and heparan sulfate proteoglycans are present in lower abundance, as well as sequestered growth factors (Beacham et al., 2007). This diversity and spatial heterogeneity of CDM components mimic more closely what is found in in vivo matrix, providing physiological properties not commonly found in traditional native protein gels. Because CDM is generated by the secretion and assembly of ECM fibers from layers of confluent cells in vitro, its topography consists of arrays of fibronectin fibers that are stacked to an approximate depth of 5-20 microns (Kutys et al., 2013). As evident in Figure 2b, each of the above described 3D in vitro ECM models provides a unique complement of matrix composition and physical architecture for studying cell migration. In this dissertation, direct matrix-specific comparisons of primary fibroblast migratory behavior are made between 3D cell-derived and type I collagen matrices.

**Mechanisms of cell migration in response to the extracellular matrix**

Interactions between cells and the ECM can profoundly affect migration rate and the particular migratory phenotype. As highlighted previously in Figure 1, a multitude of physical and chemical properties of the ECM are each sufficient to alter migratory signaling, requiring the cell to integrate each of these inputs for directed, persistent migration. Much of what is known about how the cell senses the ECM, translates and

integrates these signals, and transduces them to the migratory machinery has been elucidated from studies in 2D culture. For efficient mesenchymal migration, cells require an asymmetric morphology with defined leading and trailing edges. Polarized intracellular signaling orients protrusion of the cell leading edge, followed by integrin-mediated adhesion to the ECM, coordinated contraction of the actomyosin machinery at adhesion sites, and disassembly of adhesions at rear regions of the cell, leading to cell translocation (Figure 3a) (Lauffenburger and Horwitz, 1996; Ridley et al., 2003).

Cells interact with the ECM through cell-surface receptors, which include proteoglycans such as syndecans, the DDR-family of collagen receptors, growth factor receptors, and the 24 human integrins which are the dominant class of ECM receptor (van Dijk et al., 2013). All integrins are transmembrane, non-covalently linked heterodimers consisting of an α and β subunit. As seen in Figure 3b, mammalian genomes contain eighteen α and eight β subunit genes, whose different combination determines the ECM ligand specificity of the integrin dimer (Humphries et al., 2006). While multiple pairs of α and β integrin subunits can mediate adhesion to the same type of ECM protein, the strength of their association can vary greatly. For example, both $\alpha_v\beta_3$ and $\alpha_5\beta_1$ can bind to fibronectin, the primary component of 3D CDMs, yet the adhesion strength of $\alpha_5\beta_1$-containing adhesions can be six-fold higher (Roca-Cusachs et al., 2009). This family of integrins recognize the ECM tripeptide RGD domain (Arg-Gly-Asp) motif, which binds the integrin pair at the active site between the α and β subunits. RGD sequences are found not only in fibronectin, but other matrix ligands such as vitronectin, tenascin, fibrinogen, and laminin, where the specificity and affinity of each integrin is dependent on the fit between the protein's RGD conformation and the specific α-β active site (Humphries et

al., 2006). Far less is known about the structural recognition of the ECM by laminin/collagen binding integrins. A crystal structure of the binding between $\alpha_2$ and a type I collagen peptide identified a key motif (GFOGER) on collagen that is critical for its interaction (Emsley et al., 2000). Additionally, mutational analysis has revealed that $\alpha_2$ integrin preferentially recognizes fibrillar type I collagen, while $\alpha_1$ binds globular type I collagen with higher affinity (Kapyla et al., 2000). Integrin adhesion to specific ECM proteins is transduced to the to the intracellular face of the plasma membrane (termed outside-in signaling), where the integrin cytoplasmic tails assemble variable, multiprotein signaling/structural complexes called focal adhesions, whose individual protein components are known collectively as the adhesome.

Molecular analyses of integrin-mediated adhesions have identified ~160 distinct protein components in the adhesome (Geiger et al., 2009). When assembled into focal adhesions, these molecules serve a variety of functions that include linking ECM-bound integrins to the actomyosin machinery, nucleating cytoskeletal polymerization, and serving as a nexus for a variety of signaling events to the rest of the cell (Figure 3c). The unique molecular composition of a focal adhesion is dictated by both the specific engaged ECM ligand-integrin complex (Byron et al., 2011) and tensional forces imposed on it by actomyosin-dependent intracellular contractility in response to rigidity of the surrounding matrix (Kuo et al., 2011). Acting in concert, these ECM-specific and mechanosensitive proteins combine to form a focal adhesion signature that is unique to the surrounding matrix environment. These proteins then translate signals to the cell that are required for proliferation, polarity, differentiation, and migration. In regards to cell migration, signaling from ECM-integrin adhesions leads to the activation of the Rho

family of GTPases, which act through cytoskeleton-regulating proteins to direct cell motility.

The Rho family of GTPases consists of twenty mammalian proteins characterized by the similarity of their amino acid sequence to the first family member to be characterized, RhoA (Heasman and Ridley, 2008). These proteins are relatively small and nearly all possess the intrinsic ability to convert guanosine triphosphate (GTP) to guanosine diphosphate (GDP). This bound nucleotide regulates the activity of the GTPase through conformational changes, rendering it inactive or active in the case of GDP or GTP, respectively. The Rho GTPases mediate a variety of intracellular signaling pathways involved in the regulation of cell cycle progression (Olson et al., 1995), gene transcription (Hill et al., 1995), differentiation (Keung et al., 2011), and cell transformation (Khosravi-Far et al., 1995). However during cell migration, the major function of the Rho GTPases is regulating the polarization and assembly of the actin cytoskeleton and contractile myosin II machinery. For these roles, the best characterized Rho GTPases are Cdc42, Rac1, and RhoA.

A role for the Rho family GTPases in regulating cytoskeletal dynamics was first identified when RhoA was found to be a substrate of C3 transferase, an exoenzyme that induces cell rounding and filamentous actin disassembly in eukaryotic cells (Aktories et al., 1989). Additionally, the constitutively active form of RhoA (RhoAV14) was found to trigger the formation of bundles of parallel F-actin or stress fibers when injected into fibroblasts (Paterson et al., 1990). The ability of the Rho family of GTPases to regulate cytoskeletal remodeling was reinforced when fibroblast were injected with active RhoA, Rac1, or Cdc42 which generated stress fibers, lamellipodia and membrane ruffles, or

filopodia, respectively (Hall, 1998). Further, each of these GTPases was able to trigger the contextual formation, maturation, and disassembly of focal adhesions (Nobes and Hall, 1995). These initial demonstrations of the RhoA, Rac1, and Cdc42 function in fibroblasts have become synonymous with their general function during cell migration. The property of the Rho GTPase family to impinge on each other's activity, or crosstalk, was also observed where active Cdc42 activated Rac1 and active Rac1, in turn, could activate or inactivate RhoA (Arthur and Burridge, 2001; Nobes and Hall, 1995). More recently, there has been increasing evidence for their diverse and non-canonical functions in many different cell types.

During traditional 2D migration, Rac1, Cdc42, and RhoA are spatiotemporally polarized and activated at the leading edge of cells (Machacek et al., 2009). However during migration in 3D, polarization of Rac1 and Cdc42 can be absent during migration (Petrie et al., 2012) or the cell can exhibit variable dependence on the activity of a particular GTPase depending on matrix rigidity and composition (Deakin and Turner, 2011). Requirements for the Cdc42 and Rac1 effectors N-WASP and Scar/WAVE, regulators of actin assembly and lamellipodial protrusions, also differ during 2D and 3D migration (Tang et al., 2013). In the case of RhoA signaling, modulating RhoA-ROCK signaling switches 3D modes of motility in primary fibroblasts between lamellipodial and lobopodial-driven migration in 3D cell-derived matrix. Additionally, the mode of cancer cell migration in 3D collagen matrices depends on both traditional and non-canonical RhoA signaling pathways: amoeboid (RhoA-ROCK) and mesenchymal migration (Cdc42-MRCK) (Sahai and Marshall, 2003), as well as migratory efficiency (RhoA-ROCK1/ROCK2, RhoC) (Vega et al., 2011). Furthermore, activation of RhoA/ROCK-

regulated contractility is necessary for remodeling and alignment of matrix fibers to provide contact guidance during 3D malignant epithelial cell migration (Provenzano et al., 2008b). It is clear that the understanding of signaling mechanisms driving contextual migration in 3D, especially in the case of the Rho family GTPases, is in its infancy, with most observed differences attributed to simply changes in dimensionality rather than to a specific aspect of the ECM.

To address this outstanding and complicated question, it is important to begin by isolating experimentally and conceptually the specific roles of each of the many ECM regulators of 3D cell migration. In this dissertation, we focus on the migratory response of primary human fibroblasts upon adhesion to fibronectin or type I collagen ligands to gain a better understanding of the mechanisms behind the differential 3D migratory behaviors observed between these ECM conditions. We investigate how interaction with these ECM ligands modulates activators of the Rho family of GTPases, first specifically Rac1 for its well-documented role in regulating leading edge protrusion (Figure 3a). We then analyze how these ECM-specific signaling pathways translate to migration in 3D environments, with the goal of identifying a conserved migratory pathway that is unique to fibronectin or collagen microenvironments.

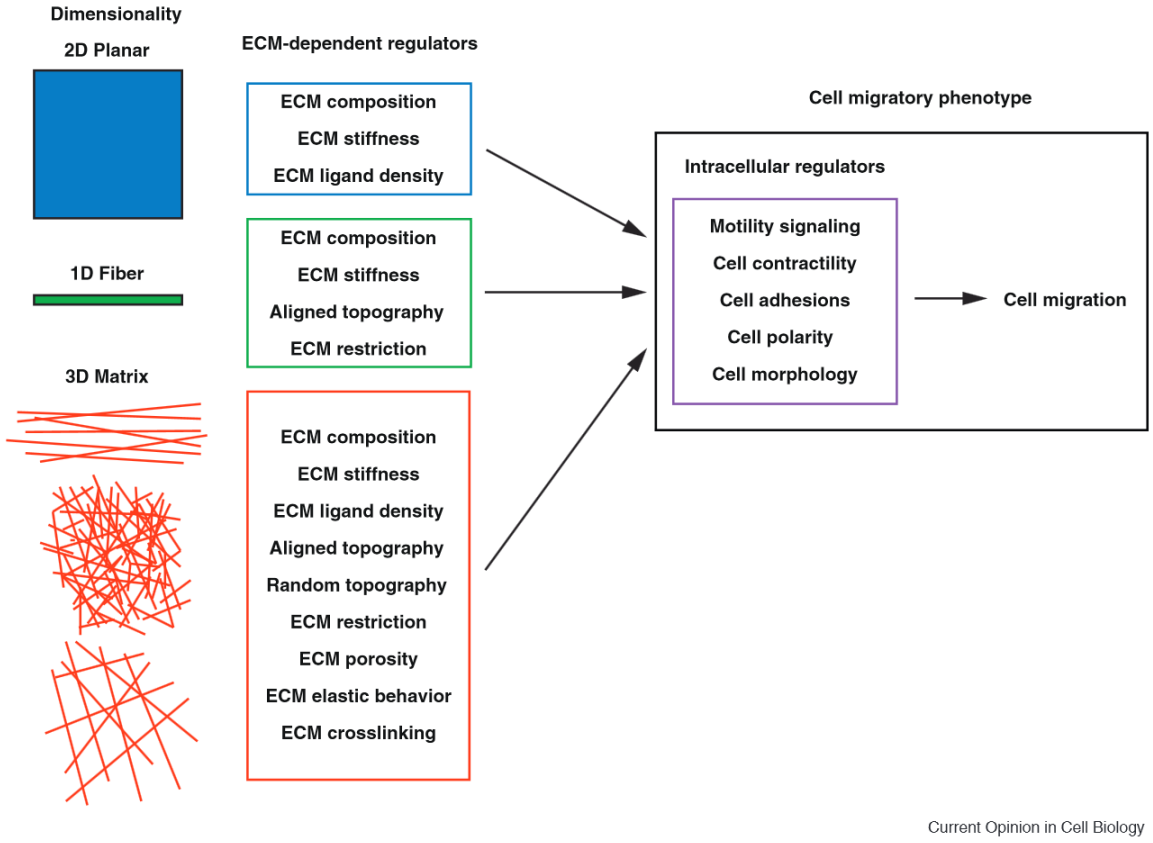


**Figure 1**: **Dimensional regulation of cell migration**. Illustration of the numerous unique ECM-dependent regulators (center column) associated with migration 2D, 1D, and 3D environments. These microenvironment regulators in turn influence intracellular regulatory pathways that govern the migratory phenotype (right panel) and determine how cell migration proceeds. Adapted from (Doyle et al., 2013).

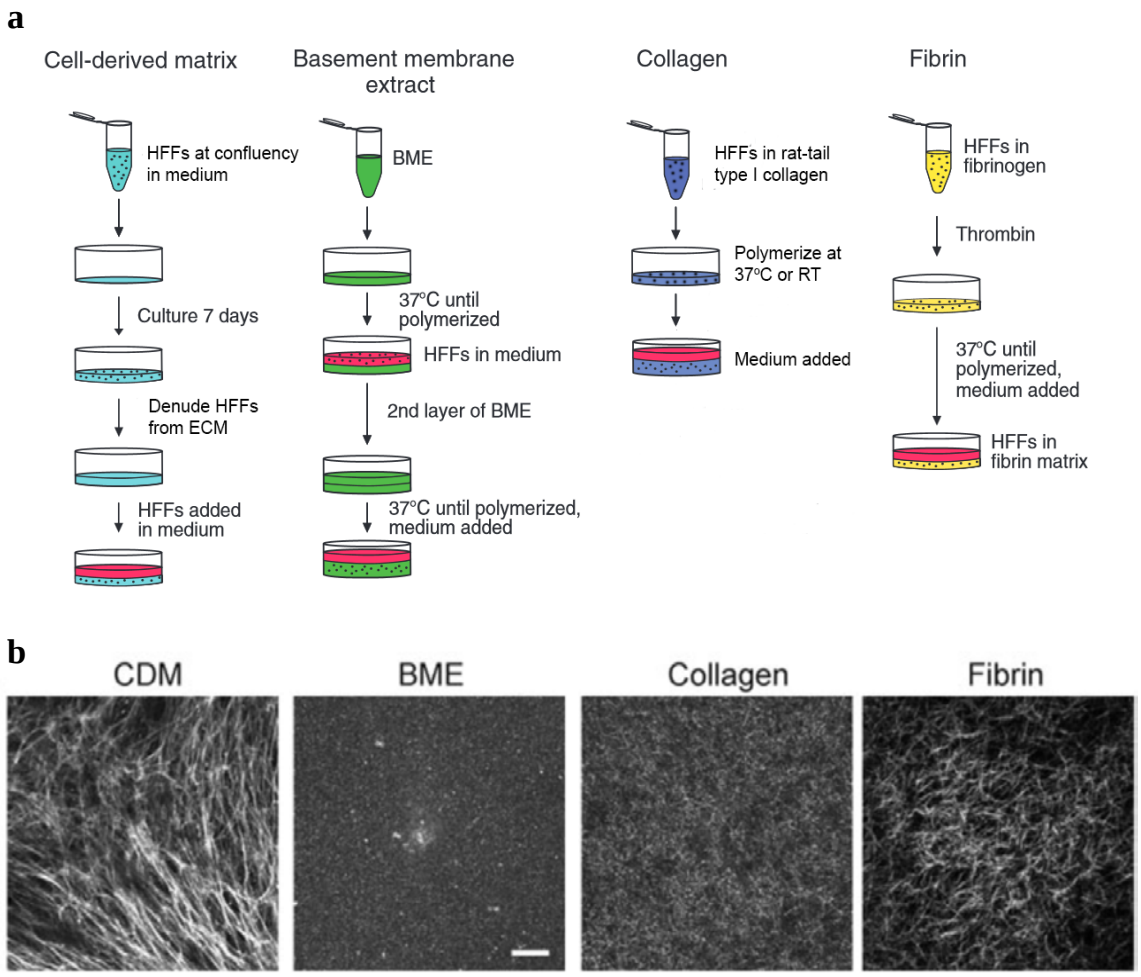


**Figure 2**: **Examples 3D in vitro ECM models and their generation**. **a** Simplified methodology for preparation of 3D in vitro cell-derived matrix, basement membrane extract, type I collagen, and fibrin ECM models. See Materials and Methods for expanded procedures for preparation of cell-derived matrix and collagen matrix. **b** Protein fiber structure of each 3D matrix. Cell-derived matrix (CDM) was visualized by fibronectin immunofluorescence stain, fibrin by fluorescently labeled fibrinogen, and basement membrane extract (BME) and collagen were visualized using reflection microscopy. Adapted from: (Hakkinen et al., 2011).

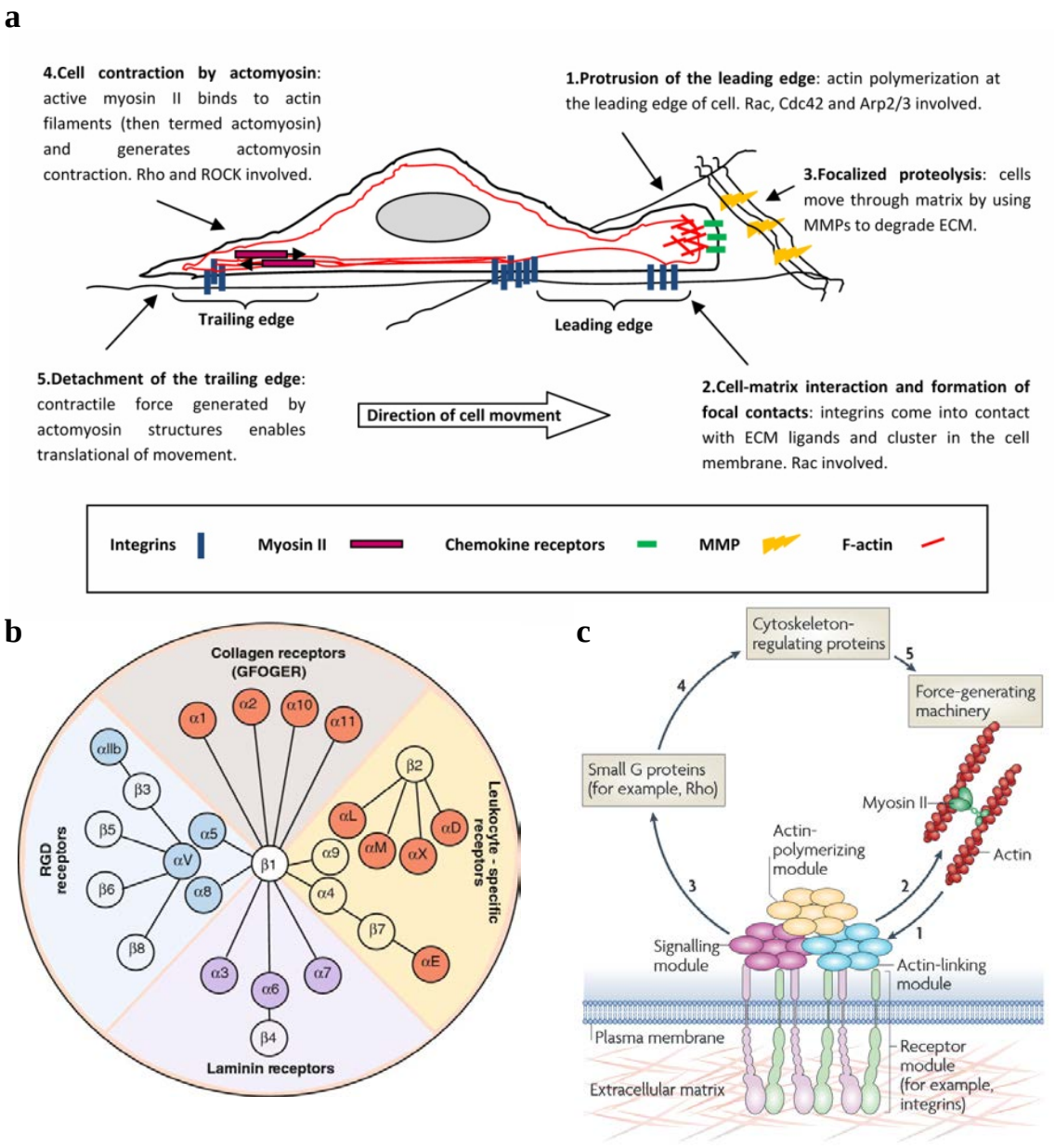


**Figure 3: Extracellular matrix-driven cell migration a** Sequential diagram of the major events during mesenchymal cell migration. **b** Diagram of the 24 human integrins and their ECM ligands. **c** Schematic of integrin-mediated focal adhesion signaling. Adapted from: (Barczyk et al., 2010; Geiger et al., 2009; Parri and Chiarugi, 2010)

# CHAPTER 1

IDENTIFICATION OF EXTRACELLULAR MATRIX-SPECIFIC GEFS

## 1.1 Introduction: GEFs and cell migration

Distinct migratory responses of cells to interactions with different ECM proteins is necessary for efficient tissue development and wound repair, and is often deregulated in cancer (Daley and Yamada, 2013; Frantz et al., 2010; Petrie et al., 2012; Provenzano et al., 2006). Integrin binding to ECM proteins triggers selective activation of the Rho GTPases, which induce cell polarization, cytoskeletal rearrangements, and contractile responses required for efficient migration in different microenvironments (Huttenlocher and Horwitz, 2011; Petrie et al., 2009; Raftopoulou and Hall, 2004). However, a fundamental unanswered question is how specific Rho GTPase signaling pathways governing migration are regulated differentially by specific ECM proteins.

Rho GTPases function as molecular switches that cycle between an inactive GDP-bound and an active GTP-bound conformation. The type of nucleotide (GDP or GTP) that is bound modulates conformational changes within the Rho GTPase switch domain region and directs effector interactions. Nucleotides are additionally stabilized by a $Mg^{2+}$ cation binding pocket, which is required for high-affinity binding to the GTPase (Goicoechea et al., 2014). The activation of Rho GTPases is mediated by guanine nucleotide exchange factors (GEFs), which catalyze the exchange of GDP for GTP. GEFs facilitate the exchange of GDP for GTP by promoting GTPase conformational

intermediates that lack both nucleotide and $Mg^{2+}$. In cells, GTP is preferentially loaded onto Rho GTPases during nucleotide exchange because GTP is present at substantially higher intracellular concentrations than GDP (Rossman et al., 2005).

To date there have been approximately 80 GEFs toward Rho GTPases identified in the human genome, which are classified into two distinct GEF families by protein structure: the Dbl family, which comprises 69 members in humans, and the DOCK family with 11 members (Meller et al., 2005; Rossman et al., 2005). The Dbl family of GEFs is named after the first mammalian GEF isolated, which was a Cdc42 GEF identified as a transforming gene from human diffuse B-lymphoma cells and subsequently designated Dbl (Schmidt and Hall, 2002). GEFs in this family are characterized by the presence of a Dbl homology (DH) catalytic domain followed by an adjacent pleckstrin homology (PH) domain. Under most conditions, the PH domain binds to phosphoinositides and localizes the GEF to plasma membranes where exchange activity commonly occurs. This conserved DH-PH motif defines the minimal structural unit required to trigger the GDP-GTP exchange reaction (Rossman et al., 2005). Outside the DH–PH domain, Dbl-family GEFs are significantly divergent and contain other protein domains that regulate the intrinsic catalytic activity of the GEF, their GTPase specificity, intracellular localization, and direct GTPase-effector targeting through additional protein-protein interactions (Goicoechea et al., 2014).

Currently, the number of GEFs in the human genome is four times higher than the number of their target Rho GTPases and continues to grow as non-canonical GEFs are continually being discovered. This complexity is compounded further by the fact that many GEFs have the ability to activate more than one GTPase, and the specificity of the

majority of GEFs has yet to be fully characterized. While tissue specificity could explain this apparent redundancy, most GEFs are ubiquitously expressed (Garcia-Mata and Burridge, 2007). A paradigm that has recently evolved is that GEFs not only serve to activate a particular GTPase, but also to facilitate and localize the connection between an upstream stimulus and downstream specific GTPase effector. This is achieved through both diversity in GEF protein domain structures and tightly regulated post-translational modifications.

There is evidence for the extracellular regulation of GEF activity by the ECM microenvironment. The Rac1 GEF P-Rex1 mediates the ErbB receptor response in breast tumorigenesis, regulating Rac1-directed cell proliferation and motility (Sosa et al., 2010). Additionally, matrix mechanical stresses translated through fibronectin adhesions activate the RhoA GEFs LARG and GEF-H1 to regulate the contractile response of the cell (Guilluy et al., 2011b). Further, certain GEFs have to been shown to associate directly, or in complex, with specific integrin subtypes suggesting their restricted, specific activation (Humphries et al., 2009; Samson et al., 2007). As emerging evidence continues to support the contextual activation of particular Rho GEFs, a model is developing in which the specific activity of Rho GTPases is controlled by the localization and activation of particular GEFs and associated with a specific cellular stimulus. Considering the reports of complex regulation of the Rho GTPases in different ECM microenvironments, it is plausible that particular GEFs are associated with specific matrix-integrin complexes governing the migratory response. We therefore hypothesized that adhesion to specific ECM molecules, such as collagen and fibronectin, would trigger differential GEF activation to regulate cell migratory responses (Figure 4a). We initially focused on

differential regulation of GEFs toward Rac1 in response to fibronectin and collagen for its well-documented roles in governing protrusion and leading edge dynamics during cell migration.

## 1.2 Fibronectin and collagen are sufficient to trigger Rac1 activation and cell migration

Previous work from our laboratory has demonstrated the role of Rac1 activity in determining the directionality, persistence, and rate of 2D cell migration. Additionally, investigations of cell motility in 3D ECM have also reported a contextual requirement for Rac1 activity for the efficient coordination of lamellipodial dynamics and mesenchymal-type migration (Pankov et al., 2005; Petrie and Yamada, 2012; Sanz-Moreno et al., 2008). Before screening for ECM-specific Rac1 GEFs, we first ensured that fibroblast adhesion to fibronectin or collagen alone was sufficient to trigger Rac1 activity and subsequent migration.

Primary human foreskin fibroblasts (HFFs) were plated onto MatTek dishes coated with human fibronectin or type I rat tail collagen in the absence of serum and incubated overnight to allow cells to reach steady-state migration. The following day, the cells were assayed for migratory behavior by timelapse microscopy for 24 hours. We observed that adhesion to either fibronectin or collagen alone was sufficient to induce cell migration in comparison to a no ECM control (Figure 5a). Characteristically, cells on fibronectin migrated in a persistent fashion, with broad, stable lamellipodia. On collagen, migration velocity was increased, yet less persistent, with a higher frequency of protrusion and less stable lamellipodia. We then assayed whether adhesion to solely fibronectin or collagen was sufficient to induce intracellular Rac1 activity. Fibroblasts were allowed to spread on fibronectin or collagen in the absence of serum over a time

course in which Rac1 activity was measured (Figure 5b). Adhesion to both fibronectin and collagen led to increases in Rac1 activity relative to a no-ECM control; however we observed different kinetics of activation over the time course, suggesting different molecular mechanisms for each ECM condition.

### 1.3 Development of an ECM-based GEF activity screen

Having established that adhesion to both collagen and fibronectin alone was sufficient to activate Rac1 and induce cell migration in HFFs, we next sought to develop a screen to identify and isolate novel Rac1 GEFs uniquely active under the two ECM conditions. It has been demonstrated previously that recombinant dominant-negative Rho GTPase mutants can be used for affinity-isolation of activated GEFs (Dubash et al., 2007; Garcia-Mata et al., 2006). Particularly, mutants that mimic the conformation of a nucleotide-free GTPase, which is an intermediate in the GDP-GTP exchange reaction, are able to form high-affinity complexes with active GEFs (Cherfils and Chardin, 1999). Taking advantage of this principle, mutant Rac1 constructs were generated containing the nucleotide-free, dominant-negative mutation RacG15A to isolate GEFs toward Rac1. Using this purified recombinant mutant, we developed an unbiased screening approach for isolating and identifying activate Rac1 GEFs from lysates of fibroblasts migrating in fibronectin- or collagen-based microenvironments.

A schematic diagram illustrating the ECM-GEF screen can be found in Figure 4b. Briefly, HFFs were serum-starved for two hours prior to plating on fibronectin or collagen-coated dishes. To avoid studying an artifact of cell spreading in response to matrix, primary fibroblasts were cultured overnight in the absence of serum to ensure that cells were undergoing steady-state migration at the time of analysis. The following day,

HFFs were lysed, and the cell lysates were incubated with GST-RacG15A conjugated to agarose beads in order to extract active GEFs. GEFs that bound to RacG15A were analyzed by SDS-PAGE, visualized by Coomassie staining, and mass spectrometry was performed on ECM-specific, excised protein bands for GEF identification. All GEFs identified using mass spectrometry were confirmed through western blot quantification.

A critical aspect during development of the ECM-GEF screen was ensuring that all relevant active GEFs were being solubilized during cell lysis. To evaluate the effects that different lysis approaches had on effectively isolating GEFs, we initially compared the profiles of GEFs associated with the recombinant RacG15A probe from HFFs under standard culture conditions using SDS-PAGE and Coomassie staining. By systematically varying lysis buffer detergents and solubilization methods, we determined the optimal strategy for extracting active GEFs by observing which method yielded the most unique protein bands on Coomassie stained gels while maintaining constant culture conditions. Surprisingly, addition of deoxycholate or NP-40 did not significantly affect the number of extracted GEFs in comparison to a 1% Triton X-100 base buffer. However comparing lysates that had been briefly sonicated to those incubated on ice yielded significantly more unique protein bands associated with the RacG15A probe. Therefore brief sonication was determined to be a crucial step for efficiently extracting the total active GEF population.

Quantitative results of select GEFs isolated from the ECM-based screen are shown in Figure 6a. Results depict the relative Western blot band intensity of mass spectrometry-identified GEFs in comparison to a no-ECM control. The majority of GEFs that were isolated showed increased activity on both fibronectin and collagen. In

particular, the promiscuous GEF SmgGDS, which has been reported to activate a wide variety of GTPases, was observed to increase its association with RacG15A strongly during cell migration on both fibronectin and collagen (Figure 6b). This result contradicts previous reports that SmgGDS does not have exchange activity toward Rac1 (Hamel et al., 2011); however, preliminary analysis of SmgGDS knockdown in HFFs suggested an inhibition of proliferation in response to fibronectin or collagen (data not shown) and warrants future investigation. Although isolating Rac1 GEFs that showed increased activity on both matrix ligands was interesting and provided insight into their function, the goal of this screen was to isolate a Rac1 GEF whose activity was specific to either fibronectin or collagen. Therefore, the primary novel finding of this screen and focus of this dissertation is that the activity of the Rac1/Cdc42 GEF βPix is specifically and robustly increased during cell migration in response to collagen versus fibronectin and null ECM controls (Figure 6c).

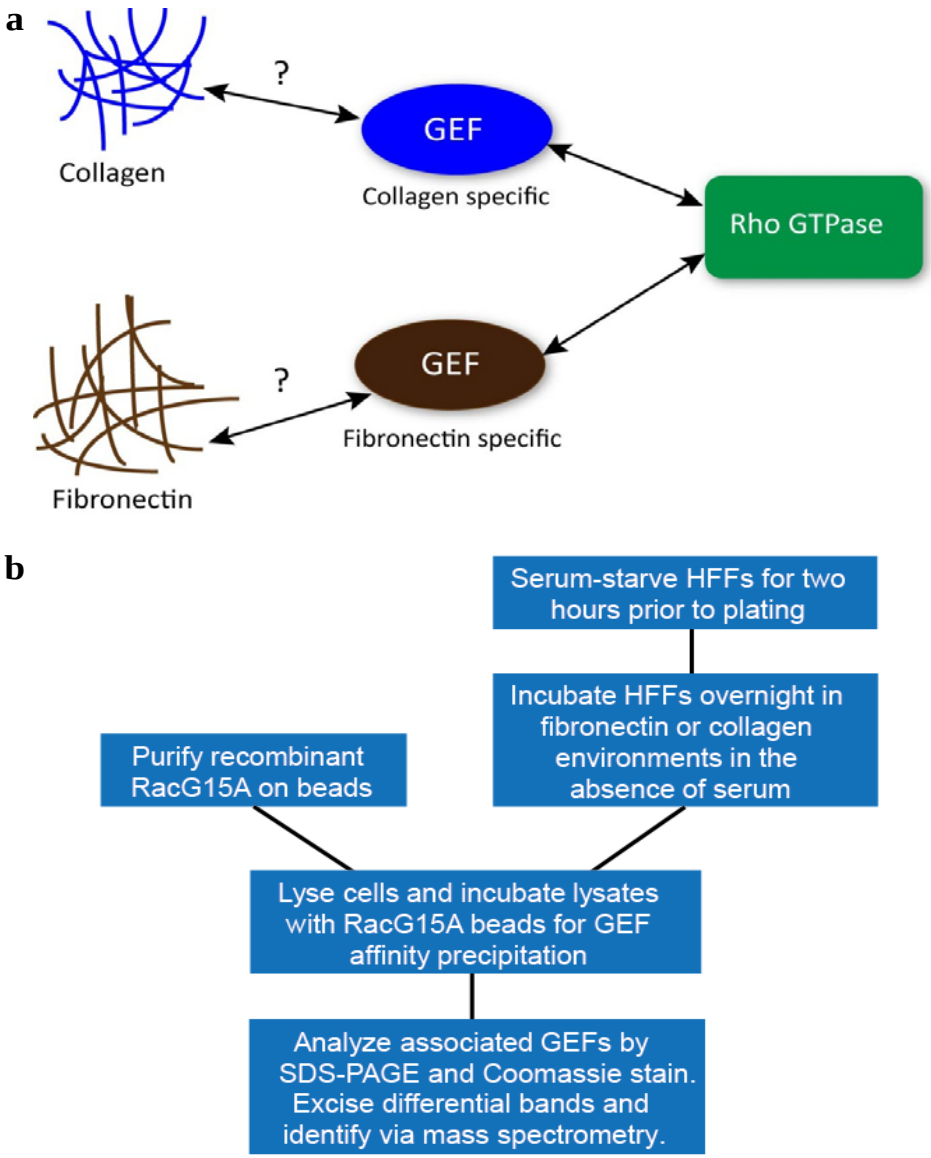


**Figure 4**: **Screen for ECM-specific regulation of Rac1 GEFs. a** Central hypothesis: adhesion to ECM ligands such as fibronectin or collagen specifically activates GEFs to modulate Rho GTPase activity and subsequent cell migration in different ECM environments. **b** Schematic diagram of the screen for ECM-specific GEFs. Briefly, HFFs were plated on ECM-coated dishes, allowed to reach steady-state migration overnight in the absence of serum, lysed, and incubated with GST-RacG15A conjugated to beads to extract active GEFs. Beads were analyzed by SDS-PAGE, Coomassie staining, and mass spectrometry of excised protein bands for identification.

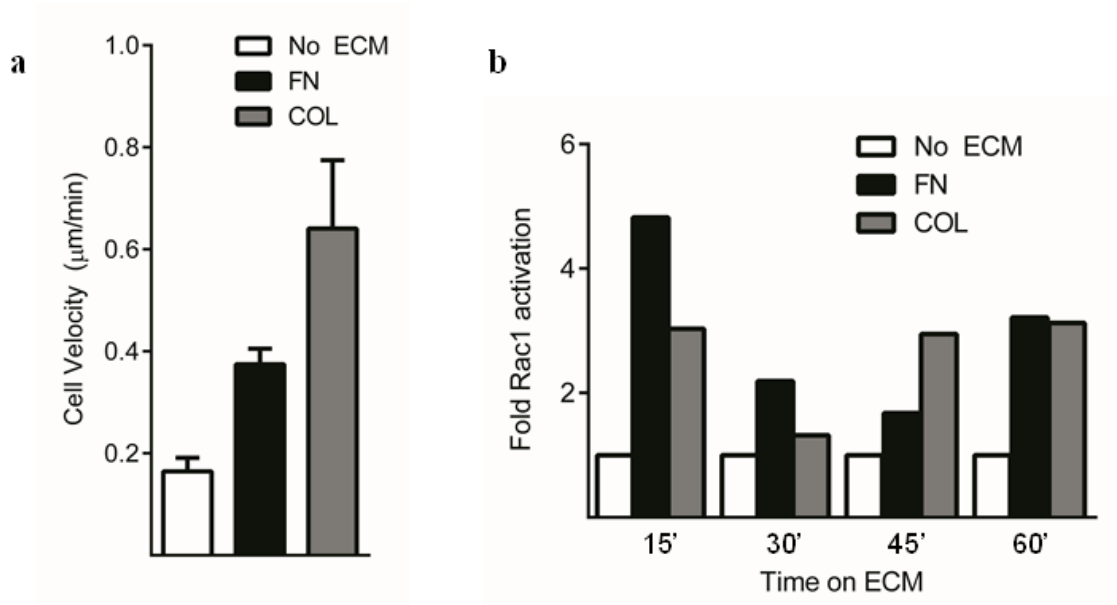


**Figure 5**: **FN and COL are sufficient to activate Rac1 and trigger cell motility. a** HFFs were allowed to reach steady-state migration overnight in the absence of serum on dishes coated with 10 μg/ml fibronectin (FN) or 50 μg/ml type I collagen (COL). The following day migration was observed by timelapse microscopy over a 24 hour period. Adhesion to both fibronectin and collagen was found to trigger motility in comparison to no-ECM control (n = 10, 13, 15 cells). **b** Time course of intracellular Rac1 activity was measured using ELISA-based activity assays (G-LISA, Cytoskeleton, Inc.), in fibroblasts spreading on fibronectin or collagen in the absence of serum. Values are reported as relative Rac1 activity increase in comparison to a no-ECM control. We observed that both fibronectin and collagen stimulated Rac1 activity in the absence of serum, but had different kinetics of activation, eventually stabilizing at similar levels of Rac1 activity (n = 2 dishes per time point).

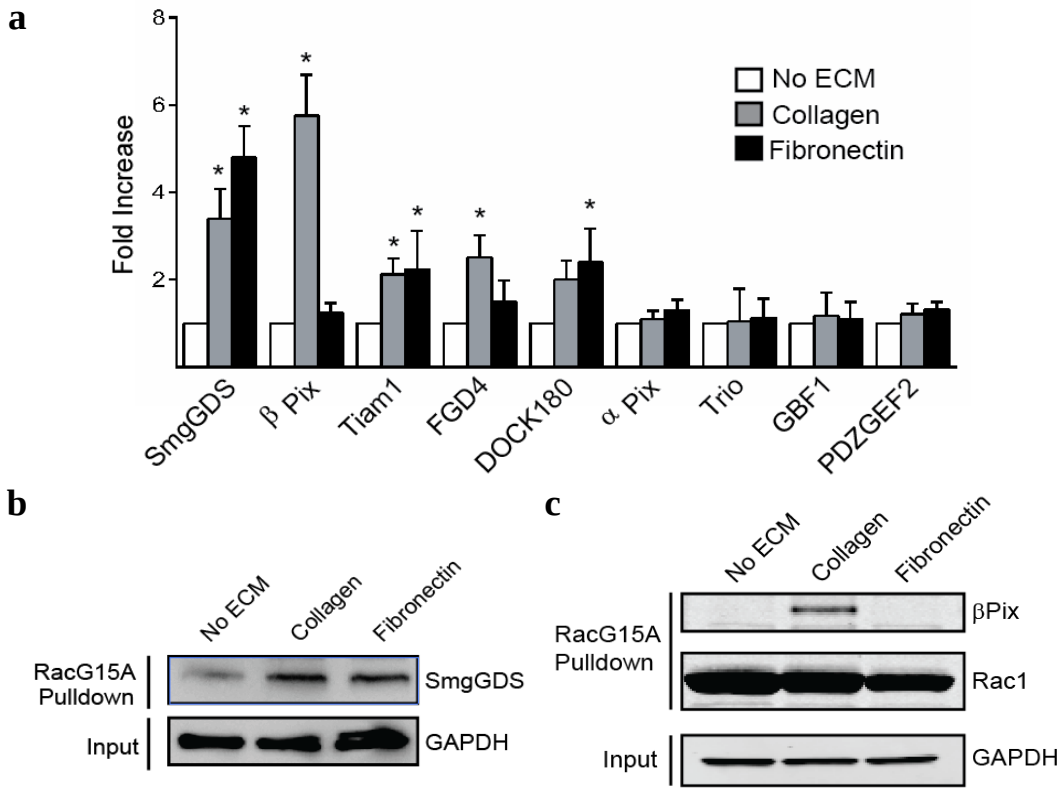


**Figure 6**: **Results of the ECM-GEF activity screen. a** Quantification of western blot band intensities of select GEFs isolated from the RacG15A ECM-GEF screen. Values are fold intensity increase above a no-ECM condition (n = 3 blots, error bars represent s.e.m, one-way ANOVA with Bonferroni multiple comparisons correction). **b** Western blot confirms up-regulation of the GEF SmgGDS binding to RacG15A when migrating in the presence of a collagen or fibronectin ECM ligand. **c** Western blot validation of βPix binding to RacG15A during migration on collagen. We observed a specific association between βPix and RacG15A only during collagen-based migration. * $P < 0.05$.

# CHAPTER 2

## βPIX: A COLLAGEN-SPECIFIC GEF CRITICAL FOR CELL MIGRATION

### 1.1 Introduction: the versatile roles of βPix

βPix was originally discovered in 1997 when it was isolated from a mouse thymus cDNA expression library screened with a monoclonal antibody recognizing a common SH3 epitope and was designated Cool-1 (Cloned out of library-1). It was observed to be widely expressed in mouse tissues and localize to the nucleus, cytoplasm, and focal complexes on the cellular level (Oh et al., 1997). Two additional Cool family members were also identified based on homology to Cool-1, and the Cool family of proteins soon encompassed $p50^{Cool-1}$, $p85^{Cool-1}$, and Cool-2 (Koh et al., 2001). The function of these proteins remained largely unknown, although GEF activity was suspected due to the presence of a tandem DH-PH motif in each of the Cool proteins. One year later, both a yeast two-hybrid screen searching for Pak3 binding proteins (Bagrodia et al., 1998) and immunoprecipitation of Pak1 (Manser et al., 1998) indicated direct binding to $p50^{Cool-1}$ and $p85^{Cool-1}$. Surprisingly, $p50^{Cool-1}$ was found to be incapable of stimulating Pak1 activity, as would have been expected if it were acting as a GEF for Cdc42 or Rac1, and it also inhibited Pak1 activation by Dbl or by activated forms of Cdc42. The $p85^{Cool-1}$ protein did not inhibit Dbl- or activated Cdc42-stimulated Pak1 activity, but itself was incapable of directly stimulating Pak1 activity (Feng et al., 2002). After this, the Cool family of proteins was re-designated Pix (Pak-interactive exchange factor) proteins, with

$p85^{Cool-1}$ as βPix, $p50^{Cool-1}$ as a smaller, inhibitory splice isoform of βPix, and the separate gene product Cool-2 as αPix.

The gene containing βPix, *ARHGEF7*, yields five alternatively spliced mRNA transcripts, yet only four distinct isoforms of βPix have been characterized. While less abundant isoforms are exclusively expressed in the brain and central nervous system, the primary 85 kDa isoform, designated βPix, is expressed ubiquitously in humans (Koh et al., 2001). The domain structure of βPix is outlined in Figure 7a. βPix is a member of the Dbl family of GEFs, containing a classical DH-PH motif flanked by a T1 domain that is also critical for GEF activity (Feng et al., 2006). Outside of this conserved region, there are numerous protein-protein interacting domains: a SH3 domain, a proline-rich domain (PRD), a Cat (Cool-associated tyrosine phosphosubstrate)/GIT (G protein-coupled receptor kinase interactor)-binding (CBD) domain, and a leucine zipper (LZ). This diverse array of domains provides the capacity for the many specialized cellular functions that have been ascribed to βPix.

For each specific intracellular function, βPix exhibits exchange activity exclusively on Cdc42 or Rac1 GTPases (Feng et al., 2002; Manser et al., 1998). This specificity is determined by whether βPix is a dimer or monomer, protein-protein interactions, and post-translational modifications (Baird et al., 2005). Outside of traditional roles in cell migration, βPix acts through Rac1 to regulate cell apoptosis by controlling adhesion-dependent epithelial survival through EBP50, as well as cytokinesis by initiating centralspindlin complex formation through a cooperative balance with the Rac1 GAP CYK4 (Bastos et al., 2012; Chen et al., 2012). Additionally, βPix also acts through Cdc42 in specialized cellular functions. The importance of βPix/Cdc42 signaling

has been reported to include regulation of proper insulin secretion in beta cells, directing EGF receptor degradation in cooperation with the E3 ligase Cbl, and modulation of β-catenin transcriptional activity in colon cancer cells (Chahdi and Raufman, 2013; Feng et al., 2006; Kepner et al., 2011).

However, what makes βPix a particularly attractive candidate GEF for an ECM-specific role in governing cell migration are previous reports of its involvement in cell polarity, protrusion, and focal adhesion turnover. In the canonical βPix pathway, the SH3 domain of βPix binds to a unique proline-rich sequence on Pak1, which is essential for Rac1 activation, and this complex localizes to focal adhesions (Manser et al., 1998). This focal adhesion localization is achieved by the interaction of βPix with proteins such as GIT1/2 (G-protein-coupled receptor kinase interactor) and PKL (paxillin kinase linker), which bind βPix at the CBD domain and also functionally link to the focal adhesion protein paxillin (Turner et al., 1999). During migration on flat two-dimensional fibronectin substrates, localization of βPix-Pak1 to focal adhesions was demonstrated to trigger focal adhesion disassembly, which was indirectly attributed to the activity of Rac1 (Nayal et al., 2006; Zhao et al., 2000). More recently, the localization of βPix to focal adhesions has been described to be negatively regulated by cellular contractility, with inhibition of myosin II leading to βPix enrichment in adhesion complexes (Kuo et al., 2011). Further investigation into the regulation of the βPix-Pak1 pathway has shown that Cdc42 acts upstream to direct βPix-Pak1 assembly. In this context, Cdc42-Pak1-βPix acts to control the polarization of cell protrusions during migration in a scratch wound assay, where Pak1 acts through βPix to spatially restrict Rac1-dependent actin polymerization to the leading edge (Cau and Hall, 2005). In addition, recent studies have begun to uncover

non-traditional roles for βPix in cell migration. βPix association with the membrane scaffolding protein Scrib leads to localized Cdc42 activity during astrocyte migration (Osmani et al., 2006), and phosphorylation of βPix by ERK/Pak2 in response to bFGF localizes βPix to lamellipodia in neuronal growth cones, controlling neurite outgrowth (Shin et al., 2002).

With the multitude of different roles reported for βPix in regulating cell physiology, it is conceivable that many are highly contextual and thus require tight regulation of βPix function. One hypothesis is that the regulation of βPix function is due to multiple phosphorylation sites on the protein (Mayhew et al., 2007). Additionally, efforts have been made to define a βPix-Pak1 "interactome" and characterize unique scaffolding and adaptor proteins that may be directing this signaling complex (Mayhew et al., 2006). However, these efforts fall short in effectively recapitulating all the stimuli, particularly extracellular, that direct βPix interactions. Therefore, it is feasible that βPix is serving a specialized role during migration in collagen environments. In this chapter, we build upon the previous observation of the collagen-specific association between βPix and RacG15A and investigate whether βPix is important for regulating cell morphology and migration in collagen.

## 2.2 Differential localization of βPix on fibronectin and collagen

βPix exists at multiple subcellular sites, including focal adhesions and plasma membrane, which is consistent with differential functions (Cau and Hall, 2005; Kuo et al., 2011; Liu et al., 2010). As an initial test for whether βPix has ECM-specific functions, we examined for altered localization of βPix during fibroblast migration on fibronectin versus fibrillar collagen. βPix has been previously shown to localize to focal

adhesions in cells migrating on fibronectin. As expected, both immunofluorescence staining for endogenous βPix and live-cell imaging of GFP-βPix showed strong localization to focal adhesions during migration on fibronectin (Figure 7b) and 3D cell-derived matrix (Figure 7c), where the primary ECM ligand is fibronectin (Kutys et al., 2013). Surprisingly, we observed a dramatic decrease in both endogenous and GFP-βPix focal adhesion localization in fibroblasts migrating on both fibrillar collagen and 3D collagen (Figure 7b, c). Instead, on fibrillar collagen βPix transitioned to non-paxillin containing structures that were localized to lamellipodia and appeared to be plasma membrane-associated. Live-cell GFP-βPix imaging provided further insight into this unique localization: βPix displayed patchwork localization on ventral cell membranes in amorphous, persistent aggregates of variable size that, while polarized to leading-edge protrusions, did not co-localize with paxillin. To further confirm this unique localization, fibroblasts migrating on fibronectin or fibrillar collagen were subjected to Triton X-100 fractionation. Subcellular fractionation revealed that on fibrillar collagen, endogenous βPix transitioned from detergent-soluble to -insoluble fractions (Figure 7d). These data demonstrate that the intracellular location of βPix changes dramatically when cells migrate on collagen compared to fibronectin, supporting the existence of ECM-specific functions observed in the initial GEF screen.

### 2.3 Collagen-specific cell morphological defects of βPix knockdown

The differential βPix focal adhesion/plasma membrane localization observed during migration on fibronectin versus fibrillar collagen strongly suggested distinct molecular functions between the two ECM conditions. To parse out these functions, we generated stable βPix knockdown lines in primary human fibroblasts using lentiviral-

based shRNA delivery. The pLentiLox 3.7 lentiviral packaging system has proven efficient in delivering shRNA hairpins and cDNA at the single-cell and organ level (Cai et al., 2007), with the viral vector (pLL 3.7) consisting of two distinct promoters governing a multiple cloning-GFP site and a shRNA hairpin site. Using this system, two distinct hairpins, one previously reported (shRNA #4, Table 2 in Materials and Methods) (Kuo et al., 2011), and one unique to this study (shRNA #2, Table 2 in Materials and Methods), were transduced into fibroblasts. FACS sorting was performed on infected populations of HFFs by using the GFP reporter to isolate high expressers and ensure adequate βPix knockdown. Both shRNA hairpins and a single, independent siRNA efficiently depleted βPix protein in HFFs (Figure 8b).

Using stable βPix knockdown fibroblasts, we next tested whether βPix had any collagen-specific functions regulating cell morphology. Nonspecific (NS) shRNA control and βPix knockdown fibroblasts were plated onto CDM or 3D collagen gels and incubated overnight in complete media. The following morning, cells were fixed and visualized by phalloidin staining, while the surrounding ECM was imaged using either fibronectin immunostaining or reflection microscopy. We observed that loss of βPix resulted in cells with a severe, rounded morphology and inability to spread in 3D collagen matrices, with a ~75% decrease in cell elongation (Figure 8c). In contrast, there were no effects on cell elongation in CDM (Figure 8a, c). Surprisingly, phalloidin staining revealed that these rounded cells were also hyper-protrusive, with a nearly three-fold increase in the number of protrusions per cell in comparison to NS fibroblasts (Figure 8d). We next investigated whether this collagen-specific morphological phenotype translated into a migratory defect.

## 2.4 Collagen-specific cell migratory defects after knockdown of βPix

To assay for collagen-specific migratory defects in the absence of βPix, stable NS and βPix shRNA fibroblasts were incubated overnight in CDM or 3D collagen matrices in complete media and migratory phase timelapse movies were obtained over 24 hours the following morning. Migration assays uncovered severe defects in motility after βPix knockdown that were specific to 3D collagen, as evident in the representative phase timelapse image (Figure 9a) and velocity quantification across ECMs (Figure 9c). This phenotype was characterized by rapid, transient formation of spatially deregulated cell protrusions that exhibited apparent deformation of adjacent collagen fibers and resulted in minimal cell motility compared to nonspecific shRNA control cells in 3D collagen. Representative migratory tracks of βPix knockdown fibroblasts in 3D collagen show that any residual motility of these cells lacks any persistence and appear to be due to stochastic oscillations of the cells within the collagen matrix (Figure 9b).

We assayed the effects of βPix knockdown across a variety of 2D and 3D ECM environments (Figure 9c). Interestingly, even high concentrations of globular collagen could not fully recapitulate the characteristic βPix knockdown phenotype in 3D collagen, whereas thin, fibrillar collagen substrates mimicked this 3D phenotype (Figure 9c). These functional differences observed between monomeric and fibrillar collagen are likely due to the preferential recognition and affinity of $\alpha_2\beta_1$ for fibrillar type I collagen (Emsley et al., 2000; Jokinen et al., 2004). Additionally, these fibrillar collagen substrates have the advantage of being thin for improved optical imaging, yet they retain the fibrillar structure of 3D collagen gels; they underscore the importance of using more-physiological polymerized collagen fibers rather than globular monomeric collagen.

To directly confirm that it was loss of βPix that drives this collagen-specific migratory phenotype, we generated a stable βPix knockdown/rescue fibroblast line. shRNA-resistant βPix cDNA was inserted into the multiple cloning site of pLL 3.7 already containing βPix shRNA hairpin #2, resulting in a cell line with knockdown of endogenous βPix and expression of a shRNA-resistant GFP-βPix at near-endogenous levels (Figure 9d). We observed that rescue of endogenous βPix knockdown with this shRNA-resistant GFP-βPix was sufficient to rescue cells from both the morphological and migratory knockdown defects in 3D collagen (Figure 9e). Thus, βPix has a critical, matrix-specific role in cell migration in fibrillar collagen environments, with knockdown leading to hyper-protrusive cells incapable of efficient migration.

### 2.5 Loss of βPix leads to robust collagen matrix remodeling and increased cell-cell adhesion specifically in collagen environments

We sought to characterize further the βPix knockdown phenotype in fibrillar collagen environments by searching for possible defects in the major cytoskeletal systems. Immunostaining for endogenous paxillin, actin, and tubulin in NS and βPix shRNA fibroblasts on fibrillar collagen revealed that the many protrusions in βPix knockdown cells contain paxillin-labeled focal adhesions, enriched actin fibers, and proper targeting of microtubules to protrusions (Figure 10a). Because there were no obvious alterations in focal adhesions, the actin cytoskeleton, or microtubules, we examined for remodeling or changes to the surrounding collagen fibers. Reflection microscopy revealed robust collagen fiber contraction and remodeling around βPix knockdown cells. Large holes were observed that were physically torn in the collagen matrix immediately adjacent to knockdown cells (Figure 10b, asterisks) along with thick, bundled arrays of remodeled collagen fibers, both indicative of high cellular contractility.

A classical characteristic of fibroblast migration is that unlike epithelial cells, they are subject to a unique form of contact inhibition of migration; such that if two migrating fibroblasts come into contact, migration is paused slightly and then redirected away from the point of collision (Thomas and Yamada, 1992). Migration of NS shRNA fibroblasts on fibrillar collagen follows this principle with fibroblasts migrating as single cells and remaining as single migratory cells, despite a pause and change of direction, after any inadvertent collisions. However if two βPix knockdown cells come into contact while migrating on fibrillar collagen, the cells strongly adhere to each other and remain as a pair. Frequently these pairs form multicellular masses, where contractile deformations between adhered cells can be observed (Figure 10c). Additionally, if a βPix knockdown cell contacts a wild type fibroblast, the knockdown cell would maintain cell-cell contact, while the wild type fibroblast would attempt to migrate away. While fibroblasts do express the cell-cell adhesion protein N-cadherin, this type of cell-cell adhesion is not usually formed between fibroblasts in culture, but traditionally between fibroblasts and epithelial cells or differentiated myofibroblasts (Mary et al., 2002). It is unclear whether βPix knockdown induces the expression of another cell-cell adhesion protein or whether the mechanism is entirely distinct, but this phenomenon warrants future investigation.

## 2.6 Conservation of collagen-specific βPix function in multiple cell types with implications during cancer cell motility

In addition to primary human foreskin fibroblasts, βPix was also essential for the migration of two immortalized fibroblasts lines (BR5 and BJ5ta) in fibrillar collagen environments. The severity of this collagen-specific βPix migratory phenotype observed in fibroblasts led us to investigate the conservation of this pathway in additional, diverse cell types. A single, independent siRNA was found to effectively deplete βPix protein in

primary human osteoblasts (NhOst), aortic smooth muscle cells (AoSMC), human umbilical vein endothelial cells (HUVEC), and invasive epithelial-derived adenocarcinoma cells (MDA-MB-231) (Figure 11b). We compared the effect of the loss of βPix on morphology and migratory behaviors of each cell type in 3D collagen versus 3D CDM (2D fibronectin versus fibrillar collagen for HUVECs). Loss of βPix led to severe morphological and migratory defects specific to collagen environments in all cell types tested. Similar to fibroblasts, βPix knockdown led to rounded, hyper-protrusive cells that robustly remodeled adjacent collagen fibers (Figure 11a), indicating that the collagen-specific function of βPix was indeed conserved across diverse cell types.

One exciting result from this analysis across different cell types was that knockdown of βPix resulted in a morphological and migratory defect in the MDA-MB-231 adenocarcinoma cell line. This cancer cell line is commonly utilized for in vivo xenograft and tail-vein tumor metastasis assays, highlighting the highly invasive and migratory potential of this line (Yang et al., 2012). Quantification of cell morphology showed that loss of βPix converted the entire cell population to rounded cells in 3D collagen with no observable effect in CDM (Figure 11c). Again, this morphological defect translated to a nearly complete inhibition of migration, with an approximate 70% decrease in cell velocity specifically in 3D collagen matrices (Figure 11d). With the clear demonstration of the importance of fibrillar collagen during tumor progression and metastasis and its abundance in certain epithelial tissues (Provenzano et al., 2006; Provenzano et al., 2008a), this result identifies a potential therapeutic role for βPix inhibition.

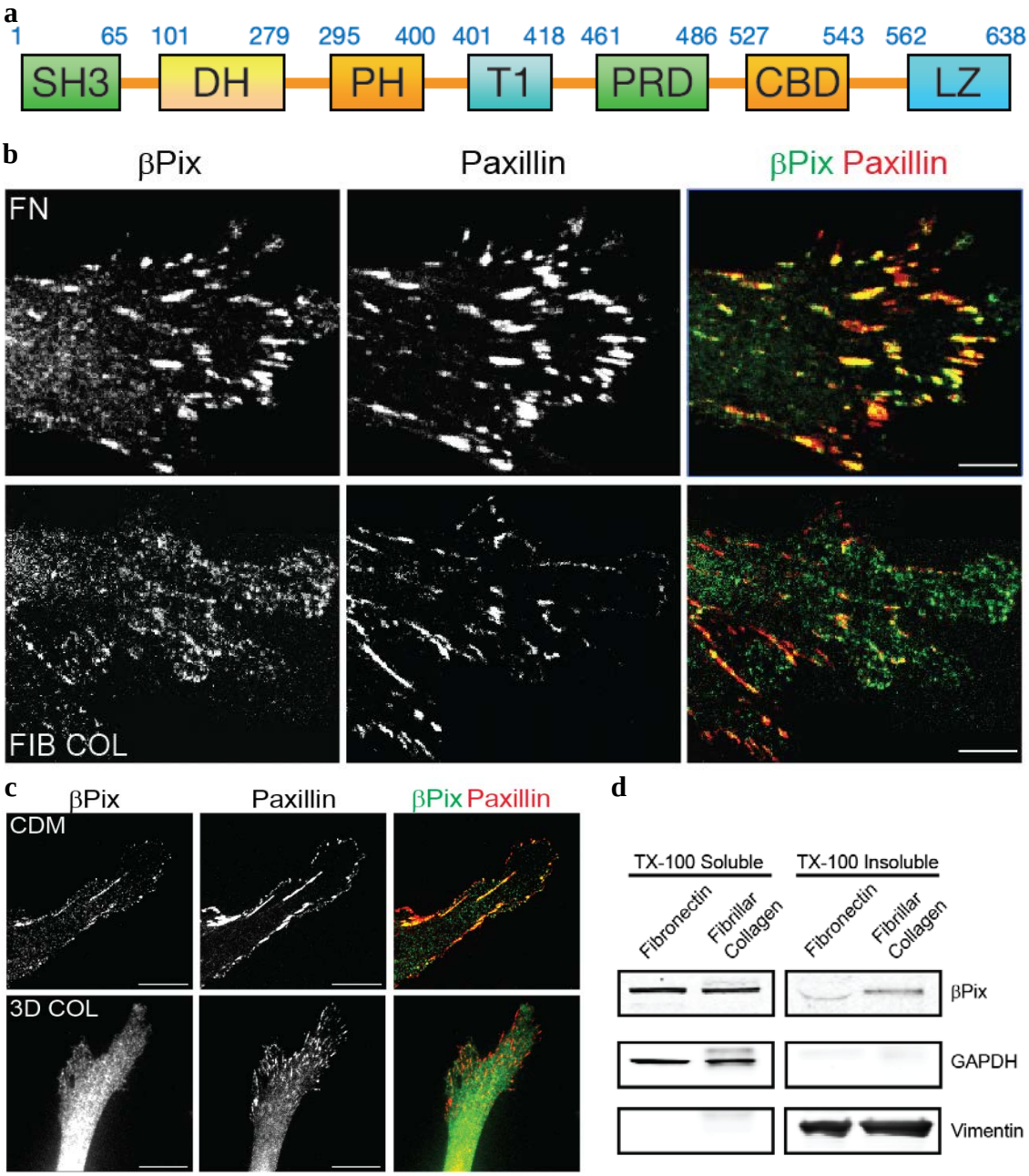
a
1
65
101
279
295
400
401
418
461
486
527
543
562
638
SH3
DH
PH
T1
PRD
CBD
LZ
b
βPix
Paxillin
βPix Paxillin
FN
FIB COL
c
βPix
Paxillin
βPix Paxillin
CDM
3D COL
d
TX-100 Soluble
TX-100 Insoluble
Fibronectin
Fibrillar Collagen
Fibronectin
Fibrillar Collagen
βPix
GAPDH
Vimentin

**Figure 7**: **ECM-dependent localization of βPix** **a** Schematic representation of βPix containing SH3, Dbl (DH) and Pleckstrin (PH) homology domains, a T1 region that regulates GEF activity, a proline-rich domain (PRD), a Cat (Cool-associated tyrosine phosphosubstrate)/GIT(G protein-coupled receptor kinase interactor)-binding (CBD) domain and a leucine zipper (LZ). **b** Composite images of the leading edge of HFFs showed loss of βPix localization to focal adhesions during migration on fibrillar collagen (FIB COL) but not fibronectin (FN). HFFs were immunostained for endogenous paxillin (red) and βPix (green); yellow indicates co-localization. Scale bars, 15 μm. **c** HFFs in 3D collagen and 3D CDM immunostained for endogenous paxillin (red) and βPix (green) display the same loss of adhesion localization as observed on fibronectin and fibrillar collagen (Fig. 7b); yellow indicates co-localization. Scale bars, 25 μm. **d** Triton X-100 fractionation of HFFs migrating on fibronectin or fibrillar collagen reveals a shift of βPix from soluble (GAPDH) to the insoluble (vimentin) fraction during migration on collagen, which was observed in three independent experiments.

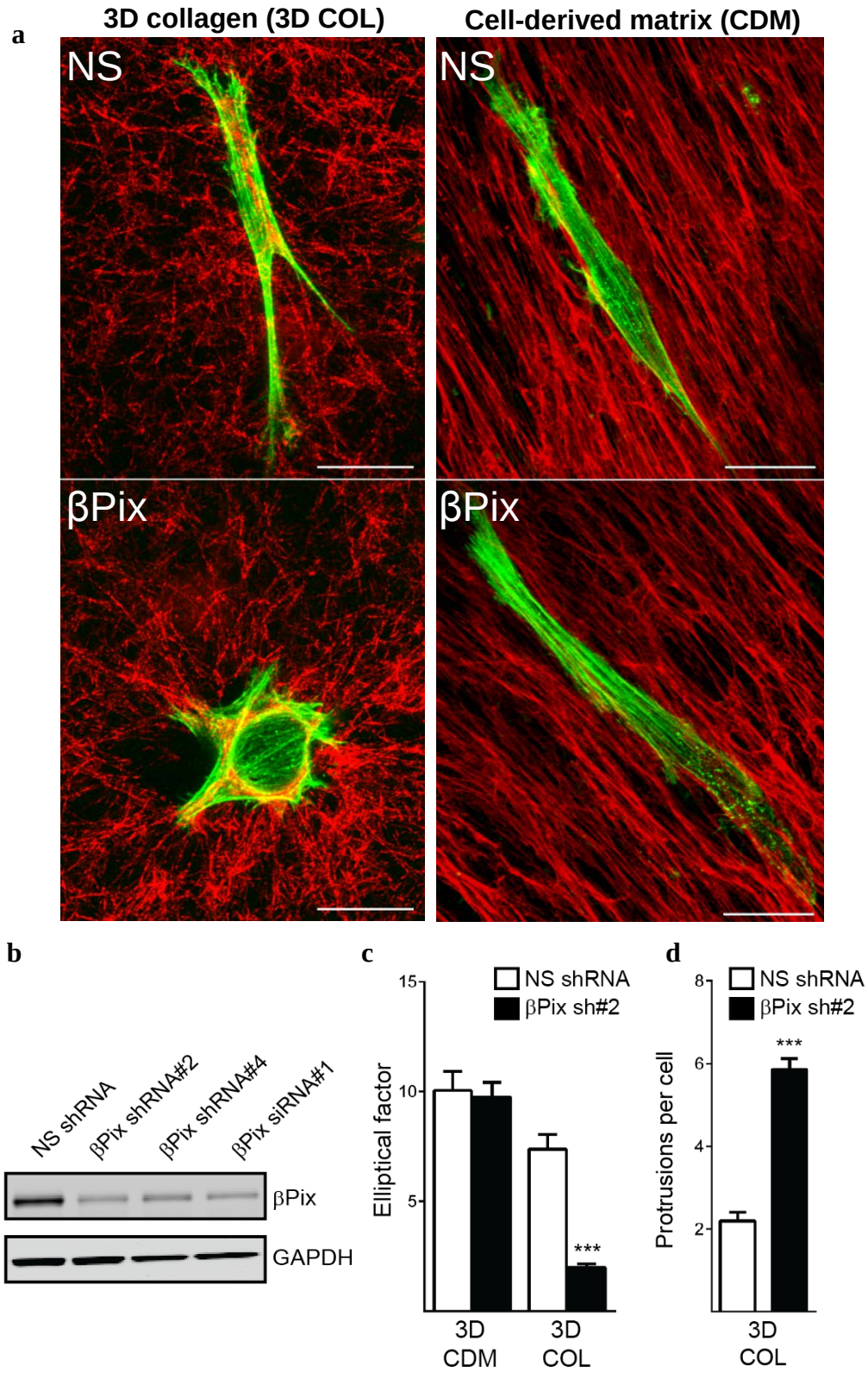
a
3D collagen (3D COL)
Cell-derived matrix (CDM)
NS
NS
βPix
βPix
b
NS shRNA
βPix shRNA#2
βPix shRNA#4
βPix siRNA#1
βPix
GAPDH
c
NS shRNA
βPix sh#2
Elliptical factor
15
10
5
***
3D CDM
3D COL
d
NS shRNA
βPix sh#2
Protrusions per cell
8
6
4
2
***
3D COL

**Figure 8**: **Collagen-specific morphological defects of βPix knockdown a** Morphological analysis of βPix knockdown in 3D fibrillar collagen (red, reflection microscopy) versus 3D cell-derived matrix (red, fibronectin) revealed defects in cell elongation after loss of βPix specific to 3D collagen. Scale bars, 25 μm. **b** Knockdown of βPix was achieved by generating HFF lines stably expressing either NS shRNA or two βPix shRNA hairpins (shRNA#2 or shRNA#4). Migration experiments were performed using each hairpin and a single siRNA toward βPix, resulting in identical phenotypes. **c** Quantification of cell elliptical factor (maximal length/width) in 3D collagen versus 3D cell-derived matrix after loss of βPix (error bars represent s.e.m., n = 44, 46 and 30, 35 cells, *t*-tests). **d** Quantification of cell protrusions (e, white arrowheads) after fixation and phalloidin staining of βPix knockdown cells in 3D collagen (error bars represent s.e.m., n = 36, 36 cells, *t*-tests). *** $P < 0.001$.

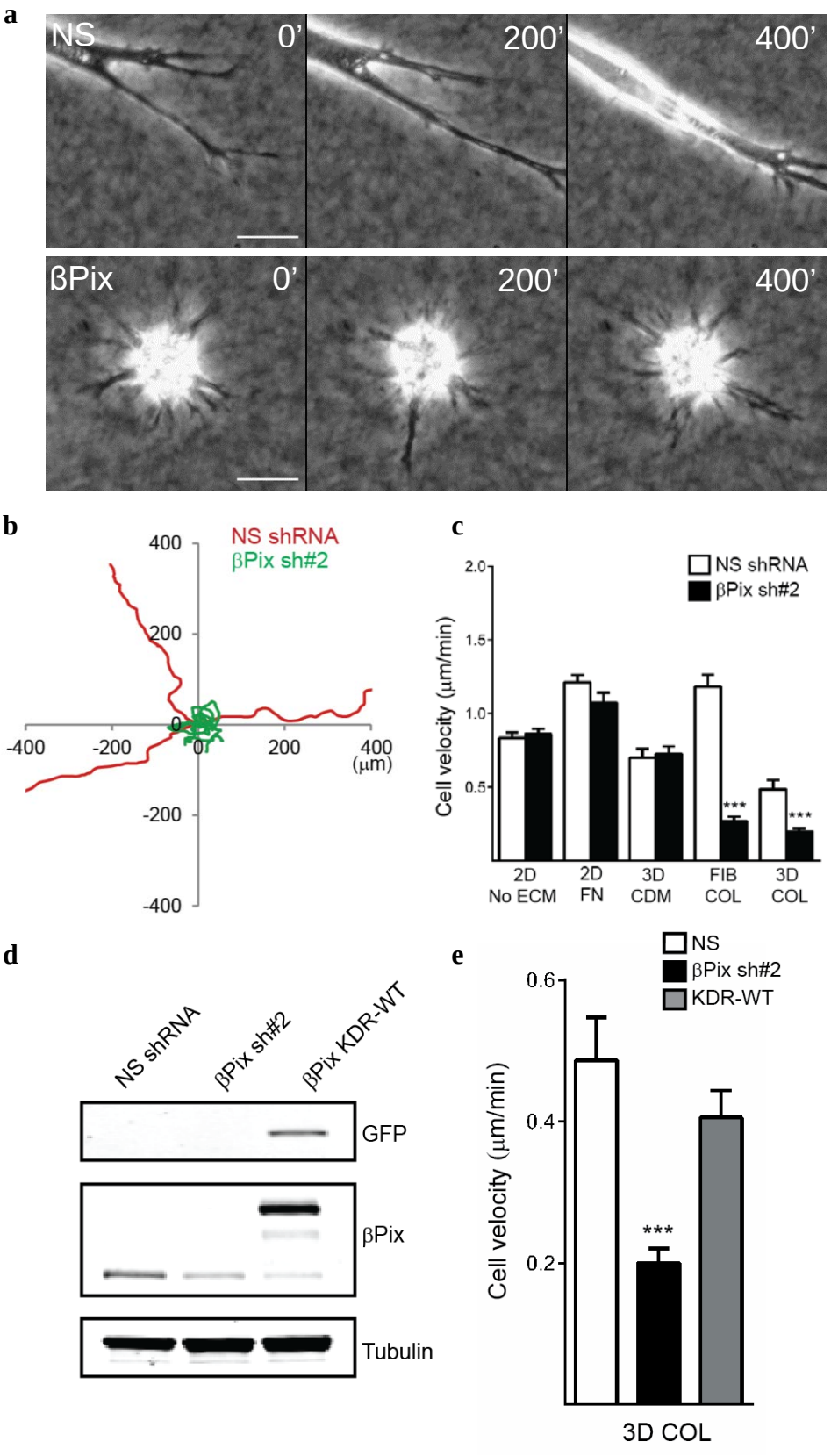
a
NS
0'
200'
400'
βPix
0'
200'
400'
b
NS shRNA
βPix sh#2
400
200
-200
-400
-400
-200
0
200
400
(μm)
c
NS shRNA
βPix sh#2
Cell velocity (μm/min)
2.0
1.5
1.0
0.5
***
***
2D No ECM
2D FN
3D CDM
FIB COL
3D COL
d
NS shRNA
βPix sh#2
βPix KDR-WT
GFP
βPix
Tubulin
e
NS
βPix sh#2
KDR-WT
Cell velocity (μm/min)
0.6
0.4
0.2
***
3D COL

**Figure 9**: **Collagen-specific migratory defects of βPix knockdown a** βPix morphological defects accompanied by migratory defects specific to fibrillar collagen matrix. Representative phase timelapse of nonspecific (NS) and βPix shRNA fibroblasts migrating in 3D collagen. White arrowheads indicate cellular protrusions; scale bars, 25 μm. **b** Migratory tracks of three NS (red) and βPix (green) shRNA fibroblasts in 3D collagen reveal loss of persistent, directional motility after βPix knockdown. **c** Quantification of cell velocities after βPix knockdown in different ECM conditions (error bars represent s.e.m., n = 20,20; 20,21; 22,22; 21,25; 25,24 cells, *t*-test). **d** Western blot of fibroblasts expressing NS shRNA, βPix shRNA#2, or βPix knockdown with a GFP-βPix rescue (βPix KDR-WT). GFP marker indicates the successful expression of the rescue construct at near endogenous levels. **e** Quantification of cell velocity of fibroblasts expressing NS shRNA, βPix shRNA, or βPix knockdown/rescue constructs in 3D collagen (error bars represent s.e.m., n = 25, 24, 25 cells, one-way ANOVA with Bonferroni correction). *** $P < 0.001$.

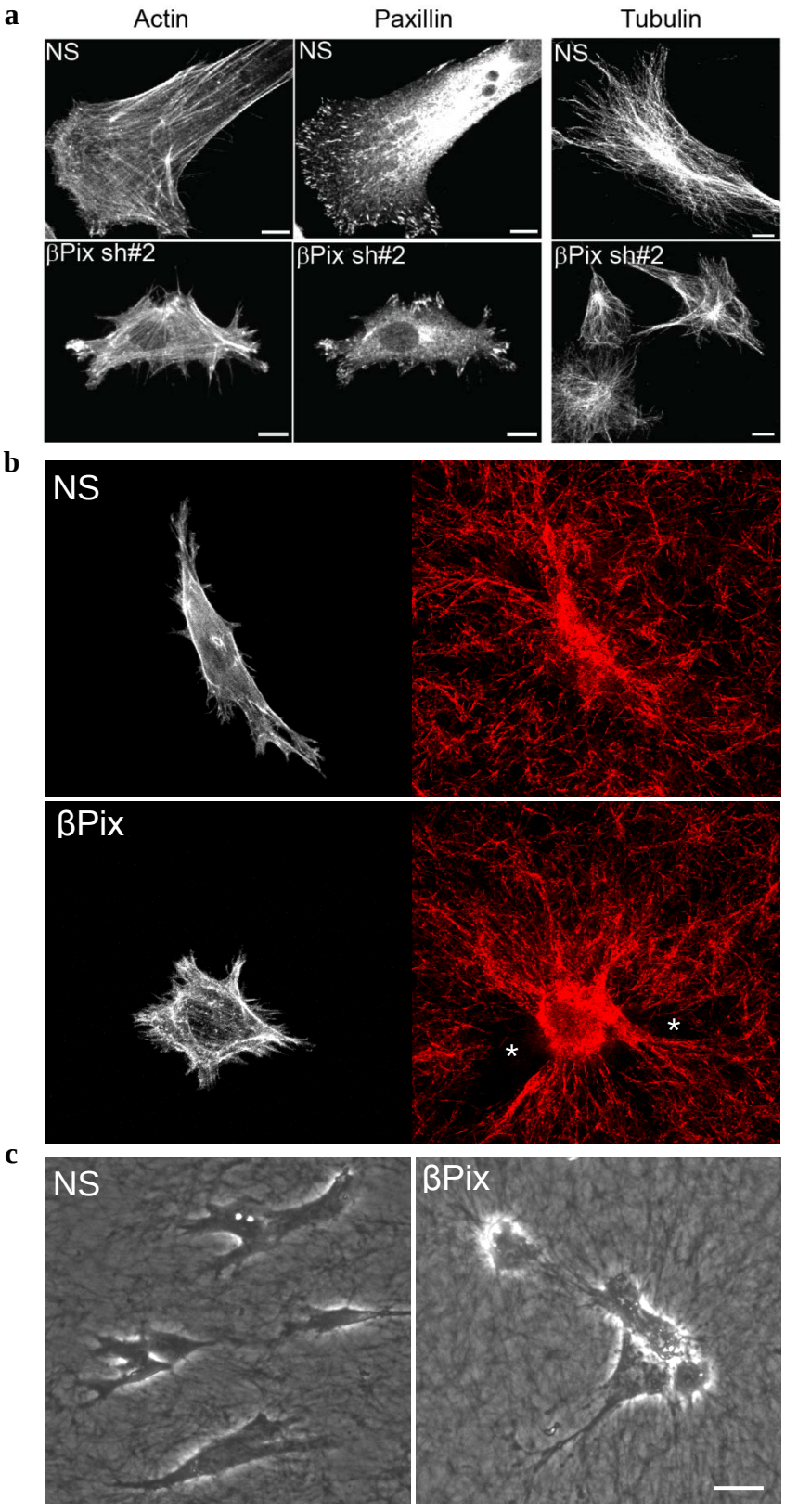
a
Actin
Paxillin
Tubulin
NS
NS
NS
βPix sh#2
βPix sh#2
βPix sh#2
b
NS
βPix
*
*
c
NS
βPix

**Figure 10**: **Loss of βPix leads to robust collagen remodeling a** Immunostaining of endogenous paxillin, actin, and β-tubulin in HFFs on fibrillar collagen expressing NS or βPix shRNA. The multiple protrusions in βPix knockdown cells had paxillin-containing adhesions, enriched actin fibers, and efficient microtubule targeting. Scale bars, 20 μm. **b** Analysis of collagen fibers (red, reflection microscopy) adjacent to NS and βPix shRNA cells revealed robust collagen contraction and remodeling with βPix knockdown (physical holes, asterisks). Scale bars, 25 μm **c** Migratory analysis of βPix knockdown fibroblasts in both 3D collagen (not pictured) and fibrillar collagen (pictured) environments revealed an increase in cell-cell adhesion in comparison to NS control. Scale bar, 50 μm.

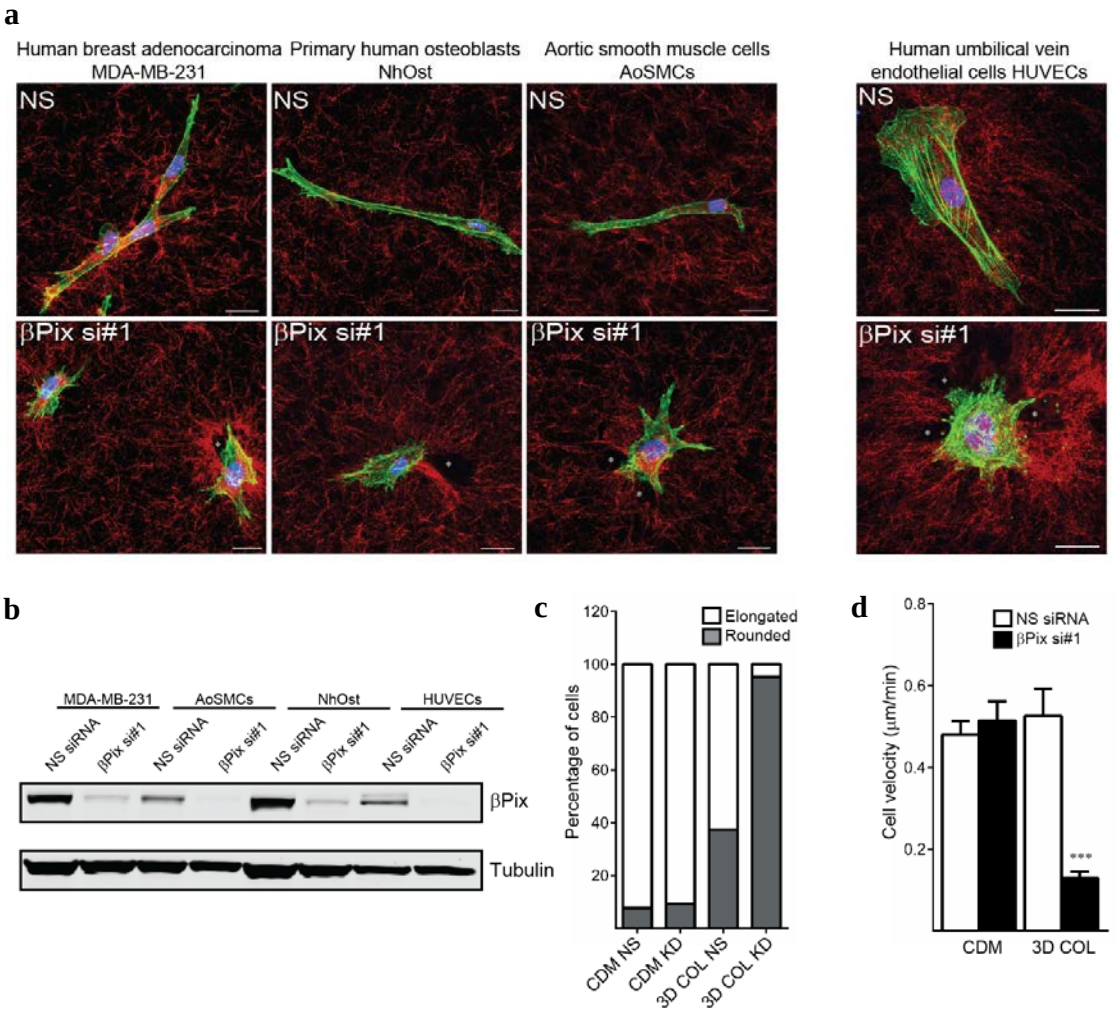


**Figure 11**: **Conservation of the βPix pathway in controlling migration in fibrillar collagen environments a** Single siRNA knockdown of βPix in human breast adenocarcinoma cells, primary human osteoblasts, human aortic smooth muscle cells, and human umbilical vein endothelial cells revealed collagen-specific morphological and migratory defects between 3D collagen and 3D cell-derived matrix (data not shown for CDM) and for HUVECs in 2D fibronectin and fibrillar collagen (green, actin; red, collagen; blue, DAPI). Scale bars, 25 μm. **b** Western blot confirmation of βPix knockdown using a single βPix siRNA. **c** Quantification of morphology of MDA-MB-

231 cells with βPix knockdown in 3D collagen versus 3D cell-derived matrix. Elongated cells defined as having an elliptical factor > 1.5 (n = 30, 30, 26, 27 cells). **d** Quantification of MDA-MB-231 cell velocity with βPix knockdown in 3D cell-derived matrix or 3D collagen. (error bars represent s.e.m., n = 19, 19, 19, 21 cells, *t*-tests).

# CHAPTER 3

## βPIX REGULATES CDC42/RHOA CROSSTALK THROUGH A NOVEL COLLAGEN-SPECIFIC INTERACTION WITH SRGAP1

### 3.1 Introduction: Cdc42, Rac1, and RhoA: 3D migration and crosstalk

The recent shift to studying cell motility in 3D ECM environments has identified substantial mechanistic differences between 2D and 3D migration. Frequently these differences are attributed to the activity and function of the Rho GTPases Cdc42, Rac1, and RhoA, as well as their regulators. In 3D environments, cells adopt modes of migration not typically observed in 2D. While the elongated, mesenchymal morphology driven by Rac1-mediated lamellipodial protrusion is found in 3D, cells also move in either amoeboid or lobopodial fashion through processes dictated mainly by Rac1 and RhoA (Petrie et al., 2012; Sahai and Marshall, 2003). Cells are able to transition between these different modes of migration in response to the properties of the extracellular matrix environment by modulating the activity of specific regulators of the Rho GTPases.

Similar to 2D, Rac1 in 3D ECM is traditionally important for promoting mesenchymal-type migration. However, the activity of Rac1 also governs the switch between mesenchymal and amoeboid migration by modulating both intracellular contractility and polarized lamellipodia formation. In certain cancer cells, knockdown of Rac1 leads to increased phosphorylation of myosin light chain (MLC) and promotes amoeboid movement. This occurs through the Rac1 effector WAVE2, which suppresses MLC phosphorylation and thus inhibits actomyosin contractility

(Sanz-Moreno et al., 2008). Rac1 can also act through the GEF NEDD9 to inhibit ROCK-meditated actomyosin contractility through Src-dependent deactivation of ROCKII (Ahn et al., 2012). Conversely in the same cancer cells, artificial activation of Rac1 promotes mesenchymal-type migration through WAVE2 by driving polarized actin assembly through the Arp2/3 complex (Sanz-Moreno et al., 2008). During fibroblast lobopodial migration in 3D CDM, however, Rac1 activity was found to be dispensable and no longer polarized to the leading edge of cells (Petrie et al., 2012).

The role of Cdc42 in governing the different modes of 3D migration is far more ambiguous. Cdc42 is involved in the establishment of 3D epithelial cell migratory polarity via its interaction with the Par3/Par6/aPKC polarity complex, which in turn regulates Rac1 via the GEF Tiam1 (Braga and Yap, 2005). Similarly, Cdc42 has been implicated in collective cancer cell invasion, where it acts through the effector MRCK to stimulate actomyosin contractility through MLC phosphorylation (Gaggioli et al., 2007). Recently, the Cdc42-specific GEF DOCK10 was identified to control invasive 3D amoeboid migration in melanoma cells. DOCK10 acts through Cdc42 to stimulate Pak2 and induce MLC phosphorylation, and inhibition of DOCK10 leads to a mesenchymal morphology (Gadea et al., 2008). However, this mechanism is limited to amoeboid migration, and very few GEFs have been identified for Cdc42 that may control 3D mesenchymal cell migration. Evidence exists indicating that Cdc42-MRCK signaling can generate cellular contractility necessary for elongated migration during 3D cancer cell migration, but how this contractile activity is distinct from the RhoA-ROCK amoeboid mechanism is unclear (Wilkinson et al., 2005). Thus, out of the three classical

Rho GTPases, the activity of Cdc42 and its specific regulators during 3D migration is least established.

Similar to Rac1, there is an overwhelming amount of evidence implicating RhoA activity in the modulation of actomyosin contractility and cytoskeleton rearrangements required for the different migratory modes during 3D migration. Classically, amoeboid cells are characterized by a rounded, less adhesive phenotype due to high levels of actomyosin contractility downstream of RhoA-ROCK signaling. The microtubule associated RhoA GEF, GEF-H1, promotes amoeboid migration in MDA-MB-231 cancer cells, and loss of GEF-H1 blocks 3D amoeboid invasion (Heck et al., 2012). Similarly, it was recently found that knockdown of the RhoA GEF Net1 inhibits amoeboid migration and promotes elongated morphology in MDA-MB-231 cells (Carr et al., 2013). While the majority of these 3D migratory studies have been limited to cancer cells, a recent investigation using primary dermal fibroblasts shows that an ECM-triggered switch between lamellipodia- and lobopodia-based 3D migration is centered around RhoA activity. This migratory switch requires a high degree of actomyosin contractility, since inhibiting RhoA, ROCK, or myosin II prevents fibroblast lobopodia migration and triggers a switch to lamellipodia-based migration (Petrie et al., 2012).

Central to the ability of cells to adapt their migratory mode in response to the extracellular matrix environment is the ability of Rho GTPases to “crosstalk” or modulate the signaling activity of each other. This occurs primarily through three mechanisms: direct regulation of GTPase activity through GEFs and GTPase-activating proteins (GAPs), regulation of Rho protein expression and stability, or through the intersection of downstream effector signaling pathways (Guilluy et al., 2011a). GAPs serve as the

agonist “off-switch” to GEFs by binding to the Rho protein and stimulating intrinsic GTPase hydrolysis, thereby inactivating it. In the case of GEF/GAP crosstalk, commonly the activity of the two Rho GTPases is separated spatio-temporally, or one of the proteins is activated while the other is inhibited.

The most frequently reported cases of Rho GTPase crosstalk in response to extracellular matrix cues are between RhoA and Rac1. Rac1/RhoA crosstalk is generally antagonistic and commonly occurs through modulation of GEF and GAP activity. A recent study showed that caveolin-1 mediates 3D extracellular matrix remodeling and cell invasion by promoting RhoA activity and inactivating Rac1 activity through the localized deactivation of p190RhoGAP (Goetz et al., 2011). During cell migration, the RhoA effector ROCK can phosphorylate and activate FilGAP, a Rac1-specific GAP, which in turn inactivates Rac1 and leads to suppression of lamellipodial protrusion (Ohta et al., 2006). The RhoA effector ROCK can also phosphorylate Par3 in its aPKC-binding region, which results in disruption of the Par3/Tiam1/aPKC/Par6 complex and leads to reduced Rac1 activity and cell migration (Nakayama et al., 2008). Conversely, Rac1 has been shown to inhibit thrombin-induced RhoA activation through the Pak1-mediated inhibition of the RhoA GEF p115-RhoGEF (Rosenfeldt et al., 2006), as well as direct suppression of RhoA activity through the binding and activation of p190RhoGAP (Bustos et al., 2008).

Although crosstalk between Cdc42 and Rac1/RhoA has been reported, the GEF/GAP regulators of Cdc42 are far less characterized and understood than the mechanisms between Rac1 and RhoA. As previously mentioned, Cdc42 activity triggers the association of βPix and Pak1, leading to the positive regulation of Rac1 activity

during in vitro wound healing assays (Cau and Hall, 2005). Although inhibitory crosstalk has been reported between Cdc42 and Rac1/RhoA (Benink and Bement, 2005; Simon et al., 2013), the few studies describing such crosstalk use localization and time-correlation studies and establish no definitive molecular mechanism involving GEF and GAP regulators.

To this point, we have identified that βPix is an ECM-specific GEF that is critical for cell migration in fibrillar collagen environments. Loss of βPix results in a severe phenotype in fibrillar collagen across diverse cell types. This phenotype is characterized by nearly complete inhibition of cell motility, rounded hyper-protrusive cells, and robust collagen matrix remodeling. In this chapter, we investigate the unique molecular mechanism behind the collagen-specific migratory function of βPix. Having isolated βPix in a screen for ECM-specific Rac1 GEFs, we first asked whether depletion of βPix can lead to collagen-specific decreases in Rac1 activity.

### 3.2 βPix acts through Cdc42, but not Rac1, during collagen migration

We first tested whether the association between βPix and Rac1 was nucleotide dependent. βPix bound specifically to a nucleotide-free mutant of Rac1, with no binding to recombinant wild type (WT) or a constitutively active mutant (Q61L) during migration on collagen (Figure 12a), which is indicative of GEF activity. To test if loss of βPix leads to collagen-specific decreases in Rac1 activity, we assayed for active Rac1 and Cdc42 in lysates from non-specific (NS) and βPix shRNA fibroblasts migrating on fibronectin or collagen using a recombinant GST-PBD (p21 binding domain of Pak1) affinity probe that binds both active Rac1 and Cdc42. Consistent with its reported function as a Rac1/Cdc42

GEF (Manser et al., 1998), we observed collagen-specific decreases not only in Rac1 (~20%), but also Cdc42 (~30%) activity with βPix knockdown (Figure 12b, c).

Having both isolated βPix in a Rac1 GEF assay and observed a collagen-specific decrease in Rac1 activity upon loss of βPix, we reasoned that knockdown of Rac1 should be sufficient to recapitulate the βPix knockdown phenotype in 3D collagen matrices. Two independent single siRNAs toward either Rac1 or Cdc42 protein were found to deplete protein levels effectively (Figure 12e, Materials and Methods Table 2), and these knockdowns cells were assayed for morphological phenotypes in 3D collagen. Surprisingly, we found that knockdown of Rac1 led to no obvious morphological defects in 3D collagen, whereas Cdc42 knockdown fully mimicked loss of βPix (Figure 12d). While Rac1 knockdown cells mirrored nonspecific siRNA controls, Cdc42 knockdowns displayed the rounded, hyper-protrusive morphology associated with βPix depletion (Figure 12d, f). In addition, Cdc42 knockdown cells appeared to be hyper-contractile, displaying robust collagen remodeling and frequently exhibiting holes in the surrounding matrix (Figure 12d, asterisks).

We tested whether the deregulated protrusive, contractile behavior of Cdc42-depleted cells was accompanied by defective migration in both 3D and thin fibrillar collagen environments. Surprisingly, knockdown of Rac1 was dispensable for migration in 3D collagen, while knockdown of Cdc42 nearly abrogated all cell motility (Figure 13a). Phase timelapse imaging additionally revealed hyper-protrusive Cdc42 knockdown cells tearing holes in the surrounding collagen matrix. We used multiple Rac-isoform knockdowns to rule out any possible compensatory roles of other Rac isoforms (Rac2, Rac3) during Rac1 knockdown. We observed that loss of Rac1 did not induce changes in

expression of other Rac isoforms (Figure 13c) and that knockdown of all Rac isoforms was insufficient to yield a phenotype similar to βPix/Cdc42 during 3D collagen migration (Figure 13b, d). These data indicate that the collagen-specific βPix knockdown phenotype is due to loss of Cdc42 activity, but not Rac1.

Similar to RacG15A, βPix also differentially bound to recombinant, nucleotide-free Cdc42G15A (Figure 13e) and additionally displayed increased but partial co-localization with Cdc42 in leading edge protrusions (Figure 13f) during migration on fibrillar collagen, but not fibronectin. Additionally, the phenotypes associated with both βPix and Cdc42 knockdown are consistent with a report that loss of Cdc42 in 3D microenvironments leads to temporally and spatially deregulated protrusions and impaired leading edge coordination (Lammermann et al., 2009). We therefore investigated whether βPix regulates the localization and activity of Cdc42 under different ECM conditions. Imaging a single-chain Cdc42 biosensor based on intramolecular fluorescence resonance energy transfer (FRET) (Komatsu et al., 2011) revealed that on fibronectin, Cdc42 activity remained polarized toward the leading edge of migrating cells expressing either nonspecific or βPix shRNA (Figure 14a). On collagen, Cdc42 activity was also polarized to the leading edge in the same regions where βPix was found to localize uniquely on the membrane. In contrast, βPix knockdown on fibrillar collagen led to a loss of this polarization and decreased overall Cdc42 activity (Figure 14a-c). Additionally, we observed similar collagen-specific decreases in Cdc42 FRET and loss of FRET polarization in 3D collagen, but not in 3D cell-derived matrix (Figure 14d), further establishing that βPix acts through Cdc42, but not Rac1, to coordinate migration in fibrillar collagen environments.

### 3.3 βPix/Cdc42 suppress and localize RhoA activity during collagen migration

As highlighted in the introduction to this chapter, crosstalk between the Rho GTPases is a common mechanism of contextually regulating the mode by which a cell migrates. Loss of Cdc42 activity alone is not sufficient to explain the severe phenotype observed with βPix knockdown. Because of the strong collagen contraction phenotype associated with loss of βPix, we speculated that βPix/Cdc42 knockdown may lead to increased RhoA activity during migration in fibrillar collagen environments. To test this hypothesis, we assayed intracellular RhoA activity during fibronectin or fibrillar collagen migration in the presence or absence of βPix by using a recombinant GST-RBD (Rho binding domain of Rhotekin) affinity probe that binds active RhoA. Knockdown of βPix resulted in a 40-60% increase in intracellular RhoA activity in fibrillar collagen, but not fibronectin (Figure 15a, b), with similar increases also observed during 3D collagen migration. Importantly, knockdown of Cdc42, but not Rac1, also increased intracellular RhoA activity levels on fibrillar collagen (Figure 15c, d).

We next used a single chain RhoA FRET biosensor (Komatsu et al., 2011; Yoshizaki et al., 2003) to determine both RhoA activity levels and localization during live-cell migration. During migration on fibronectin, we observed a gradient of RhoA activity that was highest at the rear of the cell and decreased toward the leading edge; it was unaffected by βPix knockdown (Figure 15e). This localization pattern was also observed during migration on fibrillar collagen; however, after βPix knockdown, we observed a striking loss of this RhoA gradient with a general elevation of RhoA activity (Figure 15e-g). Again, the loss of front-back RhoA FRET segregation and elevation in activity was observed in 3D collagen, but not 3D cell-derived matrix (Figure 15h),

confirming a new suppressive crosstalk mechanism between βPix/Cdc42 and RhoA in collagen microenvironments.

### 3.4 Modulation of RhoA activity is sufficient to mimic or suppress the βPix knockdown phenotype in collagen microenvironments

To demonstrate directly that increased RhoA activity is the driving mechanism behind the collagen-specific βPix/Cdc42 knockdown phenotype, we examined whether artificial increases in RhoA activity alone could mimic βPix knockdown in 3D collagen. Low-level overexpression of constitutively active RhoAQ63L, as determined by fluorescence intensity, not only mimicked the rounded morphology (Figure 16a) and robust collagen contraction (Figure 16d), but notably also the deregulated, hyper-protrusive behavior (Figure 16a-c). Expressing RhoAQ63L at comparable levels in HFFs migrating in cell-derived matrix (Figure 16e) did not perturb morphology or lead to hyper-protrusive behavior. Migration in fibrillar collagen environments (Figure 16g) was also significantly inhibited by low RhoAQ63L expression. Interestingly, similar to βPix (and Cdc42) knockdown, artificially elevating RhoA activity directly led to an increase in cell-cell adhesion between migrating fibroblasts. It appears now that this puzzling phenomenon, originally observed in the βPix knockdown cells, is a direct consequence of increased RhoA activity. Modulation of RhoA activity has been demonstrated to regulate the expression of N-cadherin in stem cells (Laplante et al., 2004) and RhoA is essential for N-cadherin-dependent cell-cell adhesions in myoblasts (Comunale et al., 2007), but it is unclear what mechanism is dominant here. How increased RhoA activity is specifically regulating cell-cell adhesion in fibroblasts in fibrillar collagen environments is of highly interest and warrants future investigation.

Finally, to test directly whether inhibiting RhoA could partially rescue the βPix knockdown phenotype, we treated βPix knockdown cells with the RhoA inhibitor C3 transferase, or with blebbistatin to inhibit cellular contractility through the RhoA effector myosin II. NS and βPix shRNA fibroblasts were incubated overnight in the presence of inhibitors, and motility was assayed by phase contrast timelapse over 24 hours starting on the following morning. We found that treating βPix knockdown cells in 3D collagen with C3 transferase could significantly rescue both morphology and migration, while blebbistatin rescued the morphology with slight increases in motility (Figure 16f, h). Interestingly, treating βPix knockdown fibroblasts with the Rho kinase inhibitor Y-27632 was unable to rescue cell morphology or migration. We conclude that βPix acts through Cdc42 to suppress and localize RhoA activity during migration in fibrillar collagen environments.

### 3.5 Identifying novel collagen-specific βPix interacting proteins

To address mechanistically how βPix acts through Cdc42 to suppress RhoA, we utilized GFP-βPix knockdown/rescue fibroblasts to isolate βPix-binding proteins from cells undergoing migration on fibronectin versus fibrillar collagen substrates. GFP-βPix was immunoprecipitated from fibroblast lysates using a high-affinity GFP-binding protein derived from a single domain camel antibody (GFP-TRAP, Chromotek), which was able to extract GFP-βPix efficiently while minimizing ECM contaminants. Coomassie blue staining of interacting proteins revealed several unique bands in comparisons between the two migratory conditions (Figure 17a). These unique bands were excised and analyzed by mass spectrometry for identification.

Immunoblotting for known binding partners such as Pak1 and GIT1 revealed decreased association on collagen compared to fibronectin, confirming the observed differential binding to βPix (Figure 17c, e). Additionally, we observed no binding of βPix to polarity-associated regulators Par6, Par3, Scrib, and aPKC in either ECM condition. With the discovery that βPix/Cdc42 were acting to suppress RhoA during migration in fibrillar collagen, we hypothesized that βPix should be promoting the collagen-specific activity of a RhoA GAP. Common RhoA GAPs p190RhoGAP and IQGAP1 both were identified by mass spectrometry, but showed no collagen-specific association with βPix (Figure 17e). Unexpectedly, mass spectrometry analysis of a strong ~130 kDa band revealed a collagen-specific association between βPix and the Rho GAP srGAP1, observed in both HFFs (Figure 17b) and MDA-MB-231 cells (Figure 17d). Depending on the context, srGAP1 can promote the GTP hydrolysis of RhoA, Cdc42, or Rac1 (Wong et al., 2001), and overexpression of srGAP1 can suppress protrusive plasma membrane dynamics (Coutinho-Budd et al., 2012). Therefore, srGAP1 was a promising candidate for contextual GAP activity toward RhoA during fibrillar collagen migration.

### 3.6 βPix has a collagen-specific association with the RhoA GAP srGAP1 that is essential for its collagen-specific function

To test whether the collagen-specific association between srGAP1 and βPix has a RhoA GAP functional role in the βPix/Cdc42 collagen pathway, we performed srGAP1 RNAi knockdown (Figure 18a) and assayed for intracellular RhoA activity. We found that intracellular RhoA activity levels increased significantly (~50-60%) during fibrillar collagen migration after loss of srGAP1, without any change on fibronectin (Figure 18b, c). Importantly, since srGAP1 has been reported to be a Rac1 GAP, we tested for ECM-specific changes in Rac1 activity upon srGAP1 knockdown. Confirming previous reports,

we observed an increase in Rac1 activity after srGAP1 knockdown during migration on fibronectin, but not during collagen migration (Figure 18g). This finding highlights that srGAP1, like βPix, has diverse cellular functions that are contextually dependent upon the ECM. We show here that in response to fibrillar collagen, srGAP1 serves as a GAP toward RhoA.

We next tested whether srGAP1 knockdown and the subsequent increase in RhoA activity led to a similar migratory phenotype in 3D collagen. Consistent with a critical role in the βPix/Cdc42 pathway, srGAP1 knockdown cells fully mimicked the phenotypic characteristics of βPix and Cdc42 knockdown in 3D collagen. Knockdown of srGAP1 resulted in rounded cells with hyperactive, de-localized protrusions and loss of persistent motility (Figure 18d-f). These cells also showed increased contraction of adjacent collagen matrix (Figure 18d) and additionally displayed increased cell-cell adhesion. This result identifies a novel interaction between a new GEF/GAP pair, defining a mechanism of Cdc42 and RhoA crosstalk. This mechanism involving βPix/Cdc42/srGAP1 serves to locally suppress RhoA activity and promote efficient cell migration in fibrillar collagen environments.

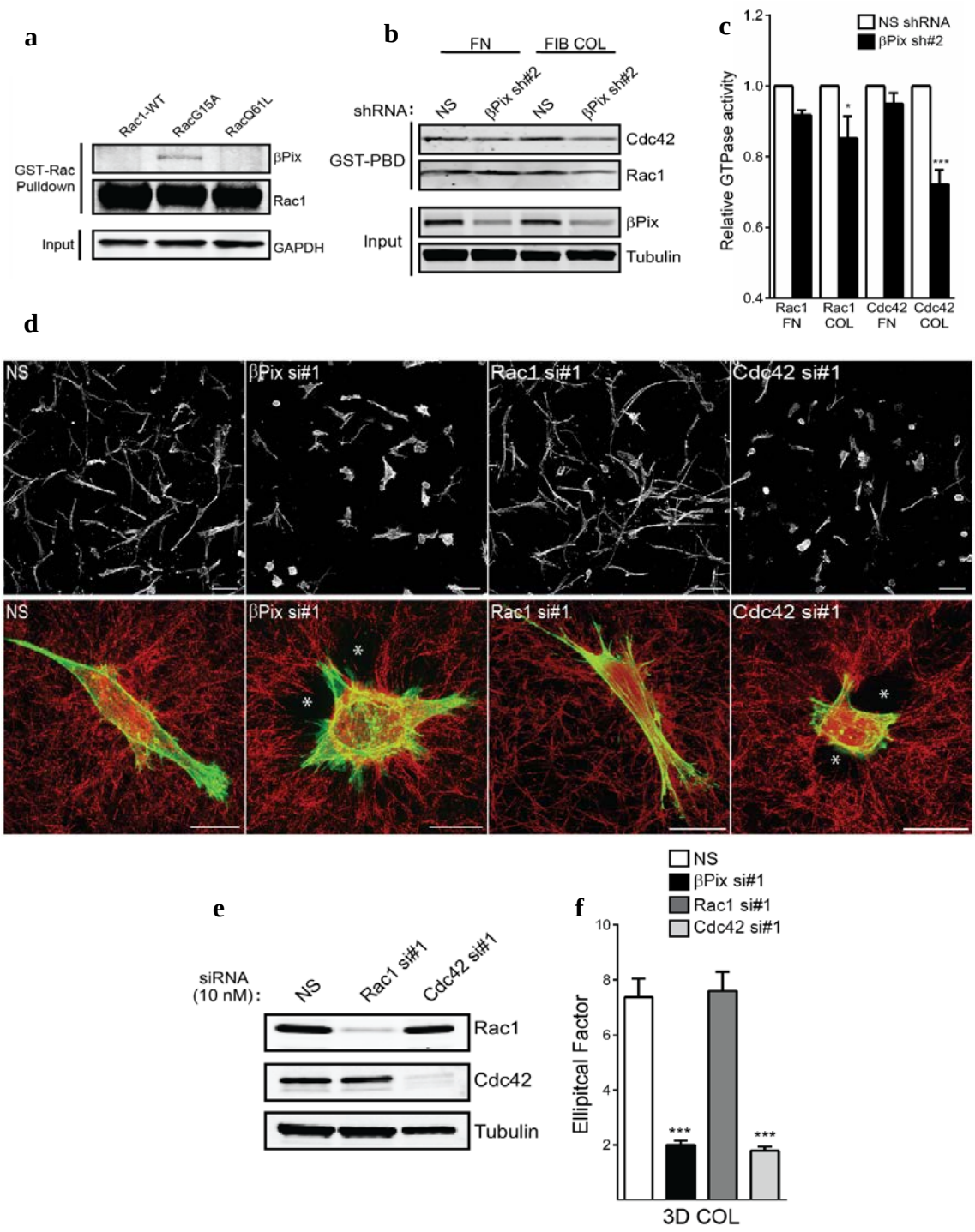
a
Rac1-WT
RacG15A
RacQ61L
GST-Rac Pulldown
βPix
Rac1
Input
GAPDH
b
FN
FIB COL
shRNA:
NS
βPix sh#2
NS
βPix sh#2
GST-PBD
Cdc42
Rac1
Input
βPix
Tubulin
c
NS shRNA
βPix sh#2
Relative GTPase activity
1.2
1.0
0.8
0.6
0.4
Rac1 FN
Rac1 COL
Cdc42 FN
Cdc42 COL
d
NS
βPix si#1
Rac1 si#1
Cdc42 si#1
e
siRNA (10 nM):
NS
Rac1 si#1
Cdc42 si#1
Rac1
Cdc42
Tubulin
f
NS
βPix si#1
Rac1 si#1
Cdc42 si#1
Ellipitcal Factor
10
8
6
4
2
3D COL

**Figure 12**: **βPix regulates cell morphology through Cdc42, but not Rac1. a** βPix specifically bound dominant-negative RacG15a and not wild type Rac1 or constitutively active Rac1 (Q61L) in lysates extracted from cells migrating on collagen. **b** Active Rac1 and Cdc42 were isolated using GST-PBD from NS and βPix shRNA-expressing HFFs migrating on fibronectin (FN) or fibrillar collagen (FIB COL). **c** Quantification of western blot band intensity revealed collagen-specific losses in both Rac1 (~20%) and Cdc42 (~30%) activity after depletion of βPix (n = 3, error bars represent s.e.m, *t*-tests)**.** **d** (Top) siRNA-treated HFFs were embedded in 3D collagen gels and incubated overnight in complete media. Cells were then fixed and stained with rhodamine-phalloidin. Maximum projections of 150 μm sections of the actin-labeled gels revealed that knockdown of Cdc42 mimicked βPix knockdown morphology, with no defects observed with Rac1 knockdown. Scale bars, 50 μm. (Bottom) Higher-power images of actin-labeled (green), siRNA-treated fibroblasts in relation to the surrounding collagen fibers (red, reflection microscopy). Knockdown of Cdc42 mimics the morphology, protrusive, and highly contractile phenotype of βPix knockdown. Holes torn in the collagen matrix are indicated by white asterisks; scale bars, 25 μm. **e** Single, independent siRNA treatments (10 nM) targeting Rac1 or Cdc42 were sufficient to deplete endogenous protein levels. **f** Quantification of cell elliptical factor (maximal length/width) in 3D collagen after Rac1 or Cdc42 siRNA treatments (error bars represent s.e.m., n = 35, 30, 35, 31 cells). * $P < 0.05$, *** $P < 0.001$.

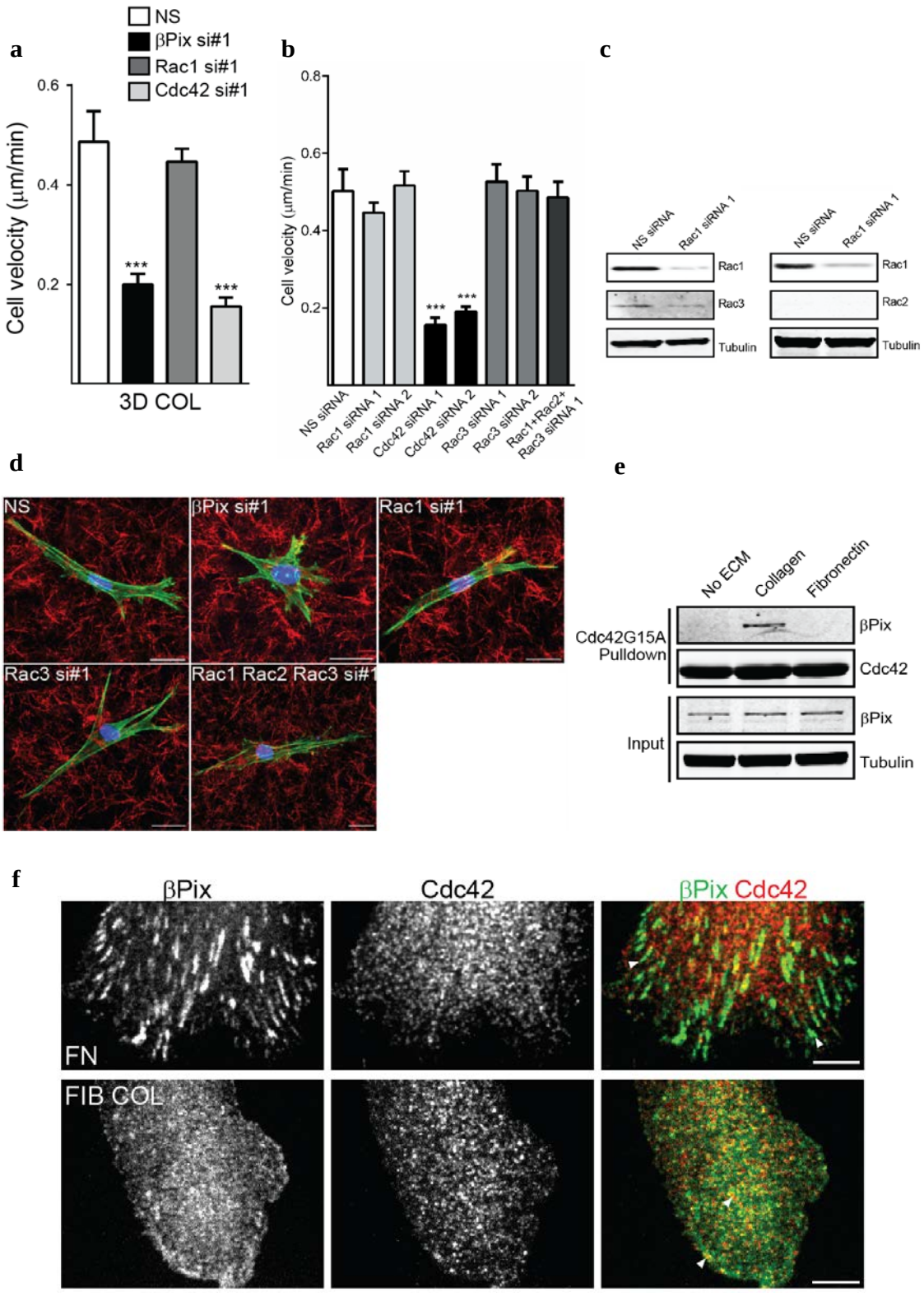
a
NS
βPix si#1
Rac1 si#1
Cdc42 si#1
Cell velocity (μm/min)
0.6
0.4
0.2
***
***
3D COL
b
Cell velocity (μm/min)
0.8
0.6
0.4
0.2
***
***
NS siRNA
Rac1 siRNA 1
Rac1 siRNA 2
Cdc42 siRNA 1
Cdc42 siRNA 2
Rac3 siRNA 1
Rac3 siRNA 2
Rac1+Rac2+ Rac3 siRNA 1
c
NS siRNA
Rac1 siRNA 1
Rac1
Rac3
Tubulin
NS siRNA
Rac1 siRNA 1
Rac1
Rac2
Tubulin
d
NS
βPix si#1
Rac1 si#1
Rac3 si#1
Rac1 Rac2 Rac3 si#1
e
No ECM
Collagen
Fibronectin
Cdc42G15A Pulldown
βPix
Cdc42
Input
βPix
Tubulin
f
βPix
Cdc42
βPix Cdc42
FN
FIB COL

**Figure 13**: **βPix regulates cell migration through Cdc42, but not Rac1. a** Quantification of cell velocity in 3D collagen for Rac1 or Cdc42 siRNA treatments (error bars represent s.e.m., n = 25, 24, 22, 24 cells, one-way ANOVA with Bonferroni multiple comparisons correction). **b** Quantification of migration velocities of GTPase siRNA-treated HFFs in 3D collagen. Two independent siRNAs toward Cdc42 mimic βPix knockdown. Additionally, Rac1 and Rac3 knockdown had no significant effect on HFF migration in 3D collagen (error bars represent s.e.m., n = 25, 22, 21, 24, 21, 19, 18, 20 cells, one-way ANOVA with Bonferroni correction). **c** Knockdown of Rac1 led to no compensatory increase in Rac3 (left) or Rac2 (right) protein levels. **d** Maximum intensity projections of phalloidin-stained HFFs in 3D collagen treated with single siRNAs toward βPix, Rac1 and Rac3, or Rac1, Rac2 and Rac3. No Rac siRNA treatment was capable of recapitulating the βPix knockdown morphological phenotype. Scale bars, 25 μm. **e** βPix also bound specifically to recombinant Cdc42G15A in lysates from cells migrating on collagen, but not fibronectin. Result represents three independent experiments. **f** Immunostaining of βPix (green) and Cdc42 (red) at the leading edge of HFFs on fibronectin or fibrillar collagen. Migration on fibrillar collagen revealed increased but partial co-localization between βPix and Cdc42 (yellow, white arrows) in comparison to cells on fibronectin. Scale bars, 10 μm. * $P < 0.05$, *** $P < 0.001$.

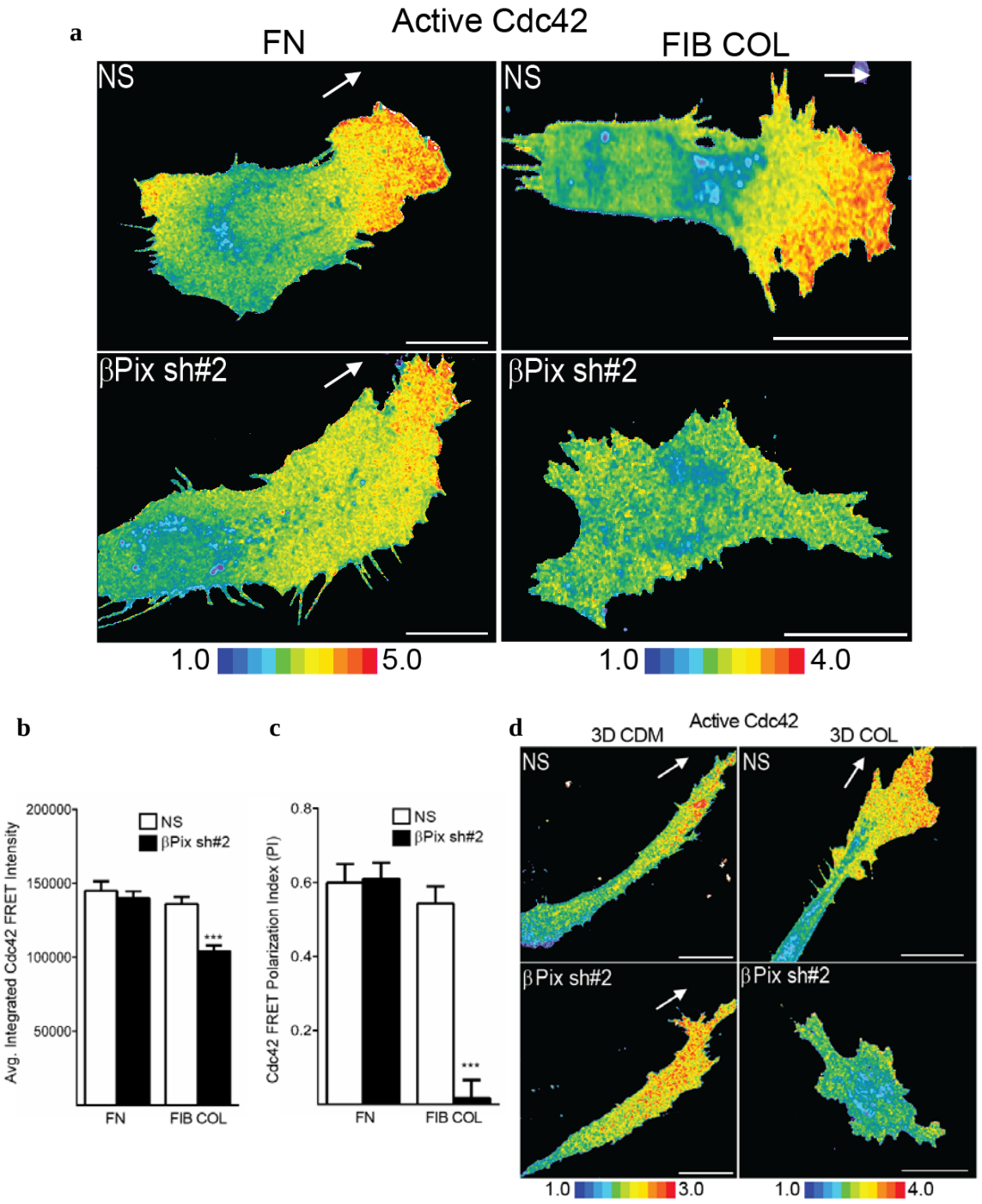
a
Active Cdc42
FN
FIB COL
NS
NS
βPix sh#2
βPix sh#2
1.0
5.0
1.0
4.0
b
Avg. Integrated Cdc42 FRET Intensity
200000
150000
100000
50000
NS
βPix sh#2
***
FN
FIB COL
c
Cdc42 FRET Polarization Index (PI)
0.8
0.6
0.4
0.2
NS
βPix sh#2
***
FN
FIB COL
d
Active Cdc42
3D CDM
3D COL
NS
NS
βPix sh#2
βPix sh#2
1.0
3.0
1.0
4.0

**Figure 14**: **FRET analysis reveals collagen-specific loss of polarized Cdc42 activity during migration. a** Maximum projections of confocal stacks of live-fibroblast migration expressing a Cdc42 biosensor on fibronectin or fibrillar collagen. Active Cdc42 was polarized toward the leading edges during migration on fibronectin in fibroblasts expressing NS or βPix shRNA. After knockdown of βPix on collagen, polarization of Cdc42 activity was lost, and overall activity was decreased. Pseudocolor intensity scales were maintained for each matrix condition; scale bars, 25 μm. White arrows designate direction of leading edge protrusions. **b** Average integrated whole cell Cdc42 FRET intensity on FN versus FIB COL (error bars represent s.e.m., n = 10, 10, 10, 10 cells, *t*-tests). **c** Quantification Cdc42 FRET polarization index on FN versus FIB COL (error bars represent s.e.m., n = 10, 10, 10, 10 cells, *t*-tests). **d** Maximum projections of confocal stacks of live-fibroblast migration expressing a Cdc42 biosensor in 3D cell-derived matrix or 3D collagen. Knockdown of βPix in 3D led to collagen-specific decreases in Cdc42 activity and loss of leading edge polarization. Scale bars, 25 μm. *** $P < 0.001$.

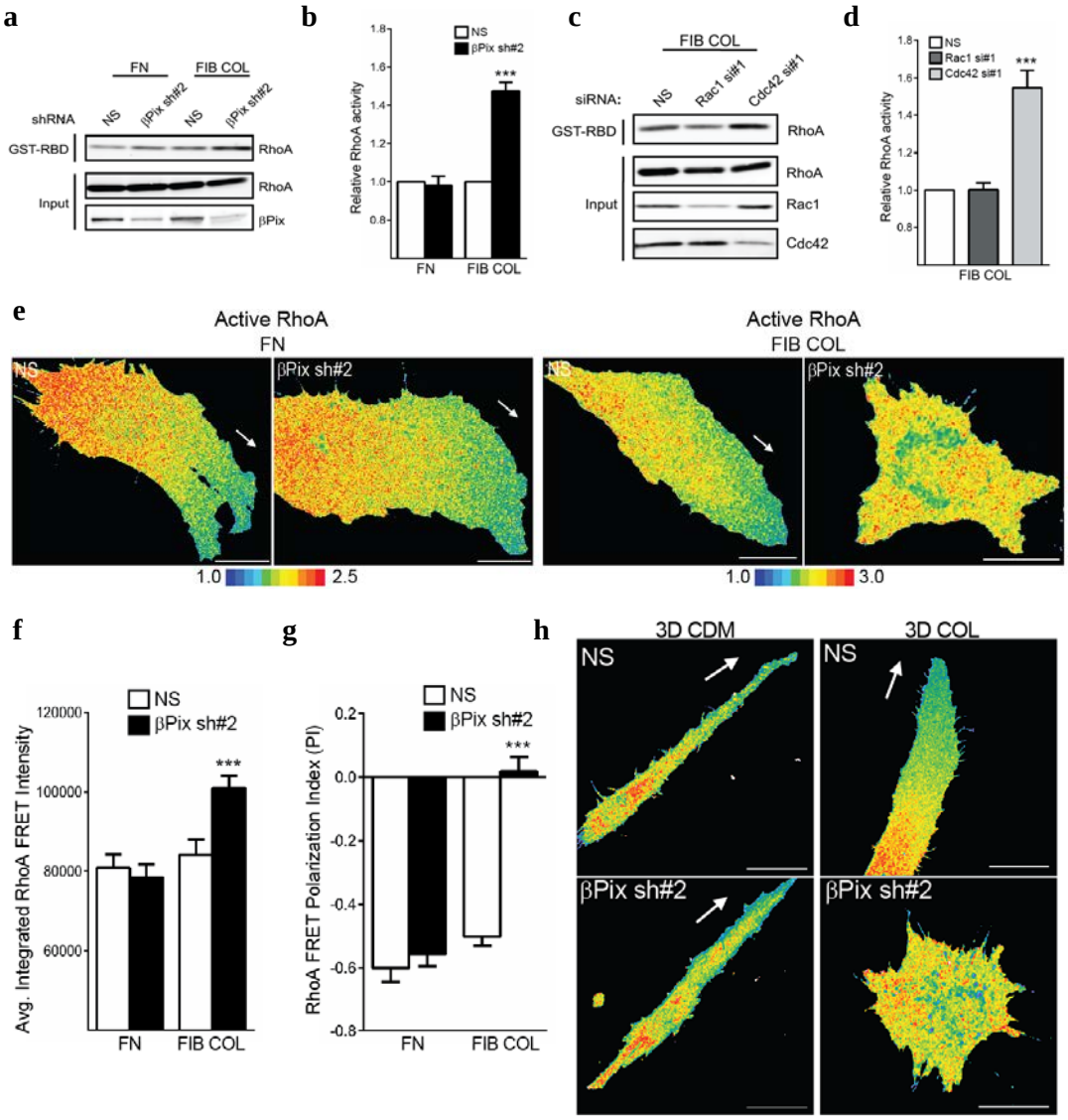
a
FN
FIB COL
shRNA
NS
βPix sh#2
NS
βPix sh#2
GST-RBD
RhoA
Input
RhoA
βPix
b
NS
βPix sh#2
***
Relative RhoA activity
1.8
1.6
1.4
1.2
1.0
0.8
FN
FIB COL
c
FIB COL
siRNA:
NS
Rac1 si#1
Cdc42 si#1
GST-RBD
RhoA
Input
RhoA
Rac1
Cdc42
d
NS
Rac1 si#1
Cdc42 si#1
***
Relative RhoA activity
FIB COL
e
Active RhoA
FN
Active RhoA
FIB COL
NS
βPix sh#2
NS
βPix sh#2
1.0
2.5
1.0
3.0
f
NS
βPix sh#2
***
Avg. Integrated RhoA FRET Intensity
120000
100000
80000
60000
FN
FIB COL
g
NS
βPix sh#2
***
RhoA FRET Polarization Index (PI)
0.2
0.0
-0.2
-0.4
-0.6
-0.8
FN
FIB COL
h
3D CDM
3D COL
NS
NS
βPix sh#2
βPix sh#2

**Figure 15**: **βPix/Cdc42 suppress and localize RhoA activity during collagen migration. a, b** RhoA activity determined using GST-RBD binding from NS and βPix shRNA-expressing HFFs migrating in fibronectin or fibrillar collagen environments; collagen-specific increases (40-60%) in RhoA activity with loss of βPix (error bars represent s.e.m, n = 3, *t*-tests). **c, d** Similarly, knockdown of Cdc42, but not Rac1, during migration on fibrillar collagen led to increased intracellular RhoA activity (error bars represent s.e.m, n = 3, one-way ANOVA with Bonferroni correction). **e** Maximum projections of confocal stacks of live fibroblast migration expressing a RhoA biosensor on fibronectin (FN) or fibrillar collagen (FIB COL). Knockdown of βPix on collagen resulted in overall elevation of RhoA activity accompanied by a loss of front-back segregation of RhoA activity. Pseudocolor intensity scales were identical for each matrix condition; scale bars, 25 μm. White arrows designate direction of leading edge protrusions. **f** Average integrated whole cell RhoA FRET intensity on FN versus FIB COL (error bars represent s.e.m., n = 10, 10, 10, 10 cells, *t*-test). **g** Quantification RhoA FRET polarization index on FN versus FIB COL (error bars represent s.e.m., n = 10, 10, 10, 10 cells, *t*-tests). **h** Maximum projections of confocal stacks of live-fibroblast migration expressing a RhoA biosensor in 3D cell-derived matrix or 3D collagen. Knockdown of βPix in 3D led to similar collagen-specific increases in RhoA activity and loss of front-back polarization of RhoA activity. Scale bars, 25 μm. *** $P < 0.001$.

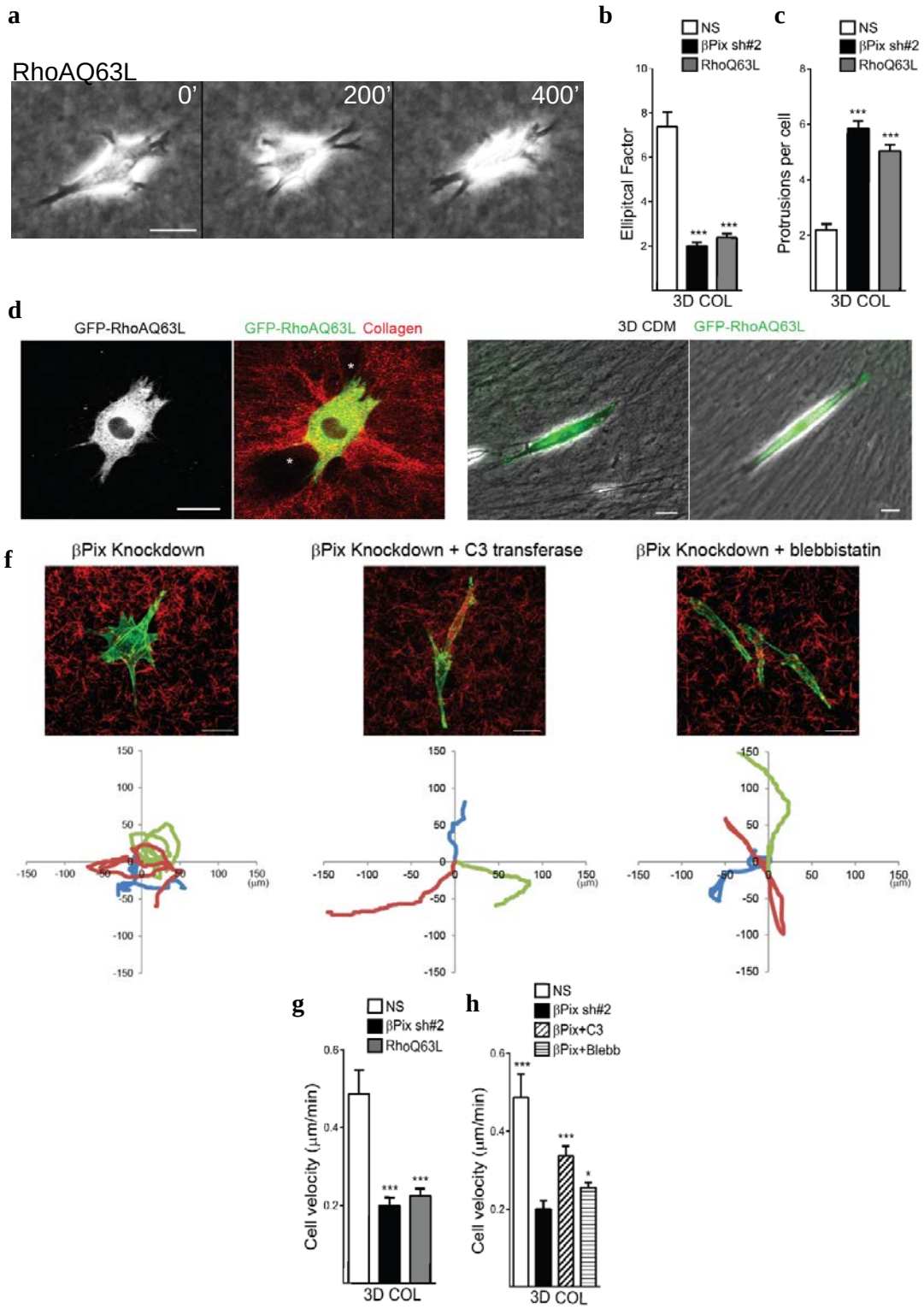
a
RhoAQ63L
0'
200'
400'
b
NS
βPix sh#2
RhoQ63L
Ellipitcal Factor
3D COL
c
Protrusions per cell
3D COL
d
GFP-RhoAQ63L
GFP-RhoAQ63L Collagen
3D CDM
GFP-RhoAQ63L
f
βPix Knockdown
βPix Knockdown + C3 transferase
βPix Knockdown + blebbistatin
(μm)
g
Cell velocity (μm/min)
3D COL
h
βPix+C3
βPix+Blebb
Cell velocity (μm/min)
3D COL

**Figure 16**: **Modulation of intracellular RhoA activity is sufficient to mimic or suppress the βPix knockdown phenotype. a** Phase contrast timelapse images of an HFF expressing low levels of GFP-RhoAQ63L in 3D collagen revealed rounded morphology, spatially and temporally deregulated protrusions (white arrowheads) and loss of persistent migration. Scale bars, 25 μm. **b** Quantification of cell elliptical factor (maximal length/width) in cells low-expressing GFP-RhoAQ63L in 3D collagen (error bars represent s.e.m., n = 30, 35, 29 cells). **c** Quantification of cell protrusions in cells with low-level GFP-RhoAQ63L expression in 3D collagen (error bars represent s.e.m., n = 36, 36, 29 cells). **d** Low-level overexpression of GFP-RhoAQ63L (grayscale, green) during 3D collagen migration (left). We found that similar to βPix and Cdc42 knockdown, RhoAQ63L leads to a rounded, notably hyper-protrusive cell with significant remodeling of collagen fibers (red; holes in the collagen matrix, white asterisks). **e** Expressing RhoAQ63L at comparable levels in HFFs migrating in cell-derived matrix (right) did not perturb morphology or lead to hyper-protrusive behaviors. Scale bar, 25 μm. **f** Maximum intensity projections of phalloidin-stain (green) βPix knockdown cells in 3D collagen (red) treated with inhibitors of RhoA (cell-permeable C3 transferase, 2 μg/ml) or myosin II (blebbistatin, 20 μM) (top). Representative migratory tracks of each condition. We found that direct inhibition of RhoA with C3 transferase significantly rescues the motility of βPix knockdown, while blebbistatin rescues to a lesser degree (bottom). **g** Quantification of cell velocity in cells with low GFP-RhoAQ63L expression in 3D collagen (error bars represent s.e.m., n = 25, 24, 21 cells). **h** βPix shRNA fibroblasts were cultured overnight in 3D collagen gels in the presence of cell-permeable C3 transferase (2 μg/mL) or blebbistatin (25 μM). Migratory velocities were assayed using 24 hour timelapse movies (error bars represent s.e.m., n = 25, 24, 20, 20 cells). One-way ANOVA with Bonferroni correction, *** $P < 0.001$, * $P < 0.05$.

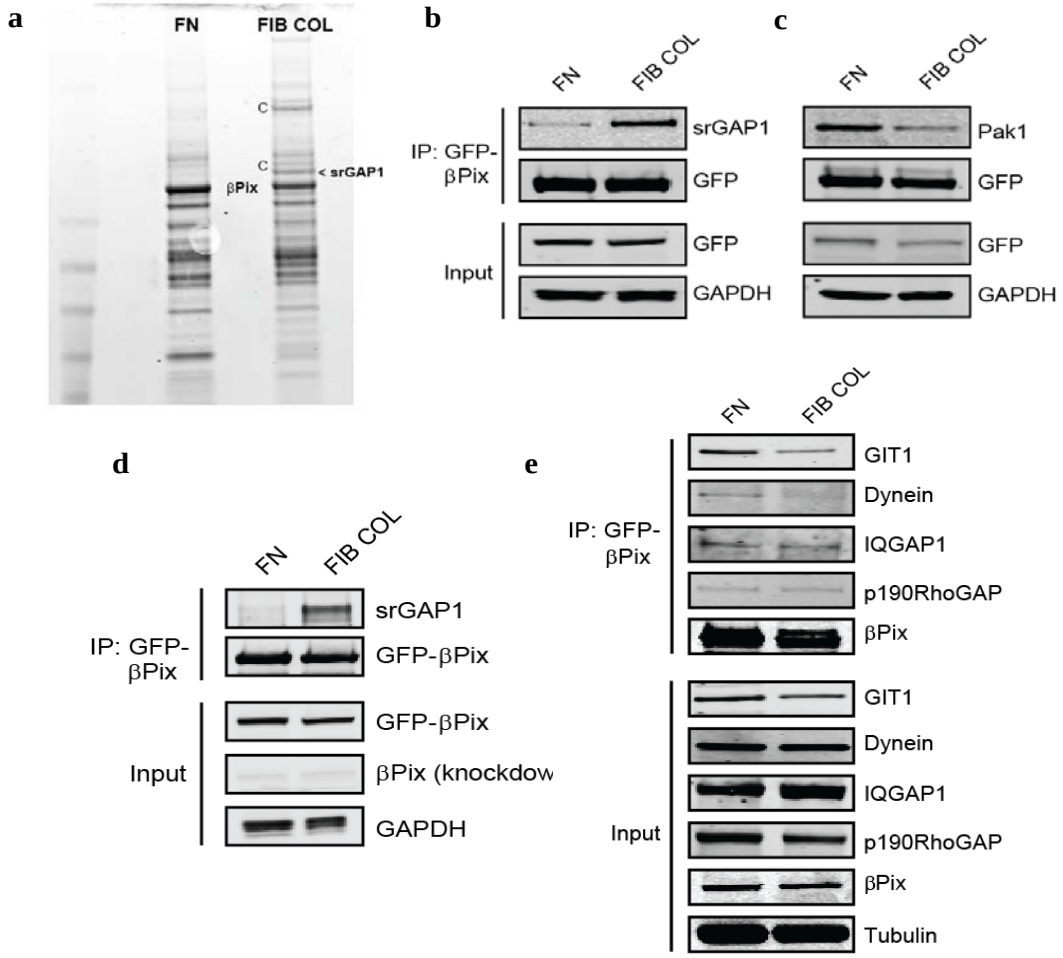


**Figure 17**: **βPix binds srGAP1 specifically during migration in fibrillar collagen. a** GFP-βPix knockdown/rescue cells were allowed to reach steady-state migration on fibronectin (FN) or fibrillar collagen (FIB COL). GFP-βPix was immunoprecipitated from cell lysates under each condition to search for matrix-specific associated proteins. Coomassie blue staining of protein bound to βPix revealed a unique ~130 kDa band (<srGAP1) and a ~65 kDa band that mass spectrometry was used to identify. "C" denotes bands from non-specific collagen binding. **b** Immunoprecipitation of GFP-βPix from βPix knockdown/rescue HFFs migrating on fibronectin (FN) versus fibrillar collagen (FIB COL) identified a novel, collagen-specific GEF/GAP interaction between βPix and srGAP1. **c** Concurrent decreased association of βPix with known effector Pak1 when migrating on fibrillar collagen. Blots are representative of three independent

experiments. **d** Immunoprecipitation of GFP-βPix from βPix knockdown/rescue MDA-MB-231 migrating on fibronectin (FN) versus fibrillar collagen (FIB COL) additionally showed collagen-specific associations between βPix and srGAP1. Blot representative of three independent experiments. **e** Immunoprecipitation of GFP-βPix from βPix knockdown/rescue HFFs migrating on fibronectin (FN) versus fibrillar collagen (FIB COL) stained for reported effectors and proteins identified from mass spectrometry. We observed a decrease in association between βPix and GIT1 on fibrillar collagen, consistent with a decrease in focal adhesion localization. Additionally, we observed a fibronectin-specific association with dynein, while observing no ECM-specificity of association with IQGAP1 or p190RhoGAP. Figure e is a composite of three individual IPs.

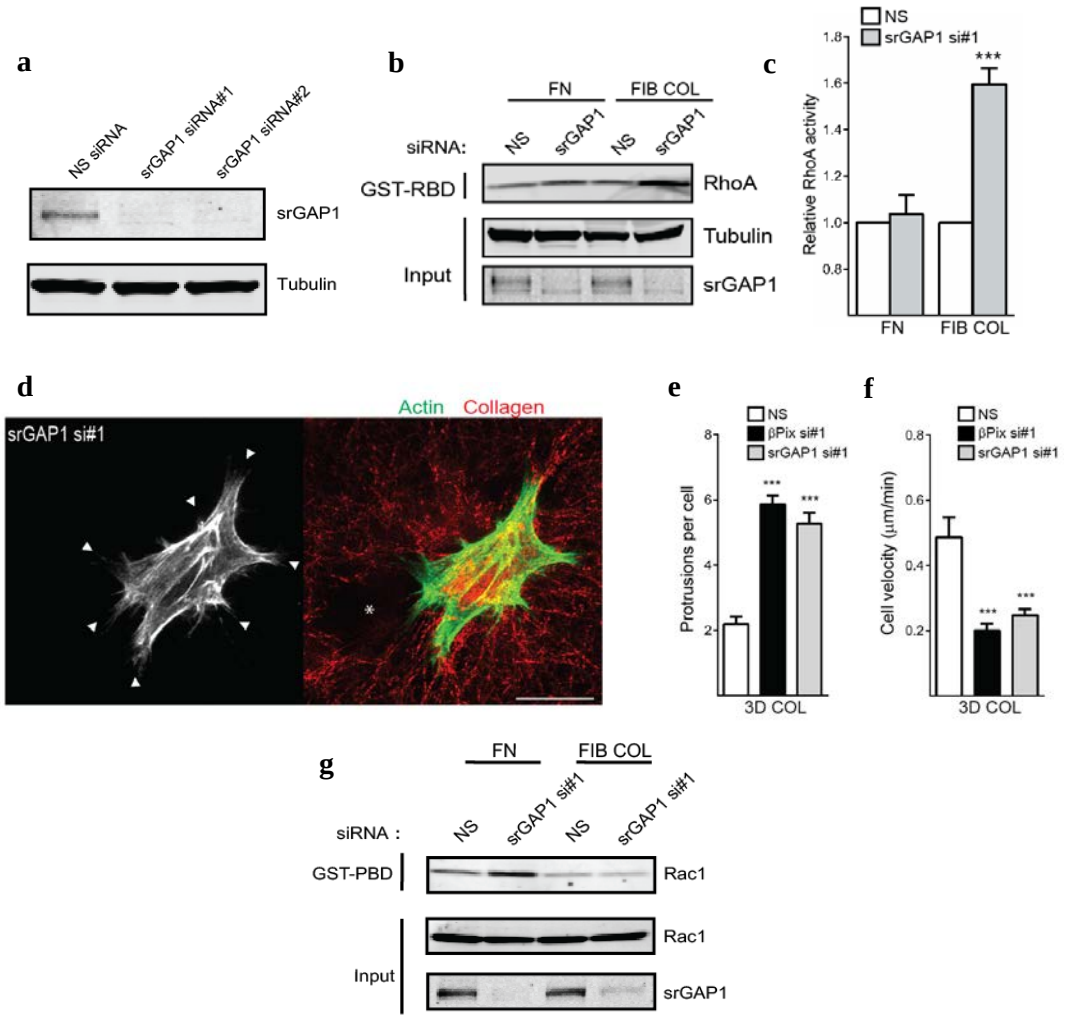


**Figure 18**: **Knockdown of srGAP1 mimics βPix/Cdc42 knockdown in fibrillar collagen. a** Single siRNA knockdown controls toward srGAP1. **b** RhoA activity determined by GST-RBD binding from NS and srGAP1 siRNA-treated HFFs migrating on fibronectin or fibrillar collagen environments. **c** Quantification of bands revealed a 40-60% collagen-specific increase in RhoA activity after loss of srGAP1 (error bars represent s.e.m, n = 3, *t*-tests). **d** srGAP1 knockdown HFFs were cultured overnight in 3D collagen gels. Fixation and labeling with Alexa488-phaloidin revealed a rounded, protrusive (white arrowheads) morphology akin to βPix knockdown. Similarly, srGAP1 knockdown fibroblasts severely altered collagen fiber arrangement (red, reflection microscopy) adjacent to the cell. Hole in matrix marked by white asterisk; scale bar, 25

μm. **e** Quantification of cell protrusions in cells treated with srGAP1 siRNA in 3D collagen (error bars represent s.e.m., n = 36, 36, 24 cells. **f** Quantification of cell velocity in cells treated with srGAP1 siRNA in 3D collagen (error bars represent s.e.m., n = 25, 24, 21 cells). **g** srGAP1 has been reported to have GAP activity toward Rac1. Active Rac1 was isolated using GST-PBD from NS and srGAP1 siRNA-treated fibroblasts migrating on fibronectin (FN) or fibrillar collagen (FIB COL). Confirming previous reports, we observed an increase in Rac1 activity with srGAP1 knockdown during migration on fibronectin, but not during collagen migration. Blot representative of two independent experiments. One-way ANOVA with Bonferroni multiple comparisons correction, *** $P < 0.001$.

# CHAPTER 4

## PHOSPHO-REGULATION OF βPIX BY FIBRILLAR COLLAGEN OCCURS THROUGH $\alpha_2\beta_1$ INTEGRIN AND PROTEIN PHOSPHATASE-2A

### 4.1 Introduction: The regulation of βPix by fibrillar collagen

Our results have revealed a matrix-specific pathway controlling migration involving a GEF/GAP interaction of βPix with srGAP1 that is critical for maintaining suppressive crosstalk between Cdc42 and RhoA during 3D collagen migration. Central to this pathway is the newly discovered, ECM-specific function of the GEF βPix. The novel protein interactions and differential activity described here complement the many preexisting, albeit contextual, roles of βPix during cell migration. Consequently, these diverse functions must necessitate that multiple tiers of regulation exist to ensure proper βPix signaling. Regarding the regulation of βPix in the identified collagen-specific pathway, outstanding questions remained: 1) how does the cell respond to fibrillar collagen to control βPix activity, 2) what post-translational modification(s) on βPix regulate its collagen-specific function, and 3) what mechanisms govern these post-translational modification(s)?

As reviewed in the Introduction, cells primarily respond to changes in ECM composition through integrin-mediated adhesion to matrix ligands. Integrins $\alpha_1\beta_1$ and $\alpha_2\beta_1$ are the major integrin collagen receptors, and each recognizes a variety of collagens, including type I collagen. Integrin $\alpha_2\beta_1$ was originally identified to play an

essential role in platelet adhesion to collagen in the blood vessel wall under flow conditions, and this adhesion was discovered to be structurally dependent on the triple-helix conformation found in fibrillar collagen (Knight et al., 2000; Morton et al., 1994). While it was identified that both $\alpha_1\beta_1$ and $\alpha_2\beta_1$ recognize the triple helical-collagen peptide motif (GFOGER) (Emsley et al., 2000), mutational analysis revealed that $\alpha_2$ integrin preferentially recognizes fibrillar type I collagen, while $\alpha_1$ binds globular type I collagen with greater affinity, yet has the highest affinity for type IV collagen (Kapyla et al., 2000). Additional cell receptors for type I collagen include the tyrosine kinase DDR receptors and syndecan-1 heparan sulfate proteoglycan. While the functions of these less-studied receptors is not fully established, an emerging trend is that they act in concert with integrins to mediate cell adhesion. In CHO cells, syndecan-1 synergistically promoted cell adhesion to type I collagen through $\alpha_2\beta_1$, while DDRs led to enhanced $\alpha_1\beta_1$ and $\alpha_2\beta_1$ integrin-mediated cell adhesion to type I collagen as a result of higher integrin activation states (Vuoriluoto et al., 2008; Xu et al., 2012).

Many contextual phosphorylation sites have been identified on βPix, providing evidence for the functional regulation of βPix through post-translational modifications. The original βPix phosphorylation sites for Pak1 were mapped to S525 and T526 (Koh et al., 2001). Similarly, bFGF and NGF were found induce phosphorylation of βPix on S525 and T526 and this phosphorylation was crucial for activation of Rac1 (Shin et al., 2002). However in response to bFGF or NGF, inhibition of ERK or Pak2, but not Pak1, prevented phosphorylation at S525 and T526 and subsequent Rac1 activation (Shin et al., 2002; Shin et al., 2004). In human mesangial cells, endothelin-1 activates PKA-dependent phosphorylation of βPix at residues S516 and T526, resulting in βPix

translocation to focal adhesions (Chahdi et al., 2005). Additionally, it was demonstrated that FAK can tyrosine phosphorylate βPix, leading to enhanced βPix binding to Rac1 and the translocation of Rac1 to focal adhesions (Chang et al., 2007). The phosphorylation of βPix has also been implicated in tumor progression, as βPix is tyrosine phosphorylated via a Src/FAK-dependent signal from the EGF receptor that triggers a complex formation with the E3 ligase Cbl and the subsequent suppression of EGF receptor degradation (Feng et al., 2006). To gain insight into the "phosphorylation code" behind βPix function, an attempt to map all βPix phosphorylation sites was made using mass spectrometry. Although the study identified 16 putative βPix phosphorylation sites, it fell short in confirming phosphorylation at many previously reported sites, including T526. This was likely due to the near impossibility of recapitulating all potential extracellular modulators of βPix activity in 2D tissue culture (Mayhew et al., 2007). However, the results from these studies confirmed the existence of tight regulatory control over the phosphorylation state of βPix and its subsequent function. It is clear that the regulation of these sites is quite complex and is influenced by a variety of kinases. Surprisingly, there have been no reports of the regulation of βPix phosphorylation by protein phosphatases.

In this chapter we focus on understanding the regulation of βPix downstream of fibrillar collagen. This includes investigating how the cell specifically responds to collagen fibers to modulate βPix activity, what post-translational modification(s) on βPix dictate this ECM-specific activity, and what are the upstream regulators of these modification(s)? We begin first by testing if the collagen-specific βPix migratory cascade is mediated by specific integrin attachment to fibrillar collagen.

## 4.2 $\alpha_2\beta_1$ integrin controls βPix function downstream of fibrillar collagen

Having identified a new collagen-specific role for βPix, we searched for the mechanisms that regulate βPix in different matrix conditions. We observed previously that differential focal adhesion localization during migration on fibronectin or fibrillar collagen was indicative of βPix function. Specifically, during migration on fibrillar collagen, βPix was dramatically localized away from focal adhesions (Figure 7b). We first tested for integrin-specific regulation of this distinct βPix localization. Previous work had shown that certain monoclonal antibodies against specific integrin subunits can mimic full integrin ligation and adhesive function (Miyamoto et al., 1995). We hypothesized that substrates coated with these integrin antibodies would be sufficient to induce differential βPix localization. Monoclonal integrin antibodies were covalently linked to glass dishes targeting $\beta_1$ (9EG7), $\alpha_5$ (mAb 16), or $\alpha_2$ (P1E6) to mimic integrin ligation. GFP-βPix knockdown/rescue cells were plated on the dishes and assayed by TIRF microscopy for loss of focal adhesion localization as a read-out of signaling to βPix (fibrillar collagen; Figure 7b). GFP-βPix strongly co-localized to focal adhesions stained for paxillin on glass or substrates targeting $\beta_1$ and $\alpha_5$ integrin (Figure 19a). However, on substrates targeting $\alpha_2$ integrin, GFP-βPix localization to focal adhesions was greatly diminished, even though paxillin-containing focal adhesions were formed normally. Conversely, treatment of cells migrating in 3D collagen with inhibitory monoclonal antibodies against specific integrins confirmed specificity for the $\alpha_2\beta_1$ integrin by blocking HFF migration (Figure 19b). These results highlight the importance of the $\alpha_2$ subunit of $\alpha_2\beta_1$ integrin in mediating βPix function during migration in fibrillar collagen environments.

## 4.3 Collagen-specific phospho-regulation at threonine 526 is critical for βPix function

βPix function has been ascribed to the differential regulation of the multiple phosphorylation sites on the protein (Mayhew et al., 2007). We therefore hypothesized that during fibroblast migration on fibronectin versus fibrillar collagen, changes in phosphorylation on βPix were essential for each ECM-specific function. To survey for ECM-specific changes in phosphorylation at specific sites on βPix, we performed phospho-proteomics on GFP-βPix isolated from lysates of knockdown/rescue cells during migration on fibronectin or fibrillar collagen. It is important to note that this analysis was not quantitative (e.g. SILAC), but instead focused on identifying the presence or absence of unique phospho-peptides without enrichment in each ECM condition. Surprisingly, between fibronectin and fibrillar collagen we obtained only a single phospho-peptide difference (Table 1, red outline) despite ensuring that complete peptide coverage of βPix was achieved during analysis of each ECM condition.

We identified a selective loss of threonine phospho-peptides at T526 only during fibrillar collagen migration. Using a phosphothreonine-specific antibody, we confirmed by western blotting decreased threonine phosphorylation on βPix isolated from GFP-βPix knockdown/rescue cells during migration on fibrillar collagen compared to fibronectin (Figure 20a). While this decrease in threonine phosphorylation supported the phospho-proteomic results, it did not directly prove that loss of phosphorylation was occurring at T526. To test whether the phosphorylation of T526 was altered, we generated stable βPix knockdown/rescue fibroblasts with either phospho-dead (KDR-T526A) or phospho-mimetic (KDR-T526E) mutations. We observed that matrix-specific differential threonine phosphorylation was lost after mutating T526 to alanine (T526A) (Figure 20a)

in GFP-βPix knockdown/rescue HFFs, confirming that the phosphorylation of T526 is altered during migration on fibronectin versus fibrillar collagen.

T526 phosphorylation has been reported to be crucial for contextual Rac1 activation (Shin et al., 2004) and βPix translocation to focal complexes (Chahdi et al., 2005), consistent with our findings of loss of these actions during migration on fibrillar collagen. To test whether the absence of phosphorylation at T526 was important for βPix migratory function in collagen, we utilized the stable βPix knockdown/rescue fibroblasts with either phospho-dead (KDR-T526A) or phospho-mimetic (KDR-T526E) mutations, with the hypothesis that mimicking phosphorylation at T526 would actually prevent morphological and migratory rescue. As predicted, re-expression of βPix with a phospho-mimetic mutation at T526 was unable to rescue the spreading defect of βPix knockdown (Figure 20b, d). T526E fibroblasts were rounded in 3D collagen matrices and also displayed robust collagen contraction and remodeling, whereas T526A βPix-expressing cells were fully rescued morphologically (Figure 20d). Consistent with knockdown of βPix, T526E cells were also unable to rescue cell migration in 3D collagen gels, while cells with T526A expression mirrored the migratory velocities of rescued KDR-WT cells (Figure 20c). To further solidify the conservation of this pathway and the importance of the T526 residue, we generated βPix knockdown/rescue phospho-variants in MDA-MB-231 adenocarcinoma cells. Similar morphological and migratory phenotypes were also observed for βPix knockdown/rescue phosphovariants in MDA-MB-231 cells (Figure 20e), as the T526E mutation again abolished cell elongation and inhibited cell motility in 3D collagen (Figure 20f, g).

Mechanistically, we were interested in how the absence of phosphorylation at T526 was directing βPix function. T526 falls just outside of the reported βPix CBD domain (Figure 7a) which is essential for directing protein-protein interactions (GIT1/2, PKL), but not for GEF activity. We therefore tested to see if phospho-mutations at T526 blocked association between βPix and the other proteins in the collagen pathway, srGAP1 and Cdc42. Immunoprecipitation of GFP-βPix knockdown/rescue phosphovariants during migration on fibrillar collagen revealed that the βPix phosphorylation mimetic (T526E) had decreased association with srGAP1, but not Cdc42 (Figure 20h). Additionally, as a negative control we observed that the T526E mutation selectively promoted the association between βPix and IQGAP1, highlighting the importance of this residue in regulating the interactions of βPix. These data indicate that absence of phosphorylation at T526 on βPix is essential for its association with srGAP1 during fibrillar collagen migration.

### 4.4 βPix has a collagen-specific association with protein phosphatase-2A that regulates phosphorylation at T526

We have discovered that the extrinsic regulation of the phosphorylation state of βPix at T526 by the extracellular matrix is critical for βPix function, with migration on fibrillar collagen resulting in an absence of phosphorylation at T526 and association with srGAP1. To investigate the upstream regulation of T526 on βPix during migration in fibrillar collagen, we utilized GFP-βPix knockdown/rescue fibroblasts (Figure 21a) to isolate collagen-specific βPix-binding proteins. In addition to srGAP1, we also isolated an approximately 65 kDa protein band that distinctly associated with βPix on fibrillar collagen. Mass spectrometry identified this band as representing a collagen-specific interaction between βPix and protein phosphatase 2A (PP2A) through the regulatory

subunit A, α isoform (PPP2R1A), which was confirmed by western blotting (Figure 21b). Additionally, we verified that this collagen-specific interaction between βPix and PPP2R1A was conserved in MDA-MB-231 cells (Figure 21c). PP2A was an intriguing candidate for the contextual regulation of βPix at T526 because a previous study reported that the phosphatase activity of PP2A can be regulated by the extracellular matrix. In fact, PP2A has been found to be activated specifically during migration in 3D collagen, but not fibronectin, and this activity is regulated by $\alpha_2\beta_1$ integrin (Ivaska et al., 2002).

We hypothesized that PP2A, through an association between βPix and the PPP2R1A subunit, is responsible for the absence of phosphorylation at T526 required during fibrillar collagen migration. To assess the role of PP2A activity, we utilized both siRNA toward the PPP2R1A subunit (Figure 21d) and okadaic acid (OKA), a potent, specific inhibitor of PP2A activity at low concentrations (Ivaska et al., 2002). We first tested whether loss of PP2A activity would modulate the phosphorylation state of βPix during fibrillar collagen migration. GFP-βPix knockdown/rescue fibroblasts migrating on fibrillar collagen were treated with NS or PPP2R1A siRNA #1. We observed that knockdown of PPP2R1A directly increased phospho-threonine levels on βPix during migration on collagen (Figure 21e). Similarly, treatment of GFP-βPix knockdown/rescue cells migrating on fibrillar collagen with okadaic acid (Figure 21f) led to an increase in threonine phosphorylation on βPix in comparison to vehicle control. These data indicate that the activity of PP2A, through an association between βPix and the PPP2R1A subunit, is essential for regulating the phosphorylation state of βPix in response to fibrillar collagen.

## 4.5 Protein phosphatase-2A activity is necessary for collagen-specific βPix function

Although we have demonstrated that inhibition of PP2A or knockdown of PPP2R1A leads to a direct increase in βPix threonine phosphorylation during migration on fibrillar collagen, it was unclear 1) whether the association between PPP2R1A and βPix is important for the collagen-specific migratory function of βPix and 2) that this change in phosphorylation is linked to the previously identified T526 residue on βPix. Inhibition of PP2A by okadaic acid has been reported to result in rounded, protrusive cells in 3D collagen (Ivaska et al., 2002), suggesting a potential role in the βPix/Cdc42/srGAP1 pathway. To test whether the interaction between βPix and PPP2R1A is functionally important for migration, we assayed morphology and migration of NS and PPP2R1A siRNA fibroblasts in 3D collagen and 3D cell-derived matrix. Knocking down PPP2R1A with two independent siRNA sequences (Figure 22a) revealed the same collagen-specific morphological defects, including the hyper-contraction of adjacent collagen fibers, mirroring βPix knockdown (Figure 22c). As expected, these morphological defects were accompanied by altered migration, with a nearly complete loss of motility in 3D collagen and only slight decreases in cell-derived matrix (Figure 22d). Likewise, we confirmed that inhibition of PP2A with 1 nM okadaic acid yielded the same collagen-specific morphological defects as previously reported and mimicked the knockdown of PPP2R1A in 3D collagen (Figure 22b). Okadaic acid treatment also led to a collagen-specific loss of cell motility (Figure 22e). These data indicate that the activity of PP2A, through the association of βPix and PPP2R1A, is critical for modulating the phosphorylation and subsequent function of βPix during fibrillar collagen migration.

We next sought to link the functional association between βPix with PPP2R1A to reduced T526 phosphorylation. To test this connection, we performed loss-of-function experiments by treating βPix knockdown/rescue wild type and T526A fibroblasts with PPP2R1A siRNA and assaying cell morphology and migration in 3D collagen. While knocking down PPP2R1A led to severe morphological and migratory defects in βPix KDR-WT fibroblasts, βPix KDR-T526A fibroblasts showed rescue of the morphological phenotype (Figure 23a, b) and partially rescued the migratory defect (Figure 23c) resulting from PPP2R1A knockdown in 3D collagen. These data indicate that PP2A is critical for mediating the absence of phosphorylation at T526 on βPix during migration in fibrillar collagen environments.

Here, we have uncovered the upstream regulatory mechanisms of βPix in response to fibrillar collagen. Our data strongly suggest that binding of $\alpha_2\beta_1$ to fibrillar collagen leads, through PP2A (PPP2R1A), to the loss of phosphorylation at T526 on βPix, which promotes association with srGAP1. However, we have not rigorously excluded the possibility that decreased kinase activity may also contribute to the absence of phosphorylation at T526. As mentioned previously, T526 is a phosphorylation site for Pak1 and PKA, and is implicated in Pak2 signaling (Chahdi et al., 2005; Koh et al., 2001). The observation of decreased association between βPix and Pak1 during migration in fibrillar collagen (Figure 17c) is consistent with the idea that decreased activity of a kinase phosphorylating βPix could also contribute to regulating T526 phosphorylation in response to fibrillar collagen, but this possibility remains to be investigated.

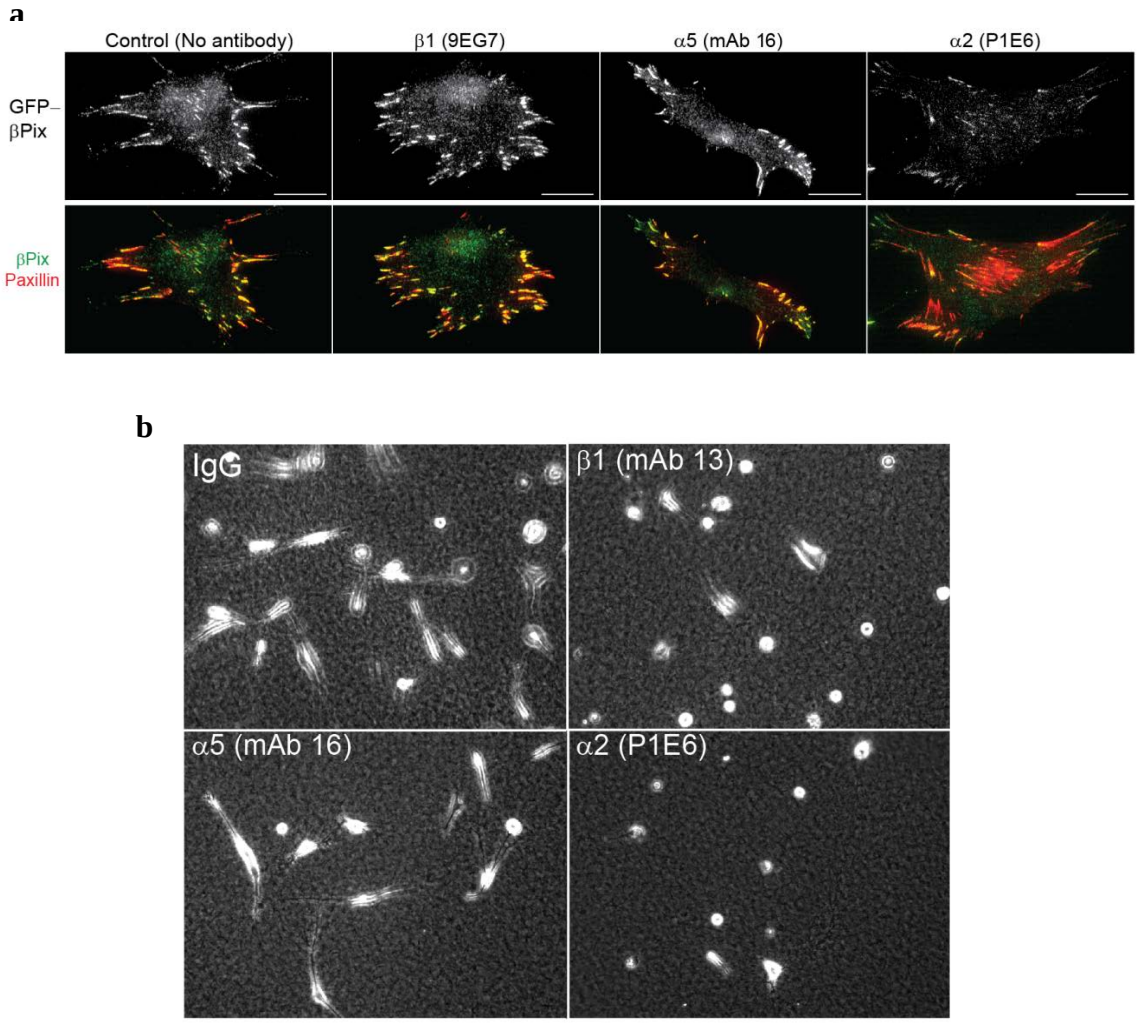


**Figure 19**: **$\alpha_2\beta_1$ integrin controls βPix function downstream of fibrillar collagen. a** Loss of focal adhesion localization was a read-out of differential βPix function on fibrillar collagen (Figure 7b). Dishes were coated with monoclonal integrin antibodies targeting $\beta_1$ (9EG7), $\alpha_5$ (mAb 16), or $\alpha_2$ (P1E6) to mimic integrin ligation. GFP-βPix knockdown/rescue cells were plated on the dishes and assayed for focal adhesion localization (red; yellow in overlay). Ligation of $\alpha_2$ resulted in a dramatic loss in GFP-βPix (grayscale) localization at paxillin (red)-containing adhesions with no changes in

overall focal adhesion profile. Scale bars, 25 μm. **b** HFFs were cultured overnight in 3D collagen gels, incubated with inhibitory integrin antibodies, ($\beta_1$-mAb 13, $\alpha_5$-mAb 16, or $\alpha_2$-P1E6) and allowed to migrate for a further 12-16 hours. Inhibition of $\beta_1$ or $\alpha_2$, but not $\alpha_5$, inhibited cell migration and spreading in 3D collagen. Experiment was performed independently at least twice with identical observations.

## βPix phospho-peptides (FN)

| Sequence | Mascot Ion Score | Modifications | Delta PPM |
|---|---|---|---|
| (R)lKsFDSLGSQQLHTR(T) | 94.88 | Phospho (+80) | 4.457 |
| (R)lKsFDSLGSQQLHTR(T) | 90.46 | Phospho (+80) | 3.828 |
| (R)TsKLFQGQYR(S) | 34.88 | Phospho (+80) | 2.432 |
| (R)TsKLFQGQYR(S) | 47.53 | Phospho (+80) | 2.666 |
| (R)sLDmTDNSNNNQLVVR(A) | 46.38 | Phospho (+80), Oxidation (+16) | 3.439 |
| (R)sLDMTDNSNNNQLVVR(A) | 76.42 | Phospho (+80) | 1.213 |
| (R)sLDmTDNSNNNQLVVR(A) | 134.6 | Phospho (+80), Oxidation (+16) | 2.127 |
| (K)ASEKPVsPK(S) | 47.06 | Phospho (+80) | -1.5 |
| (K)ASEKPVsPK(G) | 59.85 | Phospho (+80) | 0.04683 |
| (K)ASEKPVsPKGFDTTAlNK(S) | 46.8 | Phospho (+80) | 0.8139 |
| (R)msGFlYqGK(L) | 37.65 | Oxidation (+16), Phospho (+80), Deamidated (+1) | 0.475 |
| (R)msGFlYQGK(L) | 51.64 | Oxidation (+16), Phospho (+80) | 0.4719 |
| (R)msGFlYQGK(L) | 54.07 | Oxidation (+16), Phospho (+80) | 3.721 |
| (R)MsGFlYQGK(L) | 57.11 | Phospho (+80) | 3.266 |
| (R)msGFlYQGKLPTTGmTITK(L) | 62.61 | Oxidation (+16), Phospho (+80), Oxidation (+16) | 0.5766 |
| (K)EDLSKsPK(T) | 55.47 | Phospho (+80) | 0.2507 |
| (R)KPsDEEEFASR(K) | 63.35 | Phospho (+80) | -1.536 |
| (R)KPsDEEEFASRK(S) | 31.62 | Phospho (+80) | 0.1242 |
| (R)KPsDEEEFASRK(S) | 59.7 | Phospho (+80) | 0.6309 |
| (R)KStAALEEDAQILK(V) | 47.85 | Phospho (+80) | 2.844 |
| (K)StAALEEDAQILK(V) | 64.32 | Phospho (+80) | 0.7534 |
| (R)RSSLsR(L) | 25.73 | Phospho (+80) | 1.282 |

## βPix phospho-peptides (COL)

| Sequence | Mascot Ion Score | Modifications | Delta PPM |
|---|---|---|---|
| (R)lKsFDSLGSQQLHTR(T) | 84.52 | Phospho (+80) | 2.888 |
| (R)lKsFDSLGSQQLHTR(T) | 102.55 | Phospho (+80) | 1.678 |
| (R)TsKLFQGQYR(S) | 46.62 | Phospho (+80) | 2.483 |
| (R)sLDmTDNSNNNQLVVR(A) | 51.11 | Phospho (+80), Oxidation (+16) | 3.538 |
| (R)sLDmTDNSNNNQLVVR(A) | 112.98 | Phospho (+80), Oxidation (+16) | 1.916 |
| (K)ASEKPVsPK(S) | 51.63 | Phospho (+80) | -2.458 |
| (R)sLDmTDNSNNNQLVVR(A) | 39.43 | Phospho (+80) | 0.6502 |
| (K)ASEKPVsPK(S) | 26.71 | Phospho (+80) | -0.7773 |
| (K)SGTLKsPPK(G) | 24.66 | Phospho (+80) | -1.898 |
| (K)ASEKPVsPKGFDTTAlNK(S) | 31.29 | Phospho (+80), Deamidated (+1) | -0.3942 |
| (R)MsGFlYqGK(L) | 47.7 | Oxidation (+16), Phospho (+80), Deamidated (+1) | 1.448 |
| (R)msGFlYqGK(L) | 51.61 | Oxidation (+16), Phospho (+80) | 3.508 |
| (R)msGFlYQGK(L) | 57.17 | Oxidation (+16), Phospho (+80) | 2.599 |
| (R)MsGFlYQGK(L) | 37.89 | Phospho (+80) | 1.125 |
| (K)EDLSKsPK(T) | 63.28 | Phospho (+80) | -1.922 |
| (R)KPsDEEEFASRK(S) | 30.69 | Phospho (+80) | 0.1242 |
| (R)KPsDEEEFASRK(S) | 54.71 | Phospho (+80) | -0.6067 |
| (R)RSSLsR(L) | 24.23 | Phospho (+80) | 0.8997 |

**Table 1**: **ECM-specific βPix phospho-peptides.** GFP-βPix isolated from knockdown/rescue fibroblasts migrating on fibronectin or fibrillar collagen was analyzed for candidate phosphopeptides that were unique to each ECM. The resulting phosphopeptides are displayed in tabular form, showing the peptide sequence with modified residue in lowercase letters, MASCOT ion score, specific modifications, and

delta PPM of each peptide spectra. The two unique phospho-threonine peptides isolated while on fibronectin are outlined in red. Mass spectrometry analysis was performed by MS Bioworks.

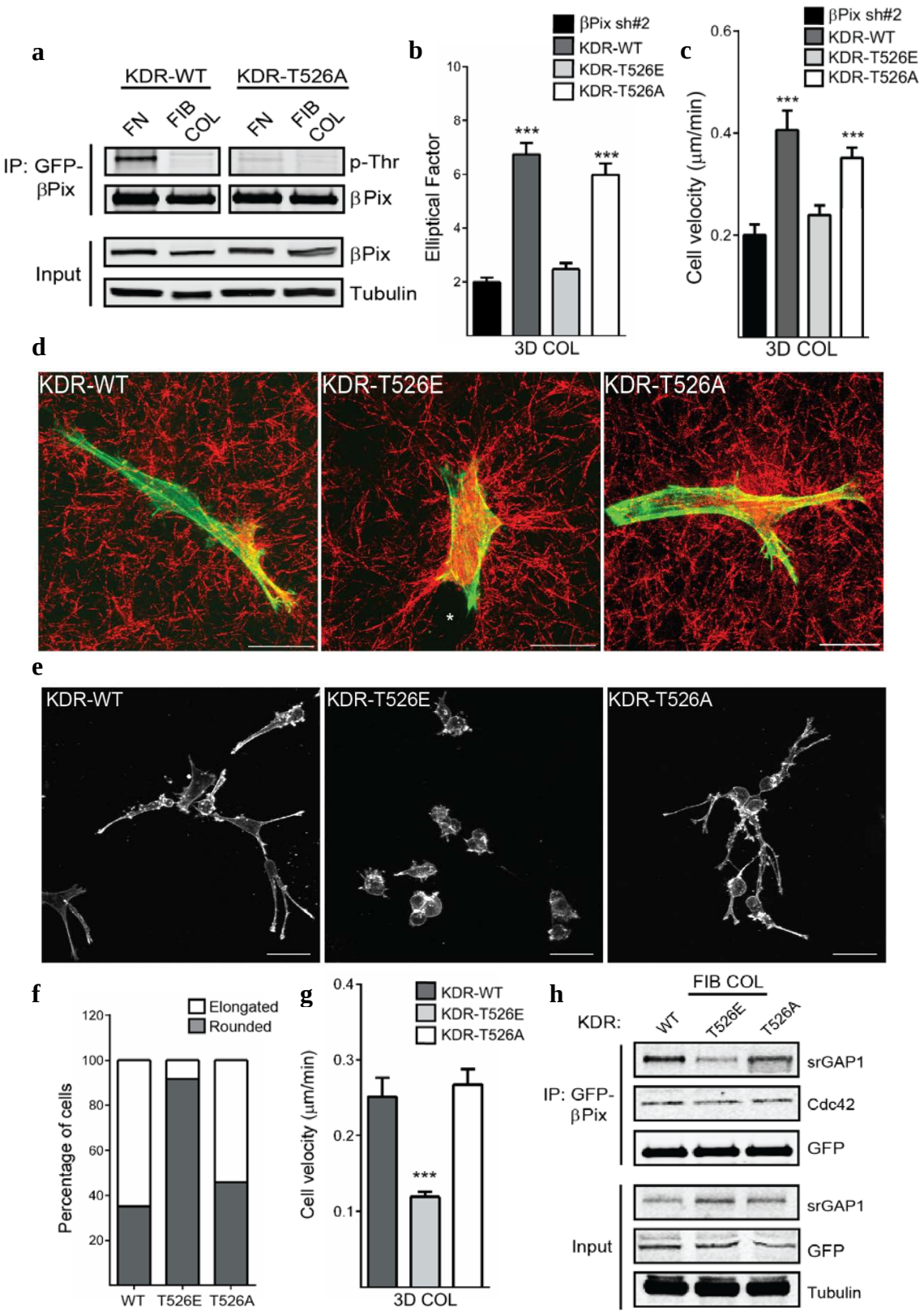
a
KDR-WT
KDR-T526A
FN
FIB
COL
FN
FIB
COL
IP: GFP-βPix
p-Thr
βPix
Input
βPix
Tubulin
b
βPix sh#2
KDR-WT
KDR-T526E
KDR-T526A
Elliptical Factor
10
8
6
4
2
***
***
3D COL
c
βPix sh#2
KDR-WT
KDR-T526E
KDR-T526A
Cell velocity (μm/min)
0.6
0.4
0.2
***
***
3D COL
d
KDR-WT
KDR-T526E
KDR-T526A
*
e
KDR-WT
KDR-T526E
KDR-T526A
f
Elongated
Rounded
Percentage of cells
120
100
80
60
40
20
WT
T526E
T526A
g
KDR-WT
KDR-T526E
KDR-T526A
Cell velocity (μm/min)
0.4
0.3
0.2
0.1
***
3D COL
h
FIB COL
KDR:
WT
T526E
T526A
IP: GFP-βPix
srGAP1
Cdc42
GFP
Input
srGAP1
GFP
Tubulin

**Figure 20**: **Collagen-specific phospho-regulation at threonine 526 is critical for βPix function and association with srGAP1. a** Western blot of KDR-WT GFP-βPix immunoprecipitated from knockdown/rescue cells migrating on fibronectin or fibrillar collagen for phospho-threonine showed a decrease in phosphorylation levels during migration on collagen. Immunoprecipitation of KDR-T526A βPix showed no change in phospho-threonine between FN and FIB COL, highlighting the functional importance of this residue. **b** Quantification of cell elliptical factor 3D collagen of βPix knockdown/rescue cells expressing wild type βPix and the phosphorylation variants (error bars represent s.e.m., n = 24, 20, 23, 19 cells, one-way ANOVA with Bonferroni correction). **c** Quantification of cell velocity in βPix knockdown/rescue phosphovariants in 3D collagen (error bars represent s.e.m., n = 25, 24, 22, 22 cells, one-way ANOVA with Bonferroni multiple comparisons correction). **d** We generated phospho-mimetic (T526E) and phospho-null (T526A) mutant βPix knockdown/rescue cells and assayed their morphology in 3D collagen. T526E βPix was insufficient to rescue the morphological and hyper-contractile phenotype of βPix knockdown (collagen fibers, red, reflection microscopy). T526A mutants efficiently rescued the βPix morphological and contractile defects. Scale bars, 25 μm. **e** Max projections of phalloidin-stained MDA-MB-231 knockdown/rescue cells expressing wild type βPix or the βPix phosphorylation variants migrating in 3D collagen. Scale bars, 50 μm. **f** Quantification of morphology of MDA-MB-231 knockdown/rescue cells expressing wild type βPix and the phosphorylation variants migrating in 3D collagen. Elongated cells defined as having an elliptical factor > 1.5 (n = 34, 36, 38 cells). **g** Quantification of migration velocities of MDA-MB-231 knockdown/rescue cells expressing wild type βPix or the phosphorylation variants migrating in 3D collagen (error bars represent s.e.m., n = 23, 21, 25 cells, one-way ANOVA with Bonferroni correction). **h** GFP-βPix was immunoprecipitated from HFFs expressing knockdown/rescue phosphovariants at Thr526 migrating on fibrillar collagen. We find that phosphorylation-mimetic (T526E) inhibits binding to srGAP1, but not Cdc42.

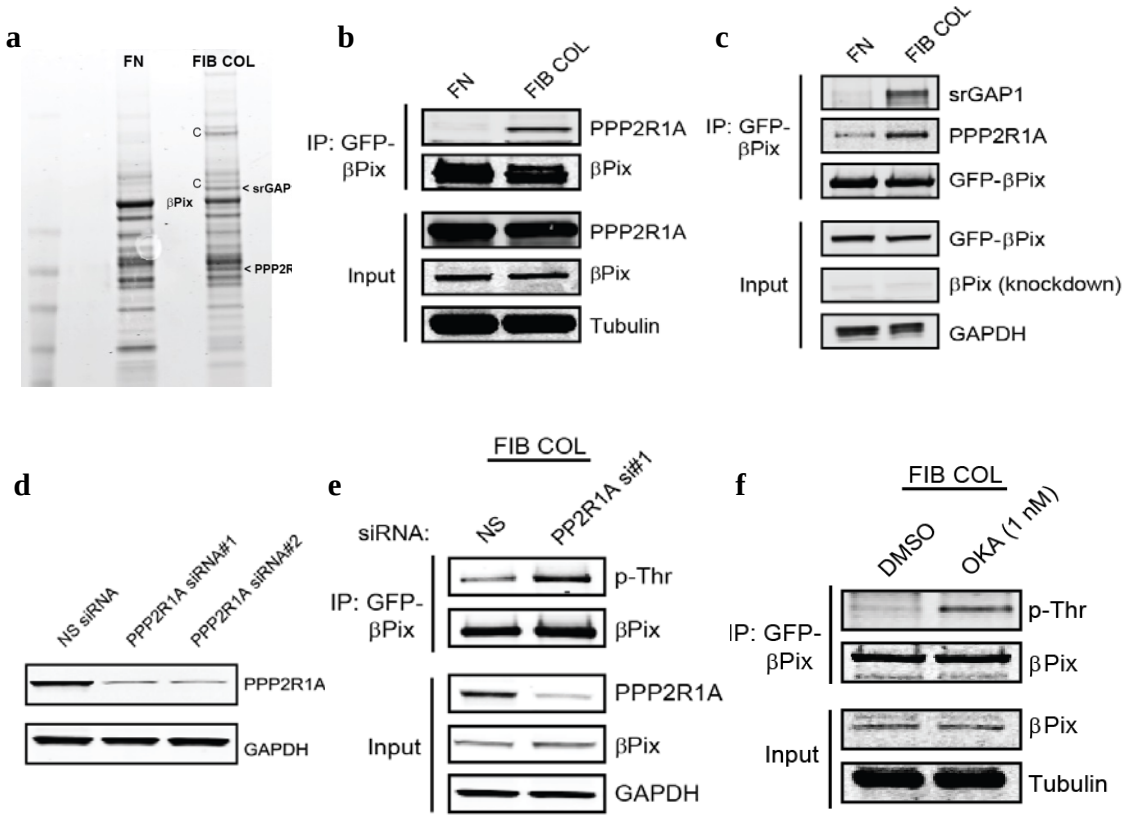


**Figure 21**: **Association between βPix and PPP2R1A regulates T526 dephosphorylation in response to fibrillar collagen. a** GFP-βPix knockdown/rescue cells were allowed to reach steady-state migration on fibronectin (FN) or fibrillar collagen (FIB COL). GFP-βPix was immunoprecipitated from cell lysates under each condition to search for matrix-specific associated proteins. Coomassie blue staining of protein bound to βPix revealed a unique ~130 kDa band (<srGAP1) and a ~65 kDa band (<PPP2R1A) that mass spectrometry identified as srGAP1 and PP2A regulatory subunit α isoform. "C" denotes bands from non-specific collagen binding. **b** Immunoprecipitation of GFP-βPix from βPix knockdown/rescue cells migrating on fibronectin versus fibrillar collagen identified a collagen-specific interaction between βPix and PP2A regulatory subunit A α isoform (PPP2R1A). **c** Immunoprecipitation of GFP-βPix from βPix knockdown/rescue MDA-MB-231 migrating on fibronectin (FN) versus fibrillar collagen (FIB COL) additionally showed collagen-specific associations between βPix and

PPP2R1A/srGAP1. **d** Single siRNA knockdown of PPP2R1A with two independent sequences. **e** GFP-βPix knockdown/rescue fibroblasts migrating on fibrillar collagen were treated with NS or PPP2R1A siRNA #1. We observed that knockdown or inhibition of PPP2R1A increased phospho-threonine levels on βPix during migration on collagen. **f** GFP-βPix knockdown/rescue fibroblasts migrating on fibrillar collagen were treated with DMSO or the PP2A inhibitor okadaic acid (OKA, 1 nM). Inhibition of PP2A with okadaic acid increased phospho-threonine levels on βPix during migration on collagen. All western blots are representative of at least three independent experiments.

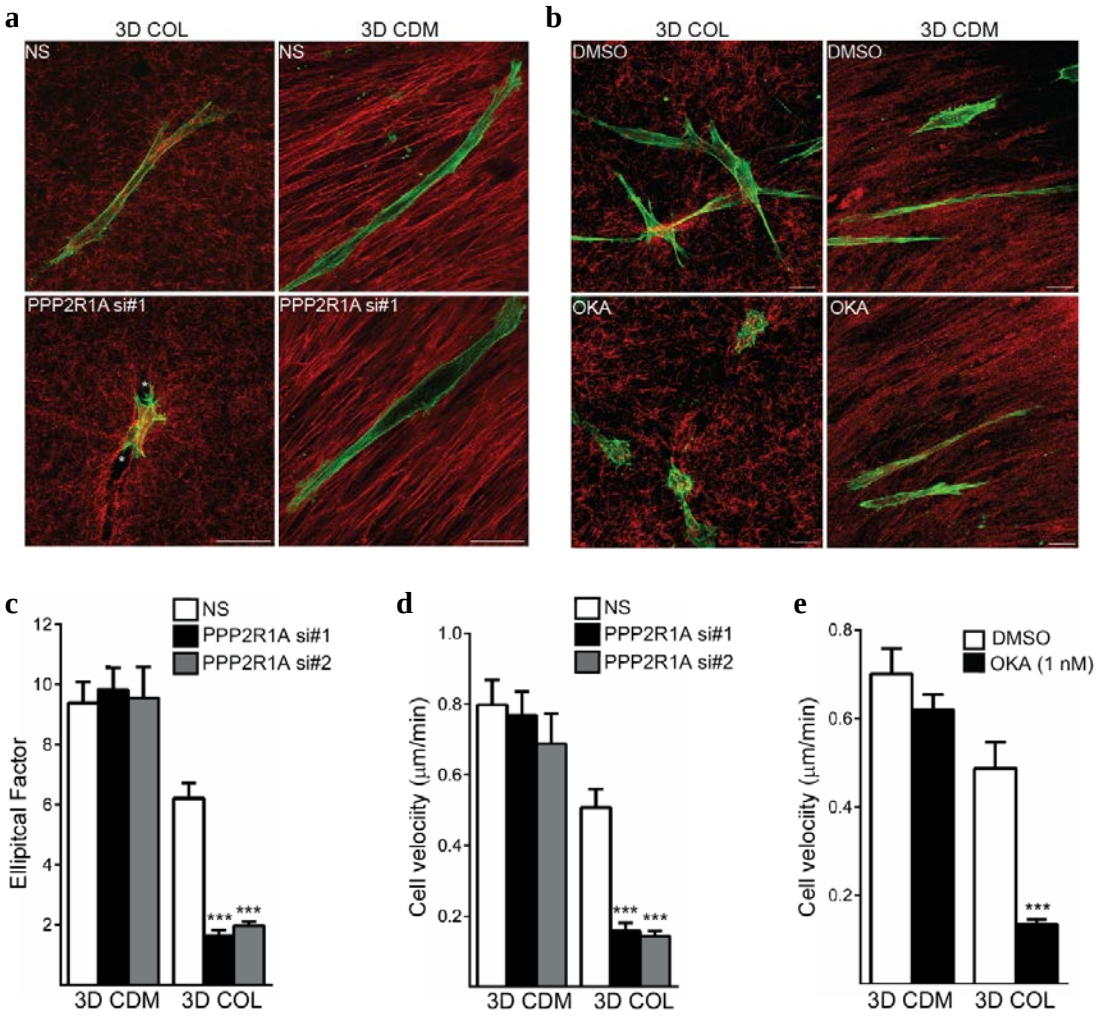


**Figure 22**: **Knockdown (PPP2R1A) or inhibition (OKA) of PP2A phenocopies βPix knockdown in 3D collagen matrices. a** Maximum projections of phalloidin-stained (green) HFFs in 3D collagen (red, reflection) or 3D cell-derived matrix (red, fibronectin immunostaining) treated with NS or with PPP2R1A siRNA #1. Scale bars 25 µm. **b** Maximum projections of phalloidin-stained (green) HFFs in 3D collagen (red, reflection) or 3D cell-derived matrix (red, reflection) treated with DMSO or with the PP2A inhibitor okadaic acid (1 nM) overnight prior to fixation. Inhibition of PP2A resulted in collagen-specific morphological defects. Scale bars 25 µm. **c** Quantification of morphology of PPP2R1A siRNA-treated HFFs in 3D collagen (error bars represent s.e.m., n = 32, 24, 19, 30, 32, 22 cells, one-way ANOVA with Bonferroni correction). **d** Quantification of

migration velocities of PPP2R1A siRNA-treated HFFs in 3D collagen. Two independent siRNAs toward PPP2R1A mimic βPix knockdown morphology and migration in 3D collagen (error bars represent s.e.m., n = 20, 22, 16, 20, 20, 17 cells, one-way ANOVA with Bonferroni correction). **e** Quantification of migration velocities of okadaic acid-treated (1 nM) HFFs in 3D collagen and 3D cell-derived matrix (error bars represent s.e.m., n = 19, 20, 20, 20, *t*-tests). *** $P < 0.001$ * $P < 0.05$.

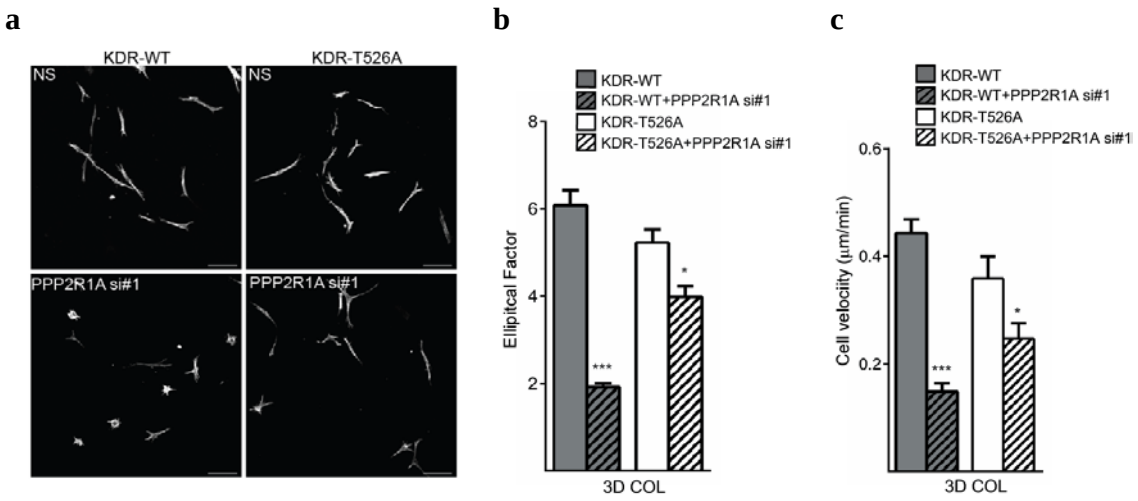


**Figure 23**: **T526A mutation in βPix knockdown/rescue cells is sufficient to rescue knockdown of PPP2R1A. a** Maximum projection of phalloidin-stained KDR-WT or KDR-T526A HFFs treated with NS or PPP2R1A siRNA #1 migrating in 3D collagen. Scale bars, 50 µm. **b** Morphological quantification of KDR-WT or KDR-T526A HFFs treated with NS or PPP2R1A siRNA #1 in 3D collagen. (error bars represent s.e.m., n = 40, 31, 35, 38 cells, *t*-tests). **c** Quantification of cell velocities in KDR-WT or KDR-T526A HFFs treated with NS or PPP2R1A siRNA #1 in 3D collagen. (error bars represent s.e.m., n = 26, 24, 24, 24 cells, *t*-tests). *** $P < 0.001$ * $P < 0.05$.

# CONCLUSION

## THE ROLE OF βPIX DURING MIGRATION IN FIBRILLAR COLLAGEN MICROENVIRONMENTS

Investigations into cell migration in 3D settings have revealed that certain extracellular matrix environments place differential requirements on the activity of the Rho GTPases for efficient migration. A fundamental unanswered question is how the specific activity of the Rho GTPases is modulated to direct cell migration when cells interact with different extracellular matrix ligands. We initiated this study with the hypothesis that adhesion to different matrix molecules, such as collagen and fibronectin, would trigger differential regulation of guanine nucleotide exchange factors to regulate migration. Our findings have established that ECM-dependent regulation of a specific GEF is a fundamental mechanism governing migration in different microenvironments, and we provide a direct mechanism for ECM-specific regulation of Rho GTPase activity directing cell migration. We demonstrate that βPix is critical for efficient migration in fibrillar collagen environments by restraining RhoA signaling. Unexpectedly, this suppression occurs through a mechanism of Rho GTPase crosstalk between Cdc42 and RhoA that is regulated by a collagen-specific interaction between the GEF/GAP pair, βPix and srGAP1. In addition, our model suggests that the collagen-specific βPix function is dictated by tight phospho-regulation of T526 on βPix. Binding of $\alpha_2\beta_1$ to

fibrillar collagen leads, through PP2A, to loss of phosphorylation at T526 on βPix and promotes association with srGAP1 (Figure 24). Taken together, we have defined a conserved migratory signaling cascade involving PP2A/βPix/srGAP1 that coordinates suppressive crosstalk between Cdc42 and RhoA that is critical for cell migration in fibrillar collagen environments.

The existence of extracellular matrix-specific pathways directing cell migration might at first seem physiologically unnecessary, considering the heterogeneous nature of most environments found in vivo. However, these mechanisms allow for an additional tier of control over the plasticity of cell migratory behavior in response to cues from each cell's extracellular environment. It provides the capacity for local changes in extracellular matrix composition and organization to elicit precise spatial control over the movement of cells during tightly regulated processes such as epithelial morphogenesis, angiogenesis and wound healing. For example, and particularly relevant to this dissertation, gradients of type I collagen fibers are sufficient to drive cytokine-independent angiogenesis. In fact, the increased angiogenic migratory response downstream of endothelial cell adhesion to fibrillar collagen was attributed to suppression of PKA activity, a reported kinase for T526 on βPix, highlighting a potential therapeutic application of this collagen-specific βPix pathway (Whelan and Senger, 2003). It is surprising that no singular Rac1 GEF was identified as specifically active in response to fibronectin. However, this finding may indicate that the migratory machinery in response to fibronectin is driven by Cdc42, RhoA, non-canonical GTPases such as RhoC/E/G and Rac2/3, or through some complex concerted action of multiple GTPases. Still, we speculate that this and other

potential extracellular matrix-specific GEF mechanisms will emerge that provide local contextual regulation of cell migration in different microenvironments.

One intriguing element of this dissertation is that we have identified a pathway of active RhoA suppression, a GTPase classically associated with controlling the contractile, or mechanotransductive, response of the cell to the microenvironment. Traditionally when we consider cell mechanotransduction, tension-sensitive proteins are activated through conformational changes in response to increased rigidity of the surrounding microenvironment. The collagen-specific βPix pathway of Cdc42-RhoA crosstalk identified here contrasts with this idea, where seemingly the activity of RhoA is inherently high, yet actively suppressed by βPix in response to fibrillar collagen. It is unclear what environmental factors may be influencing RhoA activity, whether it is induced by growth-factor signaling from serum or a physical aspect of the collagen matrix. However, what this pathway potentially provides is an alternative to the classical view of mechanotransduction, a tunable RhoA responsive mechanism that is adaptable to changes in collagen matrix rigidity. In essence, increases in matrix rigidity could modulate the phosphorylation of βPix at T526, which would decrease the activity of Cdc42/srGAP1, remove the suppressive check on RhoA, and permit the contractile forces required for efficient migration. This possibility could be tested by assaying the effect of βPix knockdown on morphology and migration, as well as the threonine phosphorylation state of βPix, in fibrillar collagen environments of increased rigidity through chemical crosslinking or altered polymerization methods.

Although there are many complex interactions and crosstalk occurring at the leading edge of cells during migration, the βPix/srGAP1 complex provides an elegant

mechanism for restricting RhoA and concentrating Cdc42 activity toward the leading edge in collagen microenvironments. How the cell is able to regulate signaling spatially and temporally across many aspects of cell physiology is currently a major area of investigation. While reports of GEFs and GAPs acting in concert to control migration mode exist (Sanz-Moreno et al., 2008), we report here a GEF/GAP interaction directly shown to spatially control intracellular Rho GTPase crosstalk. We speculate that this and other potential specific GEF/GAP interactions could provide local contextual regulation in other extracellular matrix microenvironments that affects differentiation, morphogenesis, and tumor progression through RhoA signaling (Daley et al., 2012; Engler et al., 2006; Levental et al., 2009).

The discovery of a central role for βPix in directing a conserved, collagen-specific migratory pathway has potential therapeutic implications. As mentioned earlier in the Conclusion, our identification of the conservation of the βPix pathway in HUVEC cells in conjunction with the evidence for type I collagen-triggered angiogenesis suggests a contextual anti-angiogenic application for the inhibition of βPix. A particularly exciting potential application can be surmised from the role of fibrillar type I collagen during tumor progression and metastasis. The linearization and perpendicular reorganization of fibrillar type I collagen to the tumor front is a classic marker of malignant transformation and metastatic potential (Levental et al., 2009; Provenzano et al., 2006). These fibrillar collagen “tracks” serve as metastatic highways for transformed cells, facilitating dissemination away from the primary tumor (Condeelis and Pollard, 2006). Inhibition of βPix in the metastatic breast adenocarcinoma MDA-MB-231 line blocks nearly all motility of these normally highly motile cells in 3D collagen. Therefore, inhibition of

βPix may have potential as an anti-metastatic therapeutic, particularly in collagen-dense environments like the skin and breast, by preventing cell migration away from the primary tumor.

While the results of this dissertation provide a detailed mechanistic understanding of the identified collagen-specific migratory pathway, future areas of investigation exist. The dramatic transition of βPix away from focal adhesions to the plasma membrane on fibrillar collagen is indicative of function, but it is unclear what mechanisms regulate this transition. Approximately 40% of human Rho GEFs contain a PDZ-binding motif, a protein-protein interaction domain important for localized signal transduction (Garcia-Mata and Burridge, 2007), which βPix contains in its coiled-coil C-terminus. While we have ruled out βPix binding to the previously reported PDZ-containing proteins hScrib and Shank, it is possible that a PDZ-mediated interaction with another scaffolding protein may be directing βPix localization in response to fibrillar collagen. However, we speculate that it is the βPix interaction with srGAP1 that facilitates membrane localization. While srGAP1 does not contain a PDZ-domain, it contains two membrane-binding F-BAR domains. The critical phospho-regulation of βPix at T526 falls in its primary protein-protein interaction domain and is crucial for association with srGAP1. Preliminary evidence of transient over-expression of mApple-srGAP1 in GFP-βPix knockdown/rescue cells indicated co-localization in the membrane puncta observed on fibrillar collagen. We therefore propose that it is the association with srGAP1 that directs the localization of βPix away from the focal adhesion to the plasma membrane.

An additional future direction is investigating how Cdc42 modulates the GAP activity of srGAP1 toward RhoA. Cdc42 binding to srGAP1 may be sufficient to trigger

allosteric conformational shifts in srGAP1 that are amenable to active RhoA binding. However, more commonly Cdc42 affects the activity of a particular kinase to induce phosphorylation changes on target proteins, in this case srGAP1. Preliminary mass spectrometry analysis of βPix binding proteins did identify candidate kinases that may be involved in the Cdc42 activation of srGAP1, including Pak2, Akt, Cdk9/10, and Tao2. Additionally, the observed differential GAP activity of srGAP1 toward RhoA (on collagen) and Rac1 (on fibronectin) suggests that phospho-regulation may direct its function. To address this point, analysis of ECM-specific phosphorylation changes on srGAP1 should be conducted by methods similar to those presented in this dissertation, along with protein knockdown of candidate kinases to evaluate their potential role in the pathway.

We initiated this study with the hypothesis that cell adhesion to different extracellular matrix molecules modulates the activity of specific Rac1 GEFs to control migration. The activity of the Rac1/Cdc42 GEF βPix was identified to be specifically and robustly increased in response to collagen, and knockdown of βPix nearly abolished all motility specifically in fibrillar collagen environments. Unexpectedly, βPix was discovered to act through Cdc42 to maintain suppressive crosstalk with RhoA during migration. This crosstalk was achieved through the novel GEF/GAP interaction of βPix and srGAP1, which is regulated by the phosphorylation state of βPix at T526 by PP2A downstream of fibrillar collagen. We have established that ECM-dependent regulation of a specific GEF is a fundamental mechanism governing migration in different extracellular matrix environments. It will be of interest to expand this approach to different Rho GTPases and to determine whether modulation of GEF activity directs cell

migration in response to different chemical and physical properties of the extracellular matrix. By doing so, we would gain a greater understanding of how cells respond to and navigate the complex extracellular matrix environment found in vivo and how to potentially intervene when these processes become deregulated.

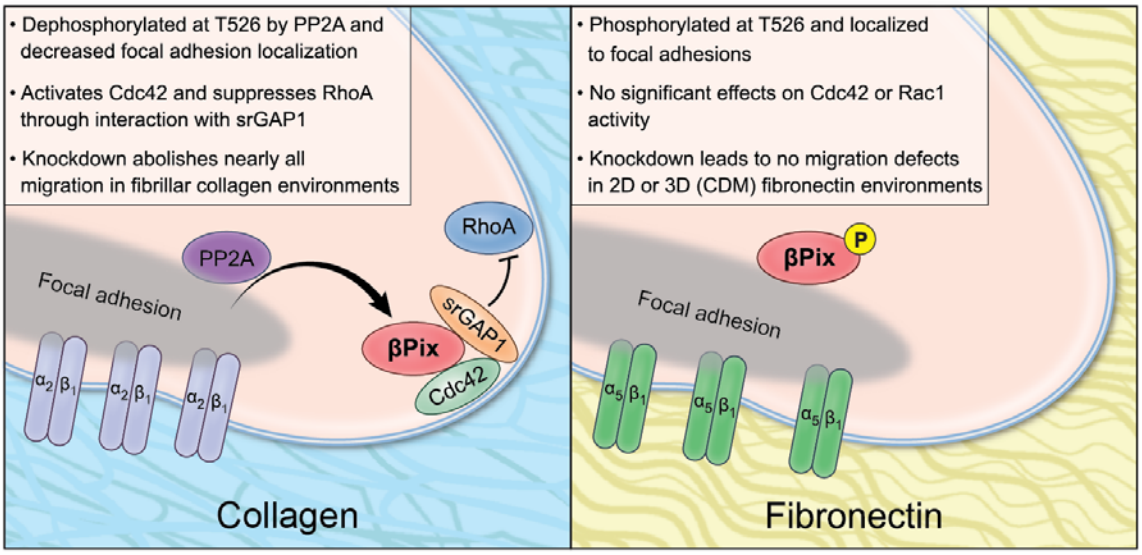


**Figure 24**: **Summary model of the collagen-specific role of βPix during migration in fibrillar collagen environments.**

## MATERIALS AND METHODS

### Cell lines and reagents

Primary human foreskin fibroblasts (HFFs), immortalized human fibroblasts (BJ5Ta and BR5, ATCC), human adenocarcinoma line MDA-MB-231, primary human osteoblasts (NhOst, Lonza), and HEK 293FT cells were cultured in phenol red-free DMEM (Hyclone) supplemented with 10% fetal bovine serum (Hyclone), 100 U/ml penicillin, 100 µg/ml streptomycin (Invitrogen), and 2 mM L-glutamine (Invitrogen) at 37°C in 10% $CO_2$ in a humidified incubator. Human umbilical vein endothelial cells (HUVECs) and human aortic smooth muscle cells (AOSMCs, Lonza) were cultured in phenol red-free DMEM (Hyclone) supplemented with 5% fetal bovine serum (Hyclone), insulin, hFGF, and hEGF (Lonza, SMGM-2 BulletKit) at 37°C in 5% $CO_2$. The following reagents were used in this study: rhodamine- and Alexa488-phallodin (Invitrogen), cell-permeable C3 transferase (Cytoskeleton), blebbistatin and okadaic acid (EMD), and GFP-TRAP GFP-binding protein (Chromotek). GFP-RhoQ63L was transfected into cells with the Nucleofector system (Lonza) using the NDHF kit (Lonza) according to the manufacturer's instructions. Equal concentrations of the DMSO vehicle were used as controls for drug studies.

### Antibodies

The anti-βPix antibody (07-1450, 1:1000), anti-GFP (3F8.2, 1:1000), anti-PAK1 (EP656Y, 1:500), anti-Rac3 (07-2151, 1:500), anti-Rac2 (07-604, 1:500), and anti-PPPR2A1 (07-250, 1:1000) were from Millipore. Anti-Rac1 (102, 1:1000), anti-Cdc42 (44, 1:500), and anti-paxillin (349, 1:100) were from BD Biosciences. Anti-RhoA antibody (ab54835, 1:1000) and anti-beta tubulin (ab6046, 1:5000) were from Abcam.

Anti-p-Threonine (42H4, 1:500) antibody was from Cell Signaling. Rabbit polyclonal antibody (5836, 1:2500) toward fibronectin was produced in-house. Anti-GAPDH (6c5, 1:5000) was from Fitzgerald and anti-actin (AC-40, 1:1000) was from Sigma. Anti-srGAP1 (286A, 1:500) was from Bethyl laboratories, and anti-SmgGDS was from Novus Biologicals.

**RNA-mediated interference**

Individual ON-TARGETplus siRNAs toward βPix, srGAP1, Rac3, Rac2, and PPP2R1A (Dharmacon-Thermo Scientific) and previously validated Rho GTPase siRNAs toward Rac1 and Cdc42 (Silencer Select, Invitrogen) were used for protein knockdown. All protein knockdowns were conducted with at least two independent RNAi sequences. For specific sequence information and labels see Supplementary Table 1. siRNAs were transfected into cells using Lipofectamine 2000 (Invitrogen) as previously described (Petrie et al., 2012).

**Lentiviral-mediated generation of stable fibroblast lines**

Stable βPix knockdown and knockdown-rescue cells lines in primary HFFs were generated using the pLL 3.7 lentiviral packing system (11795, Addgene) as described previously (Cai et al., 2007). Two independent shRNA hairpins targeting βPix regions: shRNA#2: 5'-GGAAGAAGATGCTCAGATT-3' and shRNA#4: 5'-GTAGTAAGAGCAAAGTTTA-3', along with a nonspecific control, 5'-GGAATCTCATTCGATGCAT-3' were cloned into the pLL3.7 lentiviral vector. For knockdown-rescue constructs, βPix cDNA (Origene) was cloned into pLL3.7 at the NheI-EcoRI restriction sites, creating C-terminal tagged GFP-βPix. The QuikChange Site-Directed Mutagenesis kit (Stratagene) was used to create three nucleotide substitutions

that did not perturb the amino acid sequence in βPix to generate a shRNA-resistant construct. Additionally, similar mutagenesis techniques were used to introduce phospho-mimetic (KDR-T526E) and phospho-dead (KDR-T526A) mutations into βPix cDNA in the pLL 3.7 knockdown-rescue construct. GFP or mCherry-positive cells were isolated by fluorescence-activated cell sorting (BD FACS ARIA).

**Purification of recombinant proteins**

RacG15A and Cdc42G15A were cloned into pGEX4T-1 using the EcoRI-BamHI restriction sites. pGEX4T-1 constructs containing the Rho-binding domain (3x RBD) of Rhotekin cDNA was a kind gift from Silvio Gutkind (NIDCR) and the p21-binding domain of Pak1 (PBD) was from Addgene (Plasmid 12217). Briefly, expression of the GST fusion proteins in *BL21 Escherichia coli* was induced with 200 μM isopropyl-β-$_D$-thiogalactoside (IPTG) for 12-16 hours at room temperature. Bacterial cells were lysed in buffer containing 20 mM HEPES pH 7.6, 1% Triton X-100, 150 mM NaCl, 5 mM $MgCl_2$, 1 mM dithiothreitol, protease and phosphatase inhibitor cocktails (Roche), and the proteins were purified by incubation with glutathione-Sepharose 4B beads (GE Healthcare) at 4 $^oC$.

**Mass spectrometry analysis**

Single, excised Coomassie stained bands for protein identification and phosphorylation analysis were analyzed by MS Bioworks as follows. In-gel digestion was performed using a ProGest robot (DigiLab). Gel bands were washed with 25 mM ammonium bicarbonate followed by acetonitrile, reduced with 10 mM dithiothreitol at 60°C followed by alkylation with 50 mM iodoacetamide at room temperature, digested with trypsin (Worthington) at 37°C f or 4h, and quenched with formic acid, and the

supernatant was analyzed directly without further processing. Each digested sample was analyzed by nano LC/MS/MS with a Waters NanoAcquity HPLC system interfaced to a ThermoFisher Q Exactive mass spectrometer. 30 μL of sample was loaded on a trapping column and eluted over a 75 μm analytical column at 350 nL/min; both columns were packed with Jupiter Proteo resin (Phenomenex). The mass spectrometer was operated in data-dependent mode, with MS and MS/MS performed in the Orbitrap at 70,000 and 17,500 FWHM resolution, respectively. The fifteen most abundant ions were selected for MS/MS. LC/MS/MS data were analyzed using the MASCOT algorithm, with trypsin specified as the digestion enzyme (two max missed cleavages) and all data searched against the SwissProt Human database (forward and reverse appended with common contaminant proteins). Carbamidomethylation (C) was set as fixed modification. For protein identification, Oxidation (M), Acetyl (N-term), Pyro-Glu (N-term Q), Deamidation (N,Q) were selected as variable. For phosphoanalysis, the same modifications were variable, in addition to Phospho (S-T-Y). Peptide mass tolerances were set to 10 ppm and fragment mass tolerance set to ± 0.015 Da. Mascot DAT files were parsed into the Scaffold software for validation, filtering and to create a non-redundant list per sample. The data were filtered using a minimum protein value of 80%, and a minimum peptide value of 50% (Prophet scores).

**GEF activity and GTPase activity affinity assays**

GST-RacG15A active GEF-pulldown experiments were carried out as described previously (Garcia-Mata et al., 2006). Dishes were coated with 10 μg/ml human plasma-derived fibronectin or 50 μg/ml rat tail type I collagen overnight at 4$^{o}$C. HFFs were serum starved for 2 hours prior to plating, then plated in serum-free DMEM and allowed

to reach steady-state migration over 12-16 hours. Cells were lysed in 20 mM HEPES pH 7.6, 1% Triton X-100, 150 mM NaCl, 5 mM $MgCl_2$, 1 mM dithiothreitol, protease and phosphatase inhibitor cocktails (Roche) and sonicated at 3W on ice for five seconds at $4^oC$ using a Misonix Microson XL sonicator. Lysates adjusted to equal quantities and concentration of protein were incubated with 25 µg of purified GST-RacG15A or GST-Cdc42G15A for 1 hour at $4^oC$. Samples were washed in lysis buffer (3 times for Western blotting or 5 times for mass spectrometry) and analyzed by SDS-PAGE using Novex® Tris-Glycine 4-12% polyacrylamide gels (Invitrogen). For identification of the GEFs bound to RacG15A by mass spectrometry, SDS-PAGE gels were Coomassie-stained with GelCode Blue Stain Reagent (Pierce). Bands of interest were extracted and identified using nano LC/MS/MS (MS Bioworks). For active RhoA, Cdc42 and Rac1-pulldowns, plates and cells were prepared as indicated above. Fibroblasts that were cultured overnight in complete media (RhoA) or serum-free media (Rac1, Cdc42) were lysed in 50 mM Tris pH 7.6, 200 mM NaCl, 1% Triton X-100, 0.5% deoxycholate, 5 mM $MgCl_2$, and protease and phosphatase inhibitor cocktails, sonicated at 3W on ice for five seconds, and clarified at 12,000xg for 5 minutes. Lysates were equalized for protein content and volume and rotated at $4^oC$ for 1 hour with either 20 µg GST-RBD or 30 µg GST-PBD. Bead pellets were washed three times with lysis buffer and analyzed by SDS-PAGE as described above. Polyacrylamide gels were transferred to nitrocellulose membranes using the semi-dry iBlot® transfer system (Invitrogen). Membranes were blocked with Odyssey blocking buffer (LI-COR) for one hour at room temperature. Primary antibodies were incubated with membranes in Odyssey blocking buffer containing 0.1% Tween-20 overnight at $4^oC$. Membranes were washed with TBS containing 0.1% Tween-20 (TBST)

three times over 30 minutes. IRDye-conjugated anti-mouse and rabbit secondary antibodies (1:20,000) (LI-COR) were incubated in Odyssey blocking buffer containing 0.1% Tween-20 for 30 minutes at room temperature. Membranes were then washed with TBS containing 0.1% Tween-20 (TBST) three times over 30 minutes. All Western blots were imaged and quantified using the Odyssey imaging system through the analyze module (LI-COR). Intensity values were normalized to load control (tubulin or GAPDH).

**Membrane fractionation and immunoprecipitation**

For Triton X-100 membrane fractionation, cells cultured on matrix overnight in complete media were lysed in 50 mM Tris pH 7.6, 150 mM NaCl, 1% Triton X-100, and protease and phosphatase inhibitor cocktails. Lysates were vortexed and incubated by end-over-end rotation for 20 minutes at 4$^{o}$C. Cell lysates were fractionated by centrifuging at 13,000 rpm for 15 minutes. The resulting pellets (insoluble fraction) were washed three times with lysis buffer and then denatured in 2x Novex sample buffer (Invitrogen) containing 100 µM dithiothreitol for 5 minutes at 95$^{o}$C. Pellets were compared to supernatant (soluble fraction) by SDS-PAGE using Novex® Tris-Glycine 4-12% polyacrylamide gels (Invitrogen). For immunoprecipitation of GFP-βPix from fibrillar collagen environments, cells cultured on matrix overnight in complete media were lysed in 50 mM Tris pH 7.6, 200 mM NaCl, 1% Triton X-100, 0.5% deoxycholate, 5 mM $MgCl_2$, and protease and phosphatase inhibitor cocktails (Roche), homogenized using 200-1000 µl positive displacement pipets (Anachem), sonicated at 3W on ice for three seconds, and incubated for 7 minutes with end-over-end rotation at 4$^{o}$C. Lysates were clarified by centrifugation at 12,000xg, equalized for protein content and volume, and incubated for 1 hour with 30 µl of GFP-TRAP (Chromotek) conjugated to magnetic

beads at 4°C with end-over-end rotation. For mass spectrometry analysis, beads were washed five times with lysis buffer and analyzed by SDS-PAGE and Coomassie blue staining. For the identification of srGAP1, excised gel bands were analyzed using nano LC/MS/MS (MS Bioworks).

**Generation of cell-derived matrices (CDMs)**

CDMs were prepared from HFFs as described previously[9]. MatTek dishes were coated with 0.2% gelatin for 1 h at 37°C, treated with 1% glutaraldehyde for 30 min at RT, and incubated with DME for 30 min at RT. Three washes with Dulbecco's PBS with calcium and magnesium (PBS+) followed each treatment. $4 \times 10^5$ HFFs were plated per MatTek dish, which were maintained for 10 d, adding fresh media with 50 µg/ml ascorbic acid every other day. The cells were removed from the CDM with extraction buffer (20 mM $NH_4OH$ and 0.5% Triton X-100 in PBS+) for 5 min at RT and washed with PBS+. The cell-free CDM was treated with 10 U/ml DNase (Roche) for 30 min at 37°C, washed with Dulbecco's PBS without calcium and magnesium (PBS), and stored at 4°C in PBS with 100 U/ml penicillin and 100 µg/ml streptomycin.

**Generation of fibrillar collagen matrices and time lapse microscopy**

2 mg/ml fibrillar collagen gel solutions were prepared by mixing rat tail type I collagen with 10x reconstitution buffer (0.26 M $NaHCO_3$ and 0.2 M HEPES) and 10X DME (Sigma), adjusting the pH to 7.4 with 1M NaOH, and then diluting to 2 mg/ml with PBS+ To generate thin fibrillar collagen substrates, 30 µl of solution was spread on a 20 mm MatTek dish and allowed to polymerize for 1 hour at room temperature. Using these substrates for biochemical assays facilitated cellular extraction and minimized collagen contamination in comparison to 3D collagen. Additionally, these substrates minimized

light scatter during imaging, while still providing the fibrillar collagen substrate required for the βPix knockdown phenotype. Fibroblasts were plated in complete medium overnight and assayed for motility the following day. For 3D collagen gels, cells were resuspended in PBS+ and mixed with the prepared collagen mixture. The collagen-cell mixture was spread on MatTek dishes and allowed to polymerize at room temperature for 1 hour. Complete medium was added to the gels, and the cells were assayed for motility the next day. For phase contrast microscopy timelapse imaging of fibroblasts in different matrix environments, complete medium was added prior to image acquisition. For inhibitor treatments, vehicle control or inhibitors were incubated with cells for 4-6 hours before beginning the timelapse. Random cell migration was imaged for 24 hours in 37$^{o}$C, 10% $CO_2$ environmental chambers. Timelapse videos were recorded on a microscope (Axiovert 135TV; Carl Zeiss, Inc.) fitted with a motorized xy- and z-stage focus drive (Ludl Electronic Products Ltd.) using an enhanced contrast Plan-Neofluar 10× 0.3 NA or a long-working distance Plan-Neofluar Korr 20× 0.4 NA objective (Carl Zeiss, Inc.). Images were acquired with a charge-coupled device camera (ORCA II ER; Hamamatsu Photonics). Microscopy images were adjusted for brightness and contrast and cells were tracked manually using MetaMorph software.

**Live cell fluorescence and FRET imaging**

Fibroblasts were imaged with a modified Yokogawa spinning-disk confocal scan head (CSU-21: modified by Spectral Applied Research Inc.) attached to an automated Olympus IX-81 microscope using a 60X SAPO-Chromat silicone oil objective (N.A. 1.3). A custom laser launch equipped with 442 nm (40 mW: Melles Griot), 488 nm (150 mW: Coherent), 514 nm (150 mW: Coherent), 568 nm (100 mW: Coherent), and 642 nm

(110 mW: Vortran) diode lasers supplied excitation wavelengths. A Gooch and Housego AOTF controlled shuttering and intensity for 488, 514, and 568 laser lines. 442 and 642 lines were shuttered and intensity controlled via TTL and direct voltage steps, respectively. The primary dichroics (442/568/647 and 405/488/568/647) were from Semrock. Images were captured using a backthinned EM CCD camera in 16-bit format using the 10 MHz digitization setting (Roper Scientific).

mCherry was cloned into pLL3.7 in place of GFP to allow FRET compatibility. mCherry-βPix knockdown fibroblasts were generated with the shRNA#2 hairpin. The binding of active Cdc42 or RhoA was detected by imaging the FRET-dependent, intramolecular emission fluorophore (YPet) from YPet-PAK-EV-Cdc42-CFP or YPet-RBD-EV-RhoA-CFP [24] (kind gifts from M. Matsuda). Fibroblasts were transfected as indicated using the Nucleofector system (Amaxa) according to the manufacturer's instructions. The next day, cells were trypsinized and plated onto fibronectin or fibrillar collagen matrices in complete media and allowed to adhere overnight. Cells were imaged the following morning in 5% fetal bovine serum, phenol-red free DMEM with 10 units/ml Oxyrase. Optimal FRET acquisition settings were determined for the Olympus IX-81 spinning disc microscope and strictly maintained during all subsequent FRET imaging; intensity levels of biosensor expression were similarly carefully controlled and maintained between selected cells. Ratio FRET images were obtained as previously described (Hodgson et al., 2010). Images of CFP and YPet were obtained for each z-plane under 442 nm illumination. Maximum projections of confocal z-stacks were generated using MetaMorph software. Images were first background subtracted and a binary mask was applied by thresholding to the cytoplasmic mCherry-lentiviral marker to

isolate the cellular signal. FRET ratio images were generated in MetaMorph using the arithmetic module, with a universally applied scaling factor of 1000. All resulting FRET images were processed with a 3x3 median filter to remove any hot pixels and presented in a pseudocolor map (MetaMorph). The same pseudocolor intensity scale was maintained for each ECM condition for the NS and βPix shRNA conditions. Polarization index (PI) was calculated as previously described[9] using the five highest points of FRET intensity per cell analyzed. A PI of 1 = forward polarization, 0 = nonpolarization (regions are uniformly distributed), and −1 = rearward polarization.

**Immunofluorescence**

For morphological analysis in 3D collagen or CDM and immunolocalization of Cdc42, cells cultured in complete medium were fixed with 4% paraformaldehyde in PBS+, permeabilized with 0.25% Triton X-100 in PBS+, and blocked with 1% BSA in PBS+. Rhodamine- or Alexa488-phalloidin and primary and secondary antibodies were applied in 1% BSA in PBS+ and samples were rinsed with PBS+ three times over 30 minutes between each treatment. Elliptical factor (E.F.) was calculated as the ratio of cell length to cell width at maximal points in 3D reconstructions using MetaMorph software. For localization analysis of βPix to focal adhesions on fibrillar collagen, cells were fixed-permeabilized with 3% paraformaldehyde-0.5% Triton X-100 in PBS+ at 37$^{o}$C followed by an additional fixation with 4% paraformaldehyde. Cells were blocked with 1% BSA in PBS+. Primary and secondary antibodies were applied in 1% BSA in PBS+ and rinsed three times over thirty minutes with PBS+ between each treatment. For all confocal microscope immunofluorescence analyses, cells were imaged with the same Yokogawa CSU-21/Olympus IX-81 spinning disc microscope listed for live-cell imaging with a 60X

SAPO-Chromat silicone oil objective (N.A. 1.3) for morphological imaging and a Plan Apo N 150× 1.45 NA objective (TIRFM UIS2; Olympus) for βPix localization imaging. For analysis of βPix localization to focal adhesions after plating of cells on monoclonal integrin antibodies, dishes were coated with poly-$_L$-lysine for ten minutes at room temperature, washed with PBS+, and incubated with each antibody in PBS+ for 1 hour at 37$^o$C. Dishes were washed three times with PBS+ and blocked for a further hour at 37$^o$C with 1% BSA. GFP-βPix KDR (knockdown-rescue) cells were plated in complete media overnight. The next day, the same fix-permeabilization methodology was used as described above. Cells were imaged using TIRF microscopy, performed using an Olympus IX-71 microscope using a Plan Apo N 60× 1.45 NA objective (TIRFM UIS2; Olympus). Fluorescence images were adjusted for brightness and contrast using MetaMorph software.

**Statistical analysis**

When experiments involved only a single pair of conditions, statistical differences between the two sets of data were analyzed with a two-tailed, unpaired Student *t*-test with Prism5 (GraphPad Software). For data sets containing more than two samples, one-way ANOVA with a classical Bonferroni multiple comparisons post-test was used to determine adjusted *P* values. Sample sizes of sufficient power were chosen based on similar published research and were confirmed statistically by appropriate tests. Experiments were not randomized. However, the investigator was blinded during the assessment of key morphological and migratory experiments involving βPix, Cdc42, Rac1, and srGAP1 knockdowns under different matrix conditions by using randomization of data labels. For cell tracking quantification, cells were manually tracked by M.L.K. by

through the MetaMorph Track Objects plugin. Primary statistics source data for all main and supplementary figures are available in Supplementary Table 2. Statistically significant differences are reported at *, $P < 0.05$, **, $P < 0.01$ and ***, $P < 0.001$.

| Protein Target | Sequence Name | Sequence |
|---|---|---|
| **NS (control)** | NS siRNA | UCACUCGUGCCGCAUUUCCTT |
| | NS shRNA | GGAATCTCATTCGATGCAT |
| **Rac1** | Rac1 siRNA #1 | GGAACUAAACUUGAUCUUATT |
| | Rac1 siRNA #2 | AUGAAAGUGUCACGGGUAA |
| **Rac3** | Rac3 siRNA#1 | GAAGACAGCUUGCUGAUC |
| | Rac3 siRNA#2 | AAACUGACGUCUUUCUGAU |
| **Rac2** | Rac2 siRNA #1 | UGACAACUAUUCAGCCAAU |
| **Cdc42** | Cdc42 siRNA#1 | UGAGAUAACUCACCACUGUTT |
| | Cdc42 siRNA #2 | GACGUCACAGUUAUGAUUG |
| **srGAP1** | srGAP1 siRNA#1 | UUAACGAUCUGAUUUCUUG |
| | srGAP1 siRNA#2 | CAUGAGGGCUUAGACAUUA |
| **PPP2R1A** | PPP2R1A siRNA#1 | AGGCGGAACUUCGACAGUA |
| | PPP2R1A siRNA#2 | AAACUUAACUCCUUGUGCA |
| **βPix** | βPix siRNA #1 | GAGCAUGAUGAUUGAGCGGAUA |
| | βPix shRNA #2 | GGAAGAAGATGCTCAGATT |
| | βPix shRNA #4 | GTAGTAAGAGCAAAGTTTA |

**Table 2**: **RNAi Sequence information.**

## REFERENCES


Ahn, J., V. Sanz-Moreno, and C.J. Marshall. 2012. The metastasis gene NEDD9 product acts through integrin beta3 and Src to promote mesenchymal motility and inhibit amoeboid motility. *J Cell Sci*. 125:1814-1826.

Aktories, K., U. Braun, S. Rosener, I. Just, and A. Hall. 1989. The rho gene product expressed in E. coli is a substrate of botulinum ADP-ribosyltransferase C3. *Biochem Biophys Res Commun*. 158:209-213.

Altemeier, W.A., S.Y. Schlesinger, C.A. Buell, W.C. Parks, and P. Chen. 2012. Syndecan-1 controls cell migration by activating Rap1 to regulate focal adhesion disassembly. *J Cell Sci*. 125:5188-5195.

Arthur, W.T., and K. Burridge. 2001. RhoA inactivation by p190RhoGAP regulates cell spreading and migration by promoting membrane protrusion and polarity. *Mol Biol Cell*. 12:2711-2720.

Aszodi, A., K.R. Legate, I. Nakchbandi, and R. Fassler. 2006. What mouse mutants teach us about extracellular matrix function. *Annu Rev Cell Dev Biol*. 22:591-621.

Bagrodia, S., S.J. Taylor, K.A. Jordon, L. Van Aelst, and R.A. Cerione. 1998. A novel regulator of p21-activated kinases. *J Biol Chem*. 273:23633-23636.

Baird, D., Q. Feng, and R.A. Cerione. 2005. The Cool-2/alpha-Pix protein mediates a Cdc42-Rac signaling cascade. *Curr Biol*. 15:1-10.

Baker, B.M., and C.S. Chen. 2012. Deconstructing the third dimension: how 3D culture microenvironments alter cellular cues. *J Cell Sci*. 125:3015-3024.

Barczyk, M., S. Carracedo, and D. Gullberg. 2010. Integrins. *Cell Tissue Res*. 339:269-280.

Bass, M.D., K.A. Roach, M.R. Morgan, Z. Mostafavi-Pour, T. Schoen, T. Muramatsu, U. Mayer, C. Ballestrem, J.P. Spatz, and M.J. Humphries. 2007. Syndecan-4-dependent Rac1 regulation determines directional migration in response to the extracellular matrix. *J Cell Biol*. 177:527-538.

Bastos, R.N., X. Penate, M. Bates, D. Hammond, and F.A. Barr. 2012. CYK4 inhibits Rac1-dependent PAK1 and ARHGEF7 effector pathways during cytokinesis. *J Cell Biol*. 198:865-880.

Beacham, D.A., M.D. Amatangelo, and E. Cukierman. 2007. Preparation of extracellular matrices produced by cultured and primary fibroblasts. *Curr Protoc Cell Biol*. Chapter 10:Unit 10 19.

Benink, H.A., and W.M. Bement. 2005. Concentric zones of active RhoA and Cdc42 around single cell wounds. *J Cell Biol*. 168:429-439.

Braga, V.M., and A.S. Yap. 2005. The challenges of abundance: epithelial junctions and small GTPase signalling. *Curr Opin Cell Biol*. 17:466-474.

Bustos, R.I., M.A. Forget, J.E. Settleman, and S.H. Hansen. 2008. Coordination of Rho and Rac GTPase function via p190B RhoGAP. *Curr Biol*. 18:1606-1611.

Byron, A., J.D. Humphries, M.D. Bass, D. Knight, and M.J. Humphries. 2011. Proteomic analysis of integrin adhesion complexes. *Sci Signal*. 4:pt2.

Byron, A., J.D. Humphries, and M.J. Humphries. 2013. Defining the extracellular matrix using proteomics. *Int J Exp Pathol*.

Cai, L., T.W. Marshall, A.C. Uetrecht, D.A. Schafer, and J.E. Bear. 2007. Coronin 1B coordinates Arp2/3 complex and cofilin activities at the leading edge. *Cell*. 128:915-929.

Carr, H.S., Y. Zuo, W. Oh, and J.A. Frost. 2013. Regulation of focal adhesion kinase activation, breast cancer cell motility, and amoeboid invasion by the RhoA guanine nucleotide exchange factor Net1. *Mol Cell Biol*. 33:2773-2786.

Cau, J., and A. Hall. 2005. Cdc42 controls the polarity of the actin and microtubule cytoskeletons through two distinct signal transduction pathways. *J Cell Sci*. 118:2579-2587.

Chahdi, A., B. Miller, and A. Sorokin. 2005. Endothelin 1 induces beta 1Pix translocation and Cdc42 activation via protein kinase A-dependent pathway. *J Biol Chem*. 280:578-584.

Chahdi, A., and J.P. Raufman. 2013. The Cdc42/Rac nucleotide exchange factor protein beta1Pix (Pak-interacting exchange factor) modulates beta-catenin transcriptional activity in colon cancer cells: evidence for direct interaction of beta1PIX with beta-catenin. *J Biol Chem*. 288:34019-34029.

Chang, F., C.A. Lemmon, D. Park, and L.H. Romer. 2007. FAK potentiates Rac1 activation and localization to matrix adhesion sites: a role for betaPIX. *Mol Biol Cell*. 18:253-264.

Chen, J.Y., Y.Y. Lin, and T.S. Jou. 2012. Phosphorylation of EBP50 negatively regulates beta-PIX-dependent Rac1 activity in anoikis. *Cell Death Differ*. 19:1027-1037.

Cherfils, J., and P. Chardin. 1999. GEFs: structural basis for their activation of small GTP-binding proteins. *Trends Biochem Sci*. 24:306-311.

Comunale, F., M. Causeret, C. Favard, J. Cau, N. Taulet, S. Charrasse, and C. Gauthier-Rouviere. 2007. Rac1 and RhoA GTPases have antagonistic functions during N-cadherin-dependent cell-cell contact formation in C2C12 myoblasts. *Biol Cell*. 99:503-517.

Condeelis, J., and J.W. Pollard. 2006. Macrophages: obligate partners for tumor cell migration, invasion, and metastasis. *Cell*. 124:263-266.

Coutinho-Budd, J., V. Ghukasyan, M.J. Zylka, and F. Polleux. 2012. The F-BAR domains from srGAP1, srGAP2 and srGAP3 regulate membrane deformation differently. *J Cell Sci*. 125:3390-3401.

Cox, T.R., and J.T. Erler. 2011. Remodeling and homeostasis of the extracellular matrix: implications for fibrotic diseases and cancer. *Dis Model Mech*. 4:165-178.

da Rocha-Azevedo, B., and F. Grinnell. 2013. Fibroblast morphogenesis on 3D collagen matrices: the balance between cell clustering and cell migration. *Exp Cell Res*. 319:2440-2446.

Daley, W.P., E.M. Gervais, S.W. Centanni, K.M. Gulfo, D.A. Nelson, and M. Larsen. 2012. ROCK1-directed basement membrane positioning coordinates epithelial tissue polarity. *Development*. 139:411-422.

Daley, W.P., and K.M. Yamada. 2013. ECM-modulated cellular dynamics as a driving force for tissue morphogenesis. *Curr Opin Genet Dev*. 23:408-414.

Deakin, N.O., and C.E. Turner. 2011. Distinct roles for paxillin and Hic-5 in regulating breast cancer cell morphology, invasion, and metastasis. *Mol Biol Cell*. 22:327-341.

Doyle, A.D., M.L. Kutys, M.A. Conti, K. Matsumoto, R.S. Adelstein, and K.M. Yamada. 2012. Micro-environmental control of cell migration--myosin IIA is required for efficient migration in fibrillar environments through control of cell adhesion dynamics. *J Cell Sci*. 125:2244-2256.

Doyle, A.D., R.J. Petrie, M.L. Kutys, and K.M. Yamada. 2013. Dimensions in cell migration. *Curr Opin Cell Biol*. 25:642-649.

Doyle, A.D., F.W. Wang, K. Matsumoto, and K.M. Yamada. 2009. One-dimensional topography underlies three-dimensional fibrillar cell migration. *J Cell Biol*. 184:481-490.

Dubash, A.D., K. Wennerberg, R. Garcia-Mata, M.M. Menold, W.T. Arthur, and K. Burridge. 2007. A novel role for Lsc/p115 RhoGEF and LARG in regulating RhoA activity downstream of adhesion to fibronectin. *J Cell Sci*. 120:3989-3998.

Emsley, J., C.G. Knight, R.W. Farndale, M.J. Barnes, and R.C. Liddington. 2000. Structural basis of collagen recognition by integrin alpha2beta1. *Cell*. 101:47-56.

Engler, A.J., S. Sen, H.L. Sweeney, and D.E. Discher. 2006. Matrix elasticity directs stem cell lineage specification. *Cell*. 126:677-689.

Feng, Q., J.G. Albeck, R.A. Cerione, and W. Yang. 2002. Regulation of the Cool/Pix proteins: key binding partners of the Cdc42/Rac targets, the p21-activated kinases. *J Biol Chem*. 277:5644-5650.

Feng, Q., D. Baird, X. Peng, J. Wang, T. Ly, J.L. Guan, and R.A. Cerione. 2006. Cool-1 functions as an essential regulatory node for EGF receptor- and Src-mediated cell growth. *Nat Cell Biol*. 8:945-956.

Frantz, C., K.M. Stewart, and V.M. Weaver. 2010. The extracellular matrix at a glance. *J Cell Sci*. 123:4195-4200.

Friedl, A. 2010. Proteoglycans: master modulators of paracrine fibroblast-carcinoma cell interactions. *Semin Cell Dev Biol*. 21:66-71.

Gadea, G., V. Sanz-Moreno, A. Self, A. Godi, and C.J. Marshall. 2008. DOCK10-mediated Cdc42 activation is necessary for amoeboid invasion of melanoma cells. *Curr Biol*. 18:1456-1465.

Gaggioli, C., S. Hooper, C. Hidalgo-Carcedo, R. Grosse, J.F. Marshall, K. Harrington, and E. Sahai. 2007. Fibroblast-led collective invasion of carcinoma cells with differing roles for RhoGTPases in leading and following cells. *Nat Cell Biol*. 9:1392-1400.

Garcia-Mata, R., and K. Burridge. 2007. Catching a GEF by its tail. *Trends Cell Biol*. 17:36-43.

Garcia-Mata, R., K. Wennerberg, W.T. Arthur, N.K. Noren, S.M. Ellerbroek, and K. Burridge. 2006. Analysis of activated GAPs and GEFs in cell lysates. *Methods Enzymol*. 406:425-437.

Geiger, B., J.P. Spatz, and A.D. Bershadsky. 2009. Environmental sensing through focal adhesions. *Nat Rev Mol Cell Biol*. 10:21-33.

Goetz, J.G., S. Minguet, I. Navarro-Lerida, J.J. Lazcano, R. Samaniego, E. Calvo, M. Tello, T. Osteso-Ibanez, T. Pellinen, A. Echarri, A. Cerezo, A.J. Klein-Szanto, R. Garcia, P.J. Keely, P. Sanchez-Mateos, E. Cukierman, and M.A. Del Pozo. 2011. Biomechanical remodeling of the microenvironment by stromal caveolin-1 favors tumor invasion and metastasis. *Cell*. 146:148-163.

Goicoechea, S.M., S. Awadia, and R. Garcia-Mata. 2014. I'm coming to GEF you: Regulation of RhoGEFs during cell migration. *Cell Adh Migr*. 8.

Grinnell, F., and W.M. Petroll. 2010. Cell motility and mechanics in three-dimensional collagen matrices. *Annu Rev Cell Dev Biol*. 26:335-361.

Guilluy, C., R. Garcia-Mata, and K. Burridge. 2011a. Rho protein crosstalk: another social network? *Trends Cell Biol*. 21:718-726.

Guilluy, C., V. Swaminathan, R. Garcia-Mata, E.T. O'Brien, R. Superfine, and K. Burridge. 2011b. The Rho GEFs LARG and GEF-H1 regulate the mechanical response to force on integrins. *Nature cell biology*. 13:722-727.

Hakkinen, K.M., J.S. Harunaga, A.D. Doyle, and K.M. Yamada. 2011. Direct comparisons of the morphology, migration, cell adhesions, and actin cytoskeleton of fibroblasts in four different three-dimensional extracellular matrices. *Tissue Eng Part A*. 17:713-724.

Hall, A. 1998. Rho GTPases and the actin cytoskeleton. *Science*. 279:509-514.

Hamel, B., E. Monaghan-Benson, R.J. Rojas, B.R. Temple, D.J. Marston, K. Burridge, and J. Sondek. 2011. SmgGDS is a guanine nucleotide exchange factor that specifically activates RhoA and RhoC. *J Biol Chem*. 286:12141-12148.

Heasman, S.J., and A.J. Ridley. 2008. Mammalian Rho GTPases: new insights into their functions from in vivo studies. *Nat Rev Mol Cell Biol*. 9:690-701.

Heck, J.N., S.M. Ponik, M.G. Garcia-Mendoza, C.A. Pehlke, D.R. Inman, K.W. Eliceiri, and P.J. Keely. 2012. Microtubules regulate GEF-H1 in response to extracellular matrix stiffness. *Mol Biol Cell*. 23:2583-2592.

Hern, D.L., and J.A. Hubbell. 1998. Incorporation of adhesion peptides into nonadhesive hydrogels useful for tissue resurfacing. *J Biomed Mater Res*. 39:266-276.

Hill, C.S., J. Wynne, and R. Treisman. 1995. The Rho family GTPases RhoA, Rac1, and CDC42Hs regulate transcriptional activation by SRF. *Cell*. 81:1159-1170.

Hodgson, L., F. Shen, and K. Hahn. 2010. Biosensors for characterizing the dynamics of rho family GTPases in living cells. *Curr Protoc Cell Biol*. Chapter 14:Unit 14 11 11-26.

Humphries, J.D., A. Byron, M.D. Bass, S.E. Craig, J.W. Pinney, D. Knight, and M.J. Humphries. 2009. Proteomic analysis of integrin-associated complexes identifies RCC2 as a dual regulator of Rac1 and Arf6. *Science signaling*. 2:ra51.

Humphries, J.D., A. Byron, and M.J. Humphries. 2006. Integrin ligands at a glance. *J Cell Sci*. 119:3901-3903.

Huttenlocher, A., and A.R. Horwitz. 2011. Integrins in cell migration. *Cold Spring Harb Perspect Biol*. 3:a005074.

Hynes, R.O. 2009. The extracellular matrix: not just pretty fibrils. *Science*. 326:1216-1219.

Hynes, R.O. 2012. The evolution of metazoan extracellular matrix. *J Cell Biol*. 196:671-679.

Hynes, R.O., and K.M. Yamada. 1982. Fibronectins: multifunctional modular glycoproteins. *J Cell Biol*. 95:369-377.

Ivaska, J., L. Nissinen, N. Immonen, J.E. Eriksson, V.M. Kahari, and J. Heino. 2002. Integrin alpha 2 beta 1 promotes activation of protein phosphatase 2A and dephosphorylation of Akt and glycogen synthase kinase 3 beta. *Mol Cell Biol*. 22:1352-1359.

Jokinen, J., E. Dadu, P. Nykvist, J. Kapyla, D.J. White, J. Ivaska, P. Vehvilainen, H. Reunanen, H. Larjava, L. Hakkinen, and J. Heino. 2004. Integrin-mediated cell adhesion to type I collagen fibrils. *J Biol Chem*. 279:31956-31963.

Kalluri, R., and R.A. Weinberg. 2009. The basics of epithelial-mesenchymal transition. *J Clin Invest*. 119:1420-1428.

Kapyla, J., J. Ivaska, R. Riikonen, P. Nykvist, O. Pentikainen, M. Johnson, and J. Heino. 2000. Integrin alpha(2)I domain recognizes type I and type IV collagens by different mechanisms. *J Biol Chem*. 275:3348-3354.

Kepner, E.M., S.M. Yoder, E. Oh, M.A. Kalwat, Z. Wang, L.A. Quilliam, and D.C. Thurmond. 2011. Cool-1/betaPIX functions as a guanine nucleotide exchange factor in the cycling of Cdc42 to regulate insulin secretion. *Am J Physiol Endocrinol Metab*. 301:E1072-1080.

Keung, A.J., E.M. de Juan-Pardo, D.V. Schaffer, and S. Kumar. 2011. Rho GTPases mediate the mechanosensitive lineage commitment of neural stem cells. *Stem Cells*. 29:1886-1897.

Khosravi-Far, R., P.A. Solski, G.J. Clark, M.S. Kinch, and C.J. Der. 1995. Activation of Rac1, RhoA, and mitogen-activated protein kinases is required for Ras transformation. *Mol Cell Biol*. 15:6443-6453.

Klotzsch, E., M.L. Smith, K.E. Kubow, S. Muntwyler, W.C. Little, F. Beyeler, D. Gourdon, B.J. Nelson, and V. Vogel. 2009. Fibronectin forms the most extensible biological fibers displaying switchable force-exposed cryptic binding sites. *Proc Natl Acad Sci U S A*. 106:18267-18272.

Knight, C.G., L.F. Morton, A.R. Peachey, D.S. Tuckwell, R.W. Farndale, and M.J. Barnes. 2000. The collagen-binding A-domains of integrins alpha(1)beta(1) and alpha(2)beta(1) recognize the same specific amino acid sequence, GFOGER, in native (triple-helical) collagens. *J Biol Chem*. 275:35-40.

Koh, C.G., E. Manser, Z.S. Zhao, C.P. Ng, and L. Lim. 2001. Beta1PIX, the PAK-interacting exchange factor, requires localization via a coiled-coil region to promote microvillus-like structures and membrane ruffles. *J Cell Sci*. 114:4239-4251.

Komatsu, N., K. Aoki, M. Yamada, H. Yukinaga, Y. Fujita, Y. Kamioka, and M. Matsuda. 2011. Development of an optimized backbone of FRET biosensors for kinases and GTPases. *Mol Biol Cell*. 22:4647-4656.

Kuo, J.C., X. Han, C.T. Hsiao, J.R. Yates, 3rd, and C.M. Waterman. 2011. Analysis of the myosin-II-responsive focal adhesion proteome reveals a role for beta-Pix in negative regulation of focal adhesion maturation. *Nat Cell Biol*. 13:383-393.

Kutys, M.L., A.D. Doyle, and K.M. Yamada. 2013. Regulation of cell adhesion and migration by cell-derived matrices. *Exp Cell Res*. 319:2434-2439.

Lammermann, T., J. Renkawitz, X. Wu, K. Hirsch, C. Brakebusch, and M. Sixt. 2009. Cdc42-dependent leading edge coordination is essential for interstitial dendritic cell migration. *Blood*. 113:5703-5710.

Laplante, I., R. Beliveau, and J. Paquin. 2004. RhoA/ROCK and Cdc42 regulate cell-cell contact and N-cadherin protein level during neurodetermination of P19 embryonal stem cells. *J Neurobiol*. 60:289-307.

Lauffenburger, D.A., and A.F. Horwitz. 1996. Cell migration: a physically integrated molecular process. *Cell*. 84:359-369.

Levental, K.R., H. Yu, L. Kass, J.N. Lakins, M. Egeblad, J.T. Erler, S.F. Fong, K. Csiszar, A. Giaccia, W. Weninger, M. Yamauchi, D.L. Gasser, and V.M. Weaver. 2009. Matrix crosslinking forces tumor progression by enhancing integrin signaling. *Cell*. 139:891-906.

Liu, F., L. Jia, A.M. Thompson-Baine, J.M. Puglise, M.B. Ter Beest, and M.M. Zegers. 2010. Cadherins and Pak1 control contact inhibition of proliferation by Pak1-betaPIX-GIT complex-dependent regulation of cell-matrix signaling. *Mol Cell Biol*. 30:1971-1983.

Liu, X., H. Wu, M. Byrne, J. Jeffrey, S. Krane, and R. Jaenisch. 1995. A targeted mutation at the known collagenase cleavage site in mouse type I collagen impairs tissue remodeling. *J Cell Biol*. 130:227-237.

Lo, C.M., H.B. Wang, M. Dembo, and Y.L. Wang. 2000. Cell movement is guided by the rigidity of the substrate. *Biophys J*. 79:144-152.

Lu, P., V.M. Weaver, and Z. Werb. 2012. The extracellular matrix: a dynamic niche in cancer progression. *J Cell Biol*. 196:395-406.

Lucero, H.A., and H.M. Kagan. 2006. Lysyl oxidase: an oxidative enzyme and effector of cell function. *Cell Mol Life Sci*. 63:2304-2316.

Machacek, M., L. Hodgson, C. Welch, H. Elliott, O. Pertz, P. Nalbant, A. Abell, G.L. Johnson, K.M. Hahn, and G. Danuser. 2009. Coordination of Rho GTPase activities during cell protrusion. *Nature*. 461:99-103.

Manser, E., T.H. Loo, C.G. Koh, Z.S. Zhao, X.Q. Chen, L. Tan, I. Tan, T. Leung, and L. Lim. 1998. PAK kinases are directly coupled to the PIX family of nucleotide exchange factors. *Mol Cell*. 1:183-192.

Mary, S., S. Charrasse, M. Meriane, F. Comunale, P. Travo, A. Blangy, and C. Gauthier-Rouviere. 2002. Biogenesis of N-cadherin-dependent cell-cell contacts in living fibroblasts is a microtubule-dependent kinesin-driven mechanism. *Mol Biol Cell*. 13:285-301.

Mayhew, M.W., E.D. Jeffery, N.E. Sherman, K. Nelson, J.M. Polefrone, S.J. Pratt, J. Shabanowitz, J.T. Parsons, J.W. Fox, D.F. Hunt, and A.F. Horwitz. 2007. Identification of phosphorylation sites in betaPIX and PAK1. *J Cell Sci*. 120:3911-3918.

Mayhew, M.W., D.J. Webb, M. Kovalenko, L. Whitmore, J.W. Fox, and A.F. Horwitz. 2006. Identification of protein networks associated with the PAK1-betaPIX-GIT1-paxillin signaling complex by mass spectrometry. *J Proteome Res*. 5:2417-2423.

Meller, N., S. Merlot, and C. Guda. 2005. CZH proteins: a new family of Rho-GEFs. *J Cell Sci*. 118:4937-4946.

Miyamoto, S., H. Teramoto, O.A. Coso, J.S. Gutkind, P.D. Burbelo, S.K. Akiyama, and K.M. Yamada. 1995. Integrin function: molecular hierarchies of cytoskeletal and signaling molecules. *J Cell Biol*. 131:791-805.

Morgan, M.R., H. Hamidi, M.D. Bass, S. Warwood, C. Ballestrem, and M.J. Humphries. 2013. Syndecan-4 phosphorylation is a control point for integrin recycling. *Dev Cell*. 24:472-485.

Morton, L.F., A.R. Peachey, L.S. Zijenah, A.H. Goodall, M.J. Humphries, and M.J. Barnes. 1994. Conformation-dependent platelet adhesion to collagen involving integrin alpha 2 beta 1-mediated and other mechanisms: multiple alpha 2 beta 1-recognition sites in collagen type I. *Biochem J*. 299 ( Pt 3):791-797.

Mott, J.D., and Z. Werb. 2004. Regulation of matrix biology by matrix metalloproteinases. *Curr Opin Cell Biol*. 16:558-564.

Naba, A., K.R. Clauser, S. Hoersch, H. Liu, S.A. Carr, and R.O. Hynes. 2012. The matrisome: in silico definition and in vivo characterization by proteomics of normal and tumor extracellular matrices. *Mol Cell Proteomics*. 11:M111 014647.

Nakayama, M., T.M. Goto, M. Sugimoto, T. Nishimura, T. Shinagawa, S. Ohno, M. Amano, and K. Kaibuchi. 2008. Rho-kinase phosphorylates PAR-3 and disrupts PAR complex formation. *Dev Cell*. 14:205-215.

Nayal, A., D.J. Webb, C.M. Brown, E.M. Schaefer, M. Vicente-Manzanares, and A.R. Horwitz. 2006. Paxillin phosphorylation at Ser273 localizes a GIT1-PIX-PAK

complex and regulates adhesion and protrusion dynamics. *J Cell Biol*. 173:587-589.

Nguyen-Ngoc, K.V., K.J. Cheung, A. Brenot, E.R. Shamir, R.S. Gray, W.C. Hines, P. Yaswen, Z. Werb, and A.J. Ewald. 2012. ECM microenvironment regulates collective migration and local dissemination in normal and malignant mammary epithelium. *Proc Natl Acad Sci U S A*. 109:E2595-2604.

Nobes, C.D., and A. Hall. 1995. Rho, rac, and cdc42 GTPases regulate the assembly of multimolecular focal complexes associated with actin stress fibers, lamellipodia, and filopodia. *Cell*. 81:53-62.

Oh, W.K., J.C. Yoo, D. Jo, Y.H. Song, M.G. Kim, and D. Park. 1997. Cloning of a SH3 domain-containing proline-rich protein, p85SPR, and its localization in focal adhesion. *Biochem Biophys Res Commun*. 235:794-798.

Ohta, Y., J.H. Hartwig, and T.P. Stossel. 2006. FilGAP, a Rho- and ROCK-regulated GAP for Rac binds filamin A to control actin remodelling. *Nat Cell Biol*. 8:803-814.

Olson, M.F., A. Ashworth, and A. Hall. 1995. An essential role for Rho, Rac, and Cdc42 GTPases in cell cycle progression through G1. *Science*. 269:1270-1272.

Osmani, N., N. Vitale, J.P. Borg, and S. Etienne-Manneville. 2006. Scrib controls Cdc42 localization and activity to promote cell polarization during astrocyte migration. *Curr Biol*. 16:2395-2405.

Pankov, R., Y. Endo, S. Even-Ram, M. Araki, K. Clark, E. Cukierman, K. Matsumoto, and K.M. Yamada. 2005. A Rac switch regulates random versus directionally persistent cell migration. *J Cell Biol*. 170:793-802.

Parri, M., and P. Chiarugi. 2010. Rac and Rho GTPases in cancer cell motility control. *Cell Commun Signal*. 8:23.

Paterson, H.F., A.J. Self, M.D. Garrett, I. Just, K. Aktories, and A. Hall. 1990. Microinjection of recombinant p21rho induces rapid changes in cell morphology. *J Cell Biol*. 111:1001-1007.

Petrie, R.J., A.D. Doyle, and K.M. Yamada. 2009. Random versus directionally persistent cell migration. *Nat Rev Mol Cell Biol*. 10:538-549.

Petrie, R.J., N. Gavara, R.S. Chadwick, and K.M. Yamada. 2012. Nonpolarized signaling reveals two distinct modes of 3D cell migration. *J Cell Biol*. 197:439-455.

Petrie, R.J., and K.M. Yamada. 2012. At the leading edge of three-dimensional cell migration. *J Cell Sci*. 125:5917-5926.

Provenzano, P.P., K.W. Eliceiri, J.M. Campbell, D.R. Inman, J.G. White, and P.J. Keely. 2006. Collagen reorganization at the tumor-stromal interface facilitates local invasion. *BMC Med*. 4:38.

Provenzano, P.P., D.R. Inman, K.W. Eliceiri, J.G. Knittel, L. Yan, C.T. Rueden, J.G. White, and P.J. Keely. 2008a. Collagen density promotes mammary tumor initiation and progression. *BMC Med*. 6:11.

Provenzano, P.P., D.R. Inman, K.W. Eliceiri, S.M. Trier, and P.J. Keely. 2008b. Contact guidance mediated three-dimensional cell migration is regulated by Rho/ROCK-dependent matrix reorganization. *Biophys J*. 95:5374-5384.

Raftopoulou, M., and A. Hall. 2004. Cell migration: Rho GTPases lead the way. *Dev Biol*. 265:23-32.

Raub, C.B., V. Suresh, T. Krasieva, J. Lyubovitsky, J.D. Mih, A.J. Putnam, B.J. Tromberg, and S.C. George. 2007. Noninvasive assessment of collagen gel microstructure and mechanics using multiphoton microscopy. *Biophys J*. 92:2212-2222.

Ridley, A.J., M.A. Schwartz, K. Burridge, R.A. Firtel, M.H. Ginsberg, G. Borisy, J.T. Parsons, and A.R. Horwitz. 2003. Cell migration: integrating signals from front to back. *Science*. 302:1704-1709.

Roca-Cusachs, P., N.C. Gauthier, A. Del Rio, and M.P. Sheetz. 2009. Clustering of alpha(5)beta(1) integrins determines adhesion strength whereas alpha(v)beta(3) and talin enable mechanotransduction. *Proc Natl Acad Sci U S A*. 106:16245-16250.

Rosenfeldt, H., M.D. Castellone, P.A. Randazzo, and J.S. Gutkind. 2006. Rac inhibits thrombin-induced Rho activation: evidence of a Pak-dependent GTPase crosstalk. *J Mol Signal*. 1:8.

Rossman, K.L., C.J. Der, and J. Sondek. 2005. GEF means go: turning on RHO GTPases with guanine nucleotide-exchange factors. *Nat Rev Mol Cell Biol*. 6:167-180.

Rozario, T., and D.W. DeSimone. 2010. The extracellular matrix in development and morphogenesis: a dynamic view. *Dev Biol*. 341:126-140.

Sahai, E., and C.J. Marshall. 2003. Differing modes of tumour cell invasion have distinct requirements for Rho/ROCK signalling and extracellular proteolysis. *Nat Cell Biol*. 5:711-719.

Sakai, T., M. Larsen, and K.M. Yamada. 2003. Fibronectin requirement in branching morphogenesis. *Nature*. 423:876-881.

Samson, T., C. Will, A. Knoblauch, L. Sharek, K. von der Mark, K. Burridge, and V. Wixler. 2007. Def-6, a guanine nucleotide exchange factor for Rac1, interacts

with the skeletal muscle integrin chain alpha7A and influences myoblast differentiation. *The Journal of biological chemistry*. 282:15730-15742.

Sanz-Moreno, V., G. Gadea, J. Ahn, H. Paterson, P. Marra, S. Pinner, E. Sahai, and C.J. Marshall. 2008. Rac activation and inactivation control plasticity of tumor cell movement. *Cell*. 135:510-523.

Schmidt, A., and A. Hall. 2002. Guanine nucleotide exchange factors for Rho GTPases: turning on the switch. *Genes Dev*. 16:1587-1609.

Schultz, G.S., and A. Wysocki. 2009. Interactions between extracellular matrix and growth factors in wound healing. *Wound Repair Regen*. 17:153-162.

Scott, J.E. 2003. Elasticity in extracellular matrix 'shape modules' of tendon, cartilage, etc. A sliding proteoglycan-filament model. *J Physiol*. 553:335-343.

Shin, E.Y., K.S. Shin, C.S. Lee, K.N. Woo, S.H. Quan, N.K. Soung, Y.G. Kim, C.I. Cha, S.R. Kim, D. Park, G.M. Bokoch, and E.G. Kim. 2002. Phosphorylation of p85 beta PIX, a Rac/Cdc42-specific guanine nucleotide exchange factor, via the Ras/ERK/PAK2 pathway is required for basic fibroblast growth factor-induced neurite outgrowth. *Journal of Biological Chemistry*. 277:44417-44430.

Shin, E.Y., K.N. Woo, C.S. Lee, S.H. Koo, Y.G. Kim, W.J. Kim, C.D. Bae, S.I. Chang, and E.G. Kim. 2004. Basic fibroblast growth factor stimulates activation of Rac1 through a p85 betaPIX phosphorylation-dependent pathway. *J Biol Chem*. 279:1994-2004.

Shoulders, M.D., and R.T. Raines. 2009. Collagen structure and stability. *Annu Rev Biochem*. 78:929-958.

Simon, C.M., E.M. Vaughan, W.M. Bement, and L. Edelstein-Keshet. 2013. Pattern formation of Rho GTPases in single cell wound healing. *Mol Biol Cell*. 24:421-432.

Singh, P., C. Carraher, and J.E. Schwarzbauer. 2010. Assembly of fibronectin extracellular matrix. *Annu Rev Cell Dev Biol*. 26:397-419.

Sosa, M.S., C. Lopez-Haber, C. Yang, H. Wang, M.A. Lemmon, J.M. Busillo, J. Luo, J.L. Benovic, A. Klein-Szanto, H. Yagi, J.S. Gutkind, R.E. Parsons, and M.G. Kazanietz. 2010. Identification of the Rac-GEF P-Rex1 as an essential mediator of ErbB signaling in breast cancer. *Molecular cell*. 40:877-892.

Stahl, P.J., N.H. Romano, D. Wirtz, and S.M. Yu. 2010. PEG-based hydrogels with collagen mimetic peptide-mediated and tunable physical cross-links. *Biomacromolecules*. 11:2336-2344.

Suki, B., and J.H. Bates. 2008. Extracellular matrix mechanics in lung parenchymal diseases. *Respir Physiol Neurobiol*. 163:33-43.

Tang, H., A. Li, J. Bi, D.M. Veltman, T. Zech, H.J. Spence, X. Yu, P. Timpson, R.H. Insall, M.C. Frame, and L.M. Machesky. 2013. Loss of Scar/WAVE complex promotes N-WASP- and FAK-dependent invasion. *Curr Biol*. 23:107-117.

Thomas, L.A., and K.M. Yamada. 1992. Contact stimulation of cell migration. *J Cell Sci*. 103 ( Pt 4):1211-1214.

Trappmann, B., and C.S. Chen. 2013. How cells sense extracellular matrix stiffness: a material's perspective. *Curr Opin Biotechnol*. 24:948-953.

Tsang, K.Y., M.C. Cheung, D. Chan, and K.S. Cheah. 2010. The developmental roles of the extracellular matrix: beyond structure to regulation. *Cell Tissue Res*. 339:93-110.

Turner, C.E., M.C. Brown, J.A. Perrotta, M.C. Riedy, S.N. Nikolopoulos, A.R. McDonald, S. Bagrodia, S. Thomas, and P.S. Leventhal. 1999. Paxillin LD4 motif binds PAK and PIX through a novel 95-kD ankyrin repeat, ARF-GAP protein: A role in cytoskeletal remodeling. *J Cell Biol*. 145:851-863.

van Dijk, M., S.A. Goransson, and S. Stromblad. 2013. Cell to extracellular matrix interactions and their reciprocal nature in cancer. *Exp Cell Res*.

Vega, F.M., G. Fruhwirth, T. Ng, and A.J. Ridley. 2011. RhoA and RhoC have distinct roles in migration and invasion by acting through different targets. *J Cell Biol*. 193:655-665.

Vuoriluoto, K., J. Jokinen, K. Kallio, M. Salmivirta, J. Heino, and J. Ivaska. 2008. Syndecan-1 supports integrin alpha2beta1-mediated adhesion to collagen. *Exp Cell Res*. 314:3369-3381.

Whelan, M.C., and D.R. Senger. 2003. Collagen I initiates endothelial cell morphogenesis by inducing actin polymerization through suppression of cyclic AMP and protein kinase A. *J Biol Chem*. 278:327-334.

Wierzbicka-Patynowski, I., and J.E. Schwarzbauer. 2003. The ins and outs of fibronectin matrix assembly. *J Cell Sci*. 116:3269-3276.

Wilkinson, S., H.F. Paterson, and C.J. Marshall. 2005. Cdc42-MRCK and Rho-ROCK signalling cooperate in myosin phosphorylation and cell invasion. *Nat Cell Biol*. 7:255-261.

Wise, S.G., and A.S. Weiss. 2009. Tropoelastin. *Int J Biochem Cell Biol*. 41:494-497.

Wolf, K., and P. Friedl. 2011. Extracellular matrix determinants of proteolytic and non-proteolytic cell migration. *Trends Cell Biol*. 21:736-744.

Wolf, K., M. Te Lindert, M. Krause, S. Alexander, J. Te Riet, A.L. Willis, R.M. Hoffman, C.G. Figdor, S.J. Weiss, and P. Friedl. 2013. Physical limits of cell

migration: control by ECM space and nuclear deformation and tuning by proteolysis and traction force. *J Cell Biol*. 201:1069-1084.

Wong, K., X.R. Ren, Y.Z. Huang, Y. Xie, G. Liu, H. Saito, H. Tang, L. Wen, S.M. Brady-Kalnay, L. Mei, J.Y. Wu, W.C. Xiong, and Y. Rao. 2001. Signal transduction in neuronal migration: roles of GTPase activating proteins and the small GTPase Cdc42 in the Slit-Robo pathway. *Cell*. 107:209-221.

Xu, H., D. Bihan, F. Chang, P.H. Huang, R.W. Farndale, and B. Leitinger. 2012. Discoidin domain receptors promote alpha1beta1- and alpha2beta1-integrin mediated cell adhesion to collagen by enhancing integrin activation. *PLoS One*. 7:e52209.

Yamada, K.M., and E. Cukierman. 2007. Modeling tissue morphogenesis and cancer in 3D. *Cell*. 130:601-610.

Yang, S., J.J. Zhang, and X.Y. Huang. 2012. Mouse models for tumor metastasis. *Methods Mol Biol*. 928:221-228.

Yoshizaki, H., Y. Ohba, K. Kurokawa, R.E. Itoh, T. Nakamura, N. Mochizuki, K. Nagashima, and M. Matsuda. 2003. Activity of Rho-family GTPases during cell division as visualized with FRET-based probes. *J Cell Biol*. 162:223-232.

Yurchenco, P.D. 2011. Basement membranes: cell scaffoldings and signaling platforms. *Cold Spring Harb Perspect Biol*. 3.

Zhao, Z.S., E. Manser, T.H. Loo, and L. Lim. 2000. Coupling of PAK-interacting exchange factor PIX to GIT1 promotes focal complex disassembly. *Mol Cell Biol*. 20:6354-6363.